ABSTRACT

Title of dissertation: DYNAMICS, NONLINEAR INSTABILITIES, AND CONTROL OF DRILL-STRINGS

Xie Zheng
Doctor of Philosophy, 2020

Dissertation directed by: Professor Balakumar Balachandran
Department of Mechanical Engineering

Drill strings are flexible, slender structures, which are many kilometers long. They are used to transmit the rotary motion to the drill bit in the process of drilling a bore hole. Due to the flexibility of the drill string and nonlinear interactions between the drill bit and rock, these systems often experience severe vibrations, and these vibrations may cause excessive wear of drill bit and equipment damage. The aim of this dissertation effort is to further the understanding of the underlying mechanism leading to the undesired vibratory motions of drill strings, as well as to develop a viable control strategy that is applicable for mitigation of harmful vibrations.

A reduced order drill-string model with coupled axial and torsional dynamics is constructed. Nonlinear effects associated with dry friction, loss of contact, and the state-dependent delay, which all arise from cutting mechanics are considered. For the sake of analyses, a non-dimensionalized form of the governing equations is provided. Next, in order to study the local stability of drill-string system, a linear system associated with the state-dependent delay is derived. Stability analysis of

this linearized system is carried out analytically by using the D-subdivision scheme. The obtained results are illustrated in the terms of stability crossing curves, which are presented in the plane of non-dimensional rotation speed and non-dimensional cutting depth; non-dimensional rotation speed and cutting coefficient, respectively. For the nonlinear analysis, a numerical continuation method is developed and used to follow periodic orbits of systems with friction, loss of contact, and state-dependent delay. Bifurcation diagram are constructed to capture the possible routes from either a nominal stable operational state or a stable limit-cycle motion without stick-slip to a limit-cycle motion with stick slip. It is shown that the system can experience subcritical Hopf bifurcations of equilibrium solutions and cyclic fold bifurcations. Furthermore, with the preceding work, an observer based on controller design is proposed by using a continuous pole placement method for time delay systems. The effectiveness of the controller in suppressing stick-slip behavior is shown through simulations.

The primary contributions of this dissertation are summarized as follows: i) analytical determination of the stable operational region; ii) revelation of the routes to torsional stick-slip vibrations; and iii) construction of a feasible control scheme to mitigate the destructive vibrations caused by complex nonlinear effects.

DYNAMICS, NONLINEAR INSTABILITIES, AND CONTROL OF DRILL-STRINGS

by

Xie Zheng

Dissertation submitted to the Faculty of the Graduate School of the
University of Maryland, College Park in partial fulfillment
of the requirements for the degree of
Doctor of Philosophy
2020

Advisory Committee:
Professor Balakumar Balachandran, Chair and Advisor, Mechanical Engineering
Professor Amr Baz, Department of Mechanical Engineering
Professor Nikhil Chopra, Department of Mechanical Engineering
Associate Professor Jin-Oh Hahn, Department of Mechanical Engineering
Associate Professor Maria Cameron, Department of Mathematics
(Dean's Representative)

Dedicated to my parents, wife, and daughter
for their consistent love & support.
Love you all dearly.

Acknowledgments

I would like to begin by thanking my advisor Professor Balakumar Balachandran for offering me an invaluable opportunity to work on this challenging and meaningful topic. He has always been open-minded about the research and full of insightful advice. I benefited greatly from his detailed guidance and kind support throughout my research. I learned from him that hard work, persistence, and patience are key factors to be a good researcher. It has been a real honor and pleasure to work with such an extraordinary individual .

I would also express my deep gratitude to Professor Amr Baz, Professor Nikhil Chopra, Professor Jin-Oh Hahn, and Professor Maria Cameron for agreeing to serve on my dissertation committee and sparing their invaluable time in reviewing my work. Through the courses they have taught and personal interactions with them, I have learned tremendously.

My special thanks go to Dr. Xianbo Liu, a visiting scholar in our group. Without his encouragement, insights, and expertise in nonlinear dynamics, I could not have completed this dissertation on time. I would like to thank him for helping me build a strong foundation in the field of drill system dynamics and control.

My colleagues and friends at UMD, have been enriched my doctoral life in many ways over the past few years, and they are far too many to mention their roles individually, but I would like to acknowledge them by listing their names: Vipin Agarwal; Guanjin Wang; Gizem Acar; Celeste Poley; Lautaro Cilenti; Abdulrahman Alofi; Saliou Telly; Randall Kania; Abu Bockarie Kebbie-Anthony; Preethi Ravula;

Rui Wang; Andrew Tseng; Junxi Zhu; Yimeng Dong; and Yang Yao. Two other important names to mention here: Jin Xin who has been my all-time lunch buddy, we gained considerable wisdom and weight together, and Yongsheng Liu who was my basketball mate; we ran through a lot of things in/out-side the courts.

To my family, particularly my parents, thank you for your unconditional love, continued support, and unwavering faith in me. You made me the person who I am today. Above all, I must thank my wife Linqiong, as without her love and support(mental, motivational, and financial) this dissertation would have been a distant dream. Thank you for being my chef, editor, accountant, personal trainer, and mother of my daughter. I am blessed to have known such a magnificent woman.

Finally, I am grateful for the support received for this research through Qatar National Research Fund for NPRP Project 7-083-2-041 and the Mina Martin Foundation.

Table of Contents

List of Tables

List of Figures

List of Abbreviations

BHA	Bottom hole assembly
CD-DDE	Constant delay differential equation
DDE	Delay differential equation
DOF	Degree of Freedom
ODE	Ordinary differential equation
PDC	Polycrystalline diamond compact
PID	Proportional-integral-derivative
RHP	Right Half Plane
SD-DDE	State-dependent delay differential equation
ToB	Torque on Bit
WoB	Weight on Bit
h.o.t	Higher order term
$\mathbf{I}$	Identity matrix of appropriate dimension
R^+	Positive real number
$\mathrm{Re}(\cdot)$	Real part of a complex number
$\sup(\cdot)$	supremum operator

Chapter 1: Introduction

1.1 Background

Throughout human history, energy availability has been a key enabler of living standard for human beings. In the agrarian era, people burned wood for warmth and cooking, and it remained the chief global fuel for centuries [6]. At the beginning of 18th century, the coal powered steam engine brought human beings into the industry age. With the technological breakthroughs of the 20th century, petroleum which is a much more adaptable and flexible source than coal, emerged as the major source of energy. The exploitation of oil has a long history. The earliest oil well was drilled by Chinese in AD 347 or earlier. They had depths of up to 800 feet and were drilled by using bits attached to bamboo poles [7]. With the increasing demand of petroleum, the technologies of oil drill operation have been rapidly advanced in 20th century. However, due to the strong nonlinearities in the rotary drilling systems, self-excited vibrations, which may lead to decrease of drilling efficiency, as well as accelerate the wear of drill bit and failure of the equipment, often arise in the field operations.

1.1.1 Drilling System Components

A sketch of a modern oil drilling system is shown in Figure 1.1. Briefly speaking, it contains two subsystems: the surface system (about 40-80 meters high) and the underground system(might be several kilometers long). For a detailed description of a drill-string system, one can refer to the book by Bommer [8]. The surface system consists of the following parts:

• Rotary tables, powered hydraulically or electrically, to provide the energy for the rotational motions

• Hoisting systems, including crown block, traveling block, draw-works, Kelly, and drill line, to lift the drill-strings and control the weight on the bit

• Drill mud system, to pump the drilling fluid (for taking away the heat, and providing viscous damping) through the drill string.

For the underground system, one has the following:

• Drill pipe, the length varies according to the drilling depth. Typical final hole depth goes from 1000 to 8000 m for ultra-deep drilling.

• Drill collar, heavier-weight part of the drill pipe, to provide extra weight on bit. It typically 300-500m long and with a weight of 40-60 tons at the bottom hole. Some parts of it may be thicker, and are called stabilizers, which are used to avoid large lateral motions of the drill string in the bottom hole [9].

• Drill bit, used to cut rock. Fix cutter and roller cone are two common types. A bit of fixed cutter has no moving parts (i.e., Figure 1.2 (b), (c), (d)), and is often made with polycrystalline diamond compact(PDC). The roller cone

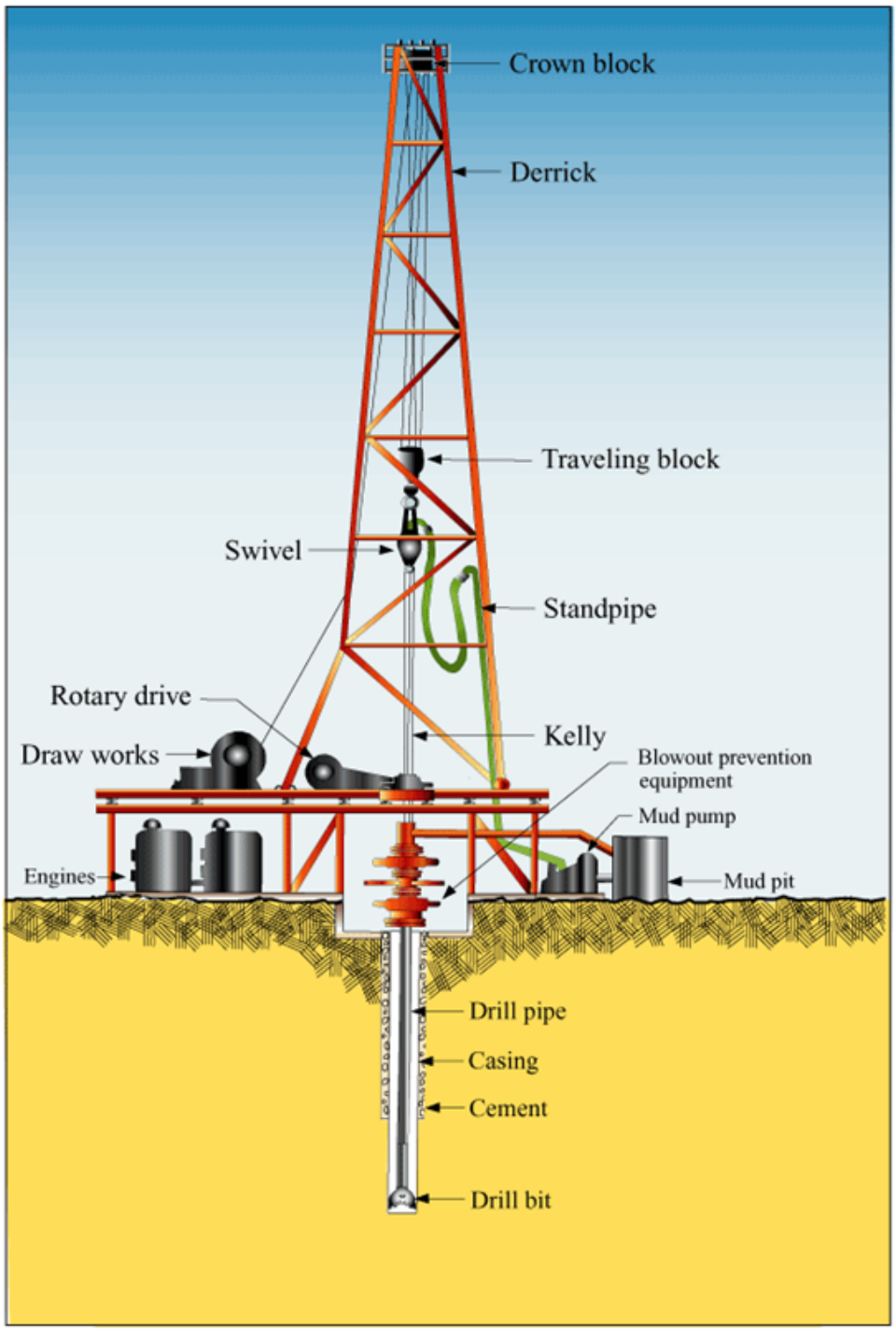

Figure 1.1: Schematic of drill-string system [1].

(see Figure 1.2(a)), on the other hand, rotates with the drill string and acts more by crushing. In addition, drill collar, together with drill bit are often times called bottom hole assembly (BHA).

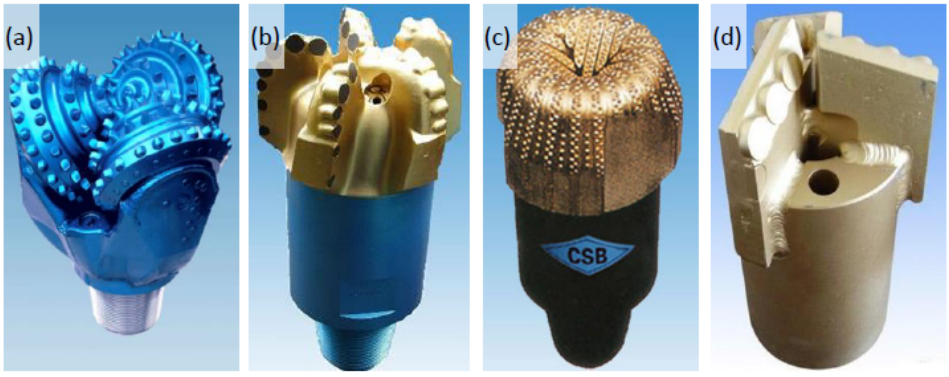

Figure 1.2: Drill bit, (a) tricone bit, (b) PDC bit, (c) diamond bit, and (d) drag bit [2].

1.1.2 Unfavorable Vibrations

As stated in last section, drill string are long and flexible slender structures that are used to transmit the rotary motion to the drill bit during drilling of a bore hole. Due to the flexibility of the drill string and nonlinear interactions between the drill bit and rock, these systems often experience different types of vibratory motions, which can be categorized as axial, torsional, and lateral vibrations. These harmful motions lead to slowing down of drilling operation, excessive wear of drill bit, and equipment failure (see Figure 1.3).

• Axial vibration. As shown in Figure 1.4(a), it is motion along the longitudinal axis of the drill components. It may cause the loss of contract between the drill

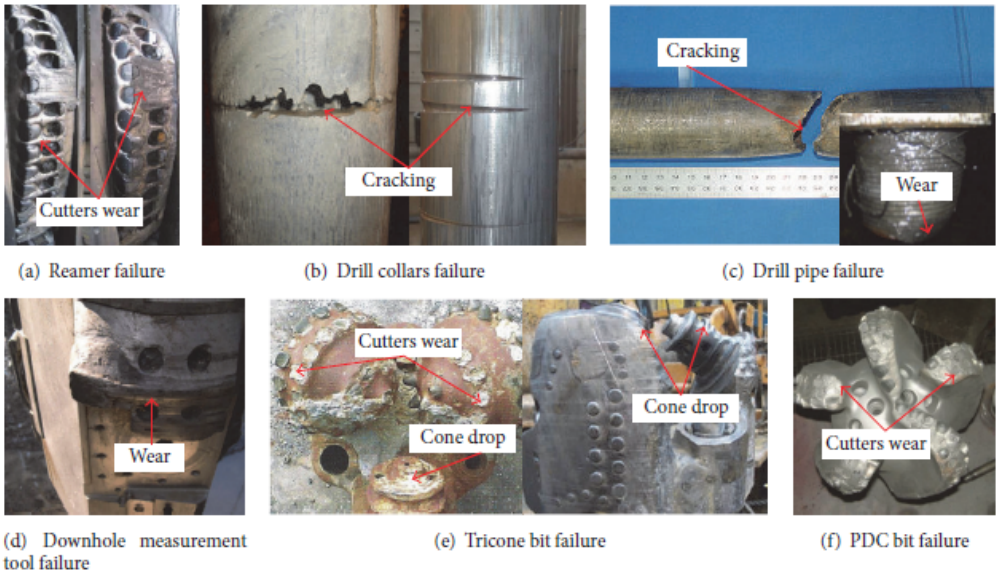

Figure 1.3: Typical drilling failures due to the different drill string vibrations [3].

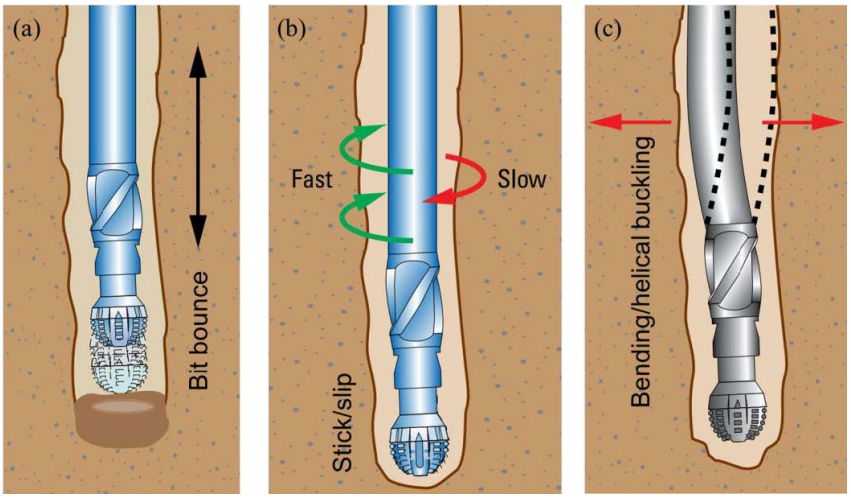

Figure 1.4: Three drill-string vibration modes: (a) axial, (b) torsional, and (c) lateral [2].

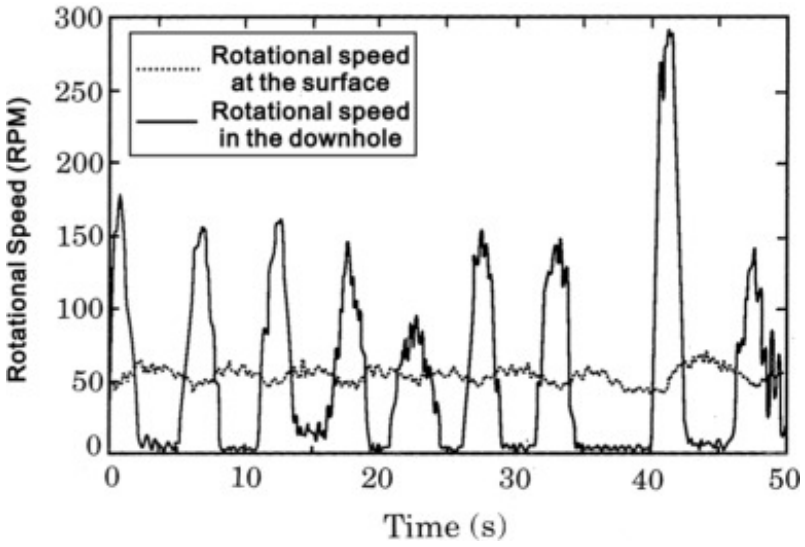

Figure 1.5: Field observed stick-slip vibration [4].

bit and the rock, which often referred to as bit bounce. Based on the level of severity, these behaviors may increase the time of drilling, provoke fatigue to the drill bit, and damage the BHA. Furthermore, due to the existence of the coupling of the cutting mechanisms, axial motions may also excite torsional and lateral vibrations.

• Torsional vibration. It can be seen from Figure 1.5 that applying a constant angular velocity at the top, does not translate into a steady rotational movement at the BHA. Instead, the BHA may suffer from one of most destructive type of vibrations: stick-slip vibrations. As the name implies, these vibrations contain two phases: the stick phase, when the drill bit motion is completely ceased, and the slip phase, when the rotational motion of the bit can speed up and be several times higher than the nominal drive speed. The discontinuous nature of the motion and high rotation speeds lead to extreme accelerations and forces, which can cause excessive wear of drill bit and equipment damage.

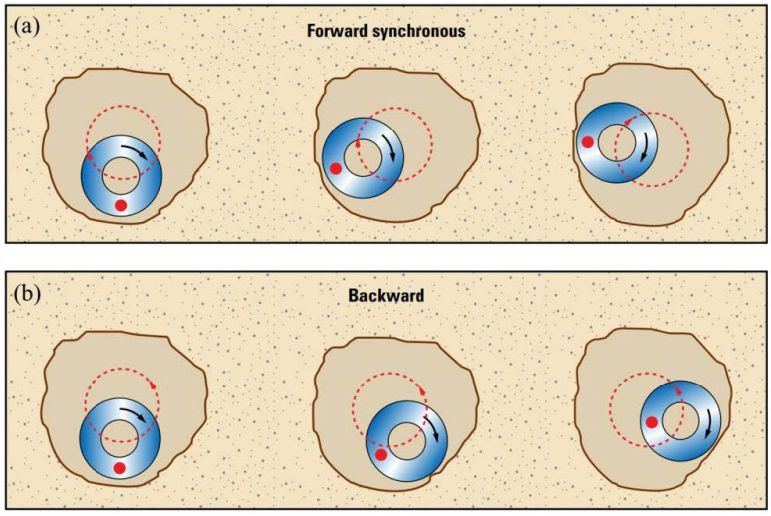

Figure 1.6: Lateral vibrations: (a) forward whirling and (b) backward whirling [4].

• Lateral vibration. As illustrated in Figure 1.4(c), deep in the hole, the lateral vibrations and shocks will happen, when the rotating BHA interacts with the borehole wall. As a result, the collisions with the borehole wall will produce eccentric hole and damage the BHA components [9]. Whirling is one of the most dangerous form of lateral vibrations, since it can not be easily discovered from the surface drill floor. As shown in Figure 1.6, one can have forward and backward whirling. For the forward whirling, the whirling direction is same as the BHA rotational direction. On the contrary, the direction of backward whirling is different with the BHA rotational direction. Furthermore, because of the geometric constraint, the backward whirling speed can be up to 5 times higher than the BHA rotary speed.

In summary, the destructiveness level of all vibrations can be written in this order in terms of undesirableness: i) backward whirling, ii) forward whirling, iii) stick slip, and iv) bit bounce.

1.2 Literature Review

1.2.1 Literature Review on Drill-string System Modeling

To understand drill-string vibrations, various models have been developed by accounting for different aspects. Models with one degree of freedom (DOF) and two degrees of freedom (2DOF) are most commonly used [10, 11]. By using a velocity-weakening friction model, Navarro-Lopez and Suarez demonstrated the occurrence of torsional stick-slip vibrations during different operations. Experimental verification of a 2DOF model was given by Mihajlovic, van Veggel, van de Wouw, and Nijmeijer [12], with a lab scaled drill-string setup. Stick-slip behavior between the well bore and drill string was found by Liao, Balachandran, Karkoub, and Abdel-Magid [13] in the numerical simulations of a discrete system with Coulomb friction and reproduced in the experimental studies. In the work of Germay, Denol, and Detournay [14], a finite element model with 58 elements has been proposed and it has been shown that higher modes are also excited.

Detournay and Defourny [15] developed a cutting mechanics model, by considering the loss of contact, friction, and wear of drill bit. The axial and torsional motion are coupled together through a state-dependent time delay [5, 16]. The coupled axial-torsional dynamics was examined in the studies of Richard, Germay, and Detournay [17] and shown to be a major cause of stick-slip motions. Systems with state-dependent delay have been reported and analyzed in many mechanical systems (e.g. milling systems [18], turning process [19]). For a drill-string system, by using

a discretized model, the local stability of system with state-dependent time delay has been studied by Liu, Vlajic, Long, Meng, and Balachandran through the semi-discretization method and eigenvalue analysis in references [5] and [20], respectively.

The nonlinear analysis for system with time delays, especially, systems with state-dependant delays is still under investigation. For a turning system, Insperger, Barton, and Stepan using a numerical continuation technique, revealed that the criticality of the Hopf bifurcation depends on the feed rate. This was in contrast to simpler constant delay models wherein only the subcritical bifurcation was found [21,22]. For a drill system with consideration of state-dependent delay, the nonlinear analysis has been carried out by using the method of multiple scales. The local bifurcation analysis has been conducted by Gupta and Wahi in reference [23]. However, in this work, only the local nonlinear analysis was carried out, the effect of other nonlinear sources(i.e., loss of contact and friction) were not taken into account.

In the current research, a discretized model is studied, motivated by the work of Germay, Denoel, and Detournay [24], who showed that a low-dimension model can describe the dynamics of a drill string well and allow for an in-depth study of effect of state-dependent delay and other nonlinear sources. The nonlinear analysis is carried out by using a numerical continuation method that is similar to those used for the turning operation cases.

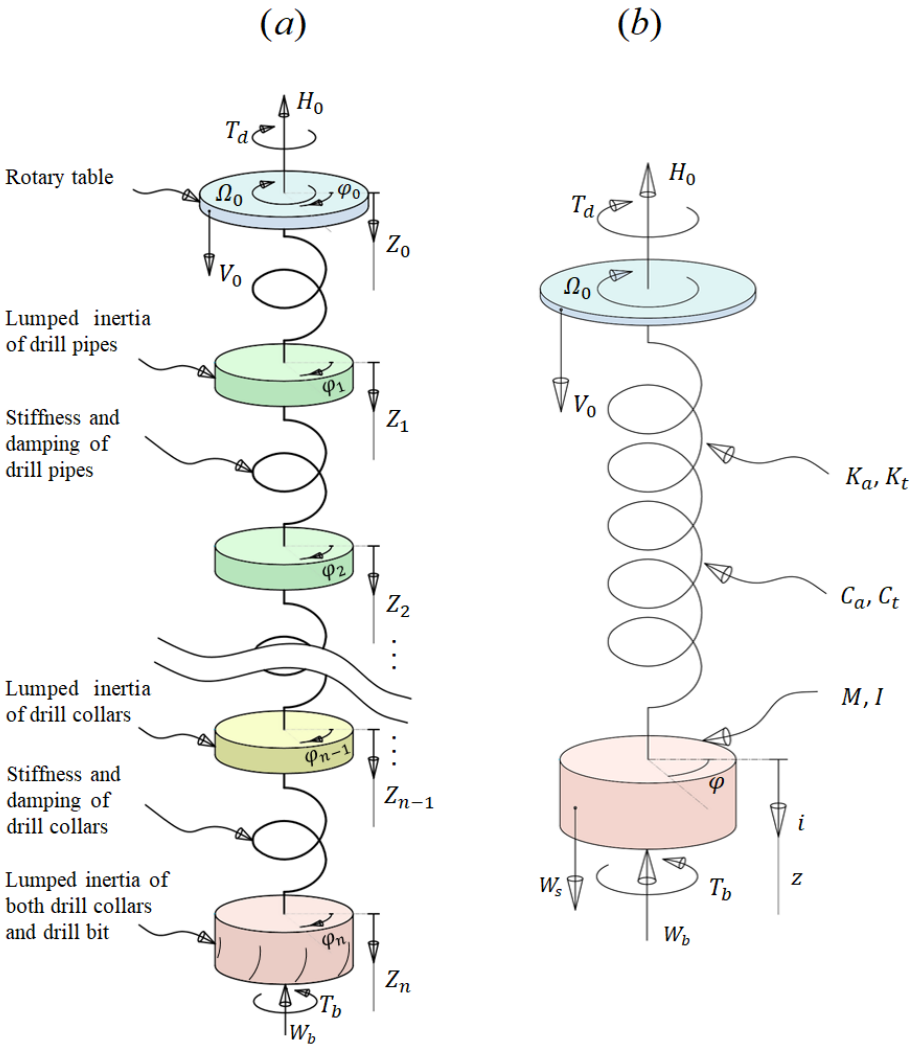

Figure 1.7: Drill-string models: (a) finite element model and (b) reduced-order model.

1.2.2 Literature Review on Systems with Time Delays

The study of a time delayed system has a long history [25, 26]. As mentioned by Michiels and Niculescu [27], the first delay differential equations (DDEs) were encountered in the work of Bernouli and Condorcet. These systems often arise in many different fields of science and engineering. Examples include biological systems [28, 29], computer networked system [30] , and semiconductor lasers [31].

Roughly speaking, a time delay system is a dynamical system represented by differential equations in some unknown function (and some of its derivatives) evaluated at arguments which are distributed over some intervals in the past [27]. Furthermore, It can be divided into two types:

- Retarded type

$$\dot{x}(t) = A_0 x(t) + \sum_{i=1}^{m} A_i x(t - \tau_i) \tag{1.1}$$

- Neutral type

$$\frac{d}{dt}\left(x(t) + \sum_{k=1}^{m} H_k x(t - \tau_k)\right) = A_0 x(t) + \sum_{k=1}^{m} A_k x(t - \tau_k) \tag{1.2}$$

where $x(t) \in \mathbf{R}^n$ is the state variable at time t, $A_i \in \mathbf{R}^{n\times n}$, $i = 0, 1, ..., m$ are real matrices, and $0 < \tau_1 < \tau_2 ... < \tau_m$ represent the time delays. Moreover, if time delays are functions of the system states, the system will be referred to as a state-dependent delay system.

1.2.3 Literature Review on Control of Drill-string Systems

In order to mitigate undesired drill-string vibrations, different control schemes have been proposed and implemented. The soft torque controller, which was patented by Shell in 1992, is widely used in industry (e.g., see [32]). With a goal of damping the first mode of torsional motion, this controller was essentially a proportional-integral (PI) controller based on the error between the measured top drive speed and a reference speed. Following this approach, soft speed as well as Z-torque controllers have been designed. However, as pointed out in the work of Kyllingstad [33], these controllers are very sensitive to time delay, and even a small amount of time delay can cause the control scheme to fail in the treatment of stick-slip vibration. Besides proportional-integral-derivative (PID) control schemes, Sarker, Riderout and Butt [34] proposed a linear quadratic regulator based controller to eliminate the stick-slip vibration with a discrete model of axial and torsional dynamics. In the study given by Vromen [35], state-feedback controller, observer-based output-feedback controller, as well as H^{∞}-based output-feedback controller were presented. However, to the best of the author's knowledge, none of them have considered the effect of time delay. In author group's previous work, based on the delayed states feedback, a PID controller was developed and implemented on a discretized system parameter model [5]. With the state-dependent delay in the model, Besselink *et al.* [36], designed both state-feedback and output-feedback control strategies with consideration of only torsional dynamics.

1.3 Scope of the Dissertation

The objective of this work is to study the effect of state-dependent delay on the drill-string dynamics, specifically related to, how the response differs from the case with constant delay, what kind of bifurcations occur in the case with state-dependent delay, and how to mitigate the stick-slip vibrations by using a suitable controller.

To answer these questions, the following work has been undertaken:

1. Model Construction: Construction of reduced-order models for varying dimensions and complexity to describe the dynamics of the drill-sting system, and use of appropriate non-dimensionalization methods to reduce the number of parameters.

2. Local Stability Analysis: Introduction of a linearization method for state-dependent delay, and comparison of the local stability analysis of the linearized state-dependent delay with the constant delay model by using D-subdivision method.

3. Nonlinear Analysis: Application of a numerical continuous method to study the nonlinear behavior of the system with a state-dependent delay. Construction of the Hopf bifurcation diagram for the fixed point of the system (constant angular speed and constant vertical speed). Determination of the parameters that are related to the criticality of the bifurcation.

4. Control Scheme: Designing of an observer that enables tracking the state of the system with time delay. Proposal of a pole placement method, to place the right most pole of the system at a desired position. Simulate the system behavior with the designed controller.

1.4 Outline

A principal aim of this dissertation is to further the understanding of the underlying mechanisms leading to the stick-slip vibrations of drill strings, as well as to develop a viable control strategy that is applicable for mitigation of harmful stick-slip vibrations. The remaining part of this dissertation is organized as follows. First, in Chapter 2, following the previous studies in the author's group [16, 37], a reduced-order drill-string model is introduced to describe the axial and torsional motion. With the goal of reducing the number of parameters, governing equations are recast in a non-dimensionlized form. In Chapter 3, the linearized model with constant time delay is obtained, and system stability is examined by using the D-subdivision method. The corresponding stability chart is given in the plane of non-dimensional axial speed and non-dimensional rotational speed for different axial-torsional damping ratios. In Chapter 4, the author has included nonlinear analysis of the system with state-dependent delay. The friction and loss of contact functions are smoothed by using a sigmoid function and a hyperbolic tangent function, and the implicit state-dependent delay is rewritten in explicit form by using a Taylor expansion to facilitate the analysis. For quasi-static variation of the depth of cut, by using a continuation method, bifurcation diagrams depicting subcritical Hopf bifurcations of equilibrium solutions and cyclic fold bifurcations are constructed. Through the bifurcation diagrams, the routes from a stable branch of equilibrium solutions or a stable branch of limit-cycle motion without stick slip to a branch of stick-slip motions are presented. In Chapter 5, an observer based controller design

is proposed. The revised continuous pole placement method for time delay system introduced by Michiels and Niculescu [27] is used for the design of the controller. Control schemes with choices of optimal control gain obtained from the numerical optimization method are developed. Through the numerical demonstration, the authors show the effectiveness of the controllers. Finally, concluding remarks and recommendation for future works are provided in Chapter 6.

Chapter 2: Drill-string modeling

2.1 Overview

In this chapter, a two degrees of freedom drill string model with coupled axial and torsion dynamics is studied. Nonlinear effects associated with dry friction, loss of contact, and the state-dependent delay, which all arise from cutting mechanics, are considered. As shown in the work of Germay, Denoel, and Detrounay, compared to more complex models, a reduced-order model can be used to capture a good qualitative description of phenomena as well, and enable an in depth analysis, providing insight into the mechanisms leading to vibrations.

The rest of the chapter is organized as follows: In Section 2.2, the reduced-order model is obtained based on a field drill rig setup. The cutting mechanism is developed by considering the loss of contact (with a Heaviside step function), dry friction (with a sign function), and time delay(with an implicit state-dependent equation). In Section 2.3, in order to reduce the number of parameters, and focus on the perturbation dynamics that is the root cause of the harmful vibrations, the non-dimensionalized form of governing equations are derived.

2.2 Reduced-order model with coupled axial-torsional motions

A sketch of drilling system being studied is shown in Figure 2.1(a). The rotary table on the top is used to drive the drill string with a constant penetration speed V_0 and a rotational speed Ω_0. The drill string includes drill pipes, drill collar, and drill bit. The drill collar which is the heavier-weight part of drill pipes together with drill bit is also known as the Bottom Hole Assembly(BHA). For a detailed description on the drill-string system, one can refer to the books such as the one by Bommer [8]. Following earlier studies [38–40], the author assumes that the well-bore is perfectly vertical and the lateral motion has no effect on axial-torsional motion. The discretized model of the system is depicted in Figure 2.1(b). With the axial displacement $Z(t)$ and the rotational displacement $\Phi(t)$, the governing equations can be written as

$$\begin{aligned} M\ddot{Z}(t) + C_a\dot{Z}(t) + K_a(Z(t) - V_0 t) &= W_s - W_b(t) \\ I\ddot{\Phi}(t) + C_t\dot{\Phi}(t) + K_t(\Phi(t) - \Omega_0 t) &= -T_b(t) \end{aligned} \tag{2.1}$$

Here, M and I are the translational inertia and rotary inertia of the BHA, respectively. Axial stiffness K_a and torsion stiffness K_t are used to capture the flexibility of the drill string. C_a and C_t represent the axial damping ratio and the torsion damping ratio due to the drill mud. W_s equals sum of the weight of drill pipe and drill collar. Furthermore, W_b and T_b, which are determined by the bit-rock interactions, are the weight and torque on the bit, respectively. Each of them can be decomposed in terms of cutting and friction components, as follows.

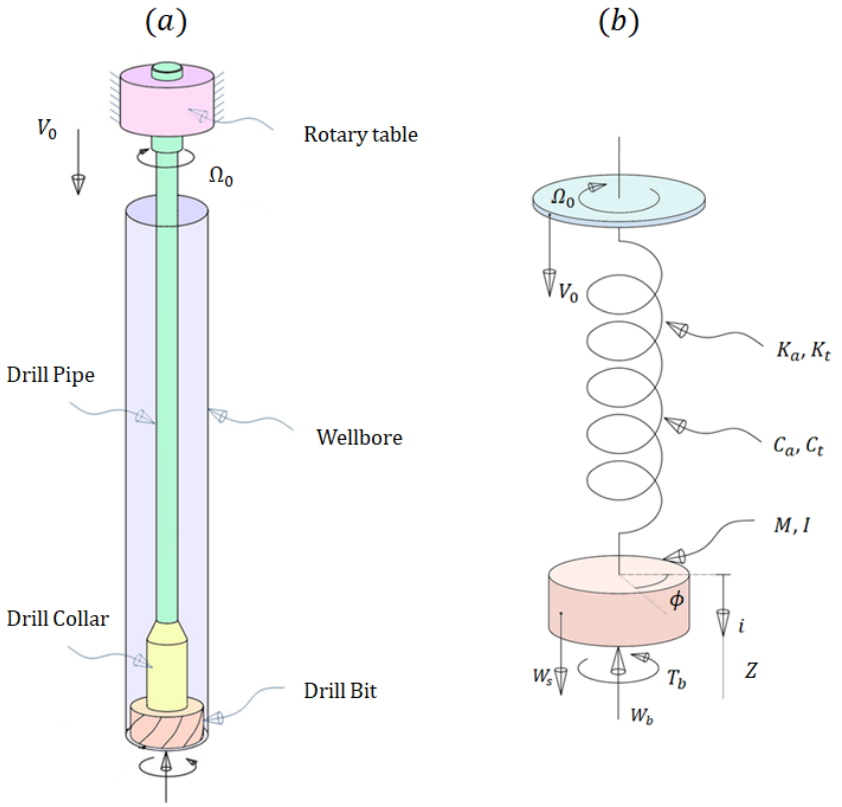

Figure 2.1: (a) Schematic of drill-string system. (b) Representative reduced-order model of drill-string system [5].

$$\begin{aligned} W_b(t) &= W_{\mathrm{bc}}(t) + W_{\mathrm{bf}}(t) \\ T_b(t) &= T_{\mathrm{bc}}(t) + T_{\mathrm{bf}}(t) \end{aligned} \tag{2.2}$$

The subscripts bc and bf denote the cutting component and the friction component of the drill bit, respectively. The cutting component is proportional to the instantaneous cutting depth of rock, while the friction component is modeled with Coulomb friction. Following the earlier work of Detournay and Defourny [15], these force and

Table 2.1: Parameters used for drilling operations

Parameter	Symbol	Value	Unit
Mass	M	3.4×10^4	kg
Axial damping	C_a	1.56×10^4	$\mathrm{N\,s\,m^{-1}}$
Axial stiffness	K_a	7.0×10^5	$\mathrm{N\,m^{-1}}$
Moment of inertia	I	116	$\mathrm{kg\,m^2}$
Torsion damping	C_t	32.9	$\mathrm{N\,s\,m\,rad^{-1}}$
Torsion stiffness	K_t	938	$\mathrm{N\,m\,rad^{-1}}$
Radius of drill bit	a	0.108	m
Wear flat length	l	0.0012	m
Intrinsic specific energy of rock	ϵ	60	MPa
Contact strength	σ	60	MPa
Cutter face inclination	ζ	0.6	-
Friction coefficient	μ	0.6	-
Geometry parameter of drill bit	γ	1	-
Number of blades on drill bit	N	4	-

torque components can be written as

$$\begin{aligned} W_{\mathrm{bc}}(t) &= \epsilon a \zeta R(d(t)) H(\dot{\Phi}(t)) \\ T_{\mathrm{bc}}(t) &= \tfrac{1}{2}\epsilon a^2 R(d(t)) H(\dot{\Phi}(t)) \\ W_{\mathrm{bf}}(t) &= \sigma a l H(d(t)) H(\dot{Z}(t)) \\ T_{\mathrm{bf}}(t) &= \tfrac{1}{2}\mu\gamma a^2 \sigma l \mathrm{sgn}(\dot{\Phi}) H(d(t)) H(\dot{Z}(t)) \end{aligned} \tag{2.3}$$

Here, ϵ, σ, and μ are the intrinsic specific energy, contact strength, and friction coefficient, which are determined by the properties of the rock being cut. a, l, ζ, and γ are the drill-bit design parameters. The parameter values provided in [5, 38] are adopted and listed in Table 1. The unit ramp function $R(\cdot)$, Heaviside step function $H(\cdot)$, and Sign function $\mathrm{sgn}(\cdot)$ that are used to describe the non-smooth behavior associated with the drill bit are given by

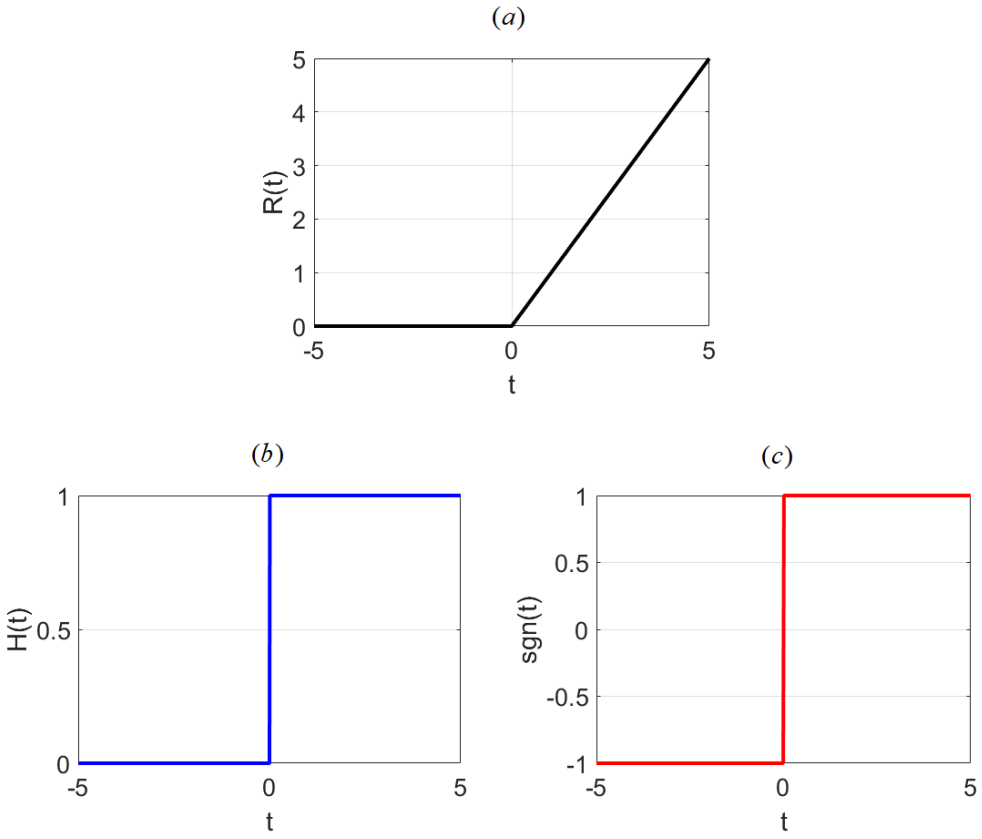

Figure 2.2: (a) Ramp function, (b) Heaviside step function, and (c) Sign function.

$$R(t) = \begin{cases} t & t \geq 0 \\ 0 & t < 0 \end{cases}$$

$$H(t) = \begin{cases} 1, & t \geq 0 \\ 0, & t < 0 \end{cases} \qquad \text{sgn}(t) = \begin{cases} 1, & t > 0 \\ 0, & t = 0 \\ -1, & t < 0 \end{cases} \tag{2.4}$$

In Figure 2.3, two successive blades of a poly-crystalline diamond compact(PDC) bit are shown. The PDC bit that is often used in drill operation is assumed to have N symmetrically distributed identical blades. For an individual blade, the

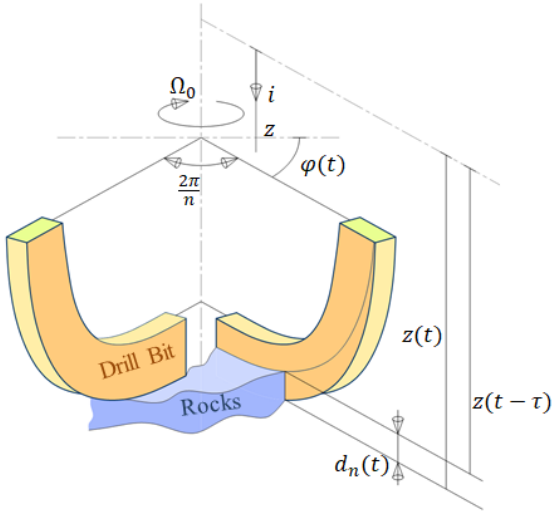

Figure 2.3: Two successive blades of a drill bit [5].

instantaneous depth of cut can be determined as

$$d_n(t) = Z(t) - Z(t-\tau) \tag{2.5}$$

Assuming that the cutting action is uniform across the N blades, the total depth of cut in Eq.(2.3) is

$$d(t) = N d_n(t) \tag{2.6}$$

and the time delay τ is determined implicitly from

$$\Phi(t) - \Phi(t-\tau) = \frac{2\pi}{N} \tag{2.7}$$

This delay represents the elapsed time for the drill bit to rotate over an angle $2\pi/N$, and it depends on the state $\Phi(t)$.

Additionally, based on the proceeding model, 5 different drilling scenarios are

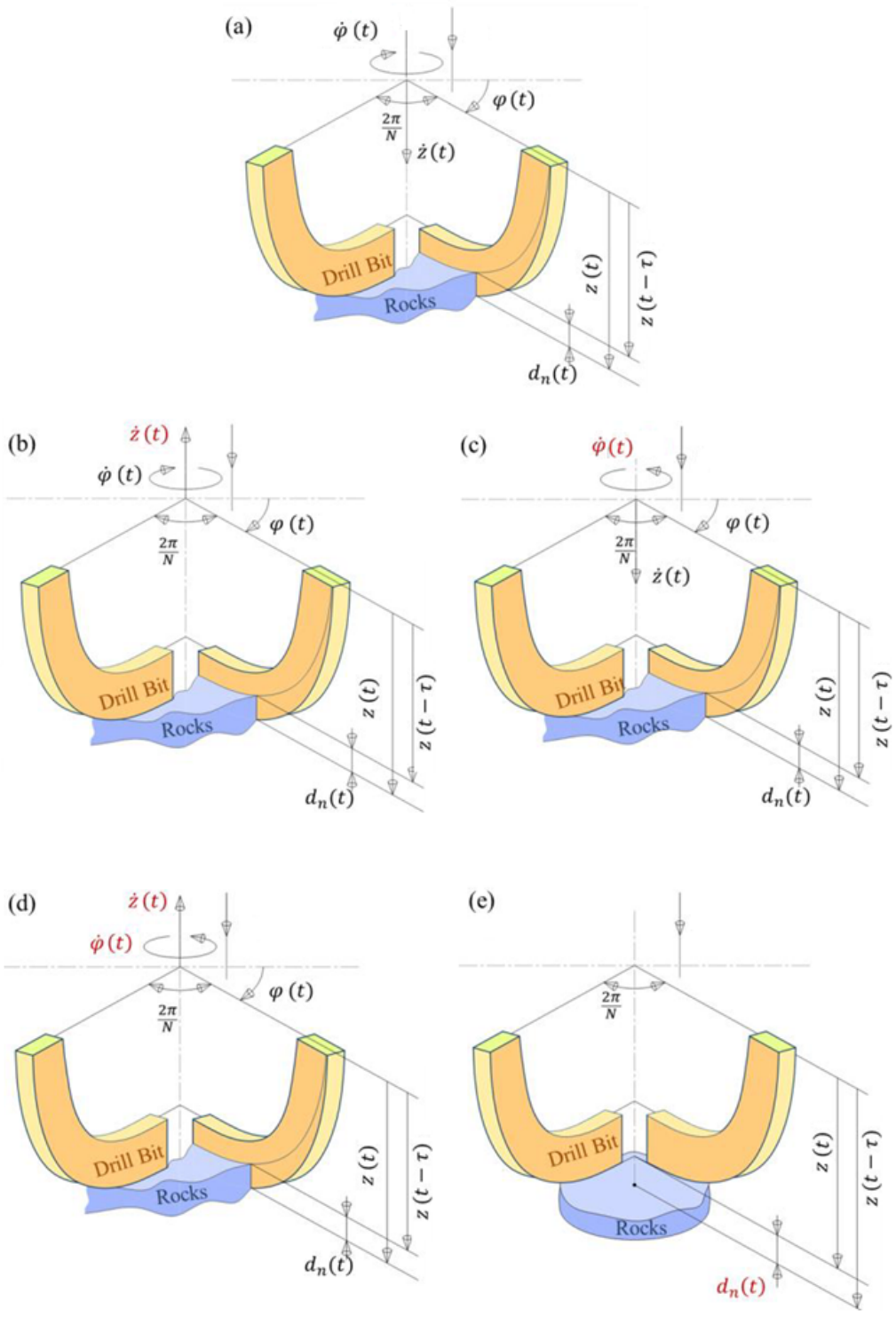

Figure 2.4: Bit-rock interaction cases: (a) stable drilling, (b) bit bounce, (c) inverse spinning of the bit, (d) bit bounce with inverse spinning, and (e) loss of contact with bit-rock. The variables in red assume negative values.

shown in Figure2.4, and presented as following:

- Case 1: $d_n \geq 0$, $\dot{Z} \geq 0$, $\dot{\Phi} \geq 0$. This is the stable drilling scenario, and it represents that the drill bit is cutting the rock and moving downwards. For this case, weight on bit $W_b > 0$, and torque on bit $T_b > 0$.

- Case 2: $d_n \geq 0$, $\dot{Z} < 0$, $\dot{\Phi} \geq 0$. This is the bit bounce scenario. Compared with stable drilling case, the drill bit is not in contact with the rock. Consequently, there is no axial friction W_{bf} and no torsional friction T_{bf}.

- Case 3: $d_n \geq 0$, $\dot{Z} \geq 0$, $\dot{\Phi} < 0$. This is inverse spinning of the bit scenario. Compared with the stable drilling case, the drill bit is suffering from severe torsional vibration, and this can cause damage to the PDC drill bit. For this case, the cutting components of the weight $W_{bc} = 0$, and of the torque $T_{bc} = 0$, and the friction components of the weight and torque are in the opposite direction to that for stable drilling.

- Case 4: $d_n \geq 0$, $\dot{Z} < 0$, $\dot{\Phi} < 0$. This is the bit bounce case with negative spinning speed scenario. For this case, the total weight on bit $W_b = 0$, and torque on bit $T_b = 0$.

- Case 5: $d_n < 0$. This is the completely loss of contact case. For this case, the total weight on bit $W_b = 0$, and torque on bit $T_b = 0$.

2.3 Non-dimensionalization

The nominal solution for Eq.(2.1), which represents the stable drilling without any vibration, can be described by:

$$\begin{aligned} \bar{Z} &= V_0 t + Z_0 \qquad \dot{\bar{Z}} = V_0 \\ \bar{\Phi} &= \Omega_0 t + \Phi_0 \qquad \dot{\bar{\Phi}} = \Omega_0 \end{aligned} \tag{2.8}$$

Here, Z_0 and Φ_0 are the respective constant deformations of the axial spring and the torsion spring. The quantities Ω_0 and V_0 represent the spinning speed of drill string and nominal penetration rate of the drill bit, respectively. On substituting Eqs.(2.3)-(2.6) into Eq.(2.1), author obtains Z_0 and Φ_0 in the form

$$\begin{aligned} Z_0 &= -\tfrac{1}{K_a}\left(2\pi\epsilon a\zeta\tfrac{V_0}{\Omega_0} + C_a V_0 + \sigma a l - W_s\right) \\ \Phi_0 &= -\tfrac{1}{K_t}\left(\pi\epsilon a^2\tfrac{V_0}{\Omega_0} + C_t\Omega_0 + \tfrac{1}{2}\mu\gamma a^2\sigma l\right) \end{aligned} \tag{2.9}$$

Next, to reduce the number of parameters, the equations of motion are written in a dimensionless form. Since the stick-slip vibration is torsion dominated, the characteristic time $t_* = \sqrt{I/K_t}$ and characteristic length $L_* = 2K_t/\epsilon a^2$ are introduced. Following earlier work [38], one can have the non-dimensional variables as

$$\begin{aligned} z &= \tfrac{Z-\bar{Z}}{L_*} \qquad \varphi = \Phi - \bar{\Phi} \\ \hat{t} &= t/t_* \qquad \hat{\tau} = \tau/t_* \end{aligned} \tag{2.10}$$

Here, the axial state z and angular state φ are perturbations of the nominal state of the drill operations. These states are functions of the dimensionless time $\hat{t}$. $\hat{\tau}$ is the dimensionless state-dependent time delay. By using the non-dimensional variables, the governing equations of axial-torsional motions can be recast as

$$\begin{aligned} \ddot{z}(\hat{t}) + 2\xi\eta\dot{z} + \eta^2 z(\hat{t}) &= -\psi\delta(\hat{t},\hat{\tau}) + \hat{W}_{\text{bf}} \\ \ddot{\varphi}(\hat{t}) + 2\kappa\dot{\varphi}(\hat{t}) + \varphi(\hat{t}) &= -\delta(\hat{t},\hat{\tau}) + \hat{T}_{\text{bf}} \end{aligned} \tag{2.11}$$

The dimensionless parameters are defined as

$$\begin{aligned} \xi &= \tfrac{C_a}{2\sqrt{K_a M}} \qquad \kappa = \tfrac{C_t}{2\sqrt{K_t I}} \\ \psi &= \tfrac{\epsilon a \zeta I}{K_t M} \qquad \eta = \sqrt{\tfrac{K_a}{M}} t_* = \sqrt{\tfrac{K_a I}{K_t M}} \end{aligned} \tag{2.12}$$

The parameters ξ and κ are the damping ratios associated with axial and torsional motions, respectively. η represents the ratio of the axial natural frequency to the torsion natural frequency. The quantity ψ is dependent upon the rock strength and drill-bit geometry. The dimensionless perturbation of cutting depth δ can be written as

$$\delta(\hat{t},\hat{\tau}) = N\left[R\left(z(\hat{t}) - z(\hat{t}-\hat{\tau}) + v_0\hat{\tau}\right)\cdot H(\dot{\varphi}(\hat{t}) + \omega_0) - v_0\hat{\tau}_0\right] \tag{2.13}$$

The dimensionless perturbation of friction components of the weight on bit $\hat{W}_{\text{bf}}$ can be expressed as

$$\hat{W}_{\text{bf}} = \frac{\sigma a l}{M L_*} t_*^2 \left[1 - H\left(z(\hat{t}) - z(\hat{t}-\hat{\tau}) + v_0\hat{\tau}\right)\cdot H\left(\dot{z}(\hat{t}) + v_0\right)\right] \tag{2.14}$$

and the dimensionless perturbation of friction components of the torque on bit $\hat{T}_{\text{bf}}$ takes the form

$$\hat{T}_{\text{bf}} = \frac{\mu\gamma\sigma a^2 l}{2I} t_*^2 \left[1 - \text{sgn}(\dot{\varphi}(\hat{t}) + \omega_0) \cdot H\left(z(\hat{t}) - z(\hat{t} - \hat{\tau}) + v_0\hat{\tau}\right) \cdot H\left(\dot{z}(\hat{t}) + v_0\right)\right] \tag{2.15}$$

where v_0 is the dimensionless penetration rate, ω_0 is the dimensionless angular speed, and $\hat{\tau}_0$ is the constant time delay.

$$\omega_0 = \Omega_0 t_* \qquad v_0 = \frac{V_0 t_*}{L_*} \qquad \hat{\tau}_0 = \frac{2\pi}{N\omega_0} \tag{2.16}$$

Furthermore, the governing equations can be recast in state-space form as

$$\dot{\mathbf{X}} = \mathbf{f}\left(\mathbf{X}(\hat{t}), \mathbf{X}(\hat{t} - \hat{\tau}(\mathbf{X}_t)), \hat{\tau}(\mathbf{X}_t)\right) \tag{2.17}$$

where $\mathbf{X} = \begin{pmatrix} z(\hat{t}) & \dot{z}(\hat{t}) & \varphi(\hat{t}) & \dot{\varphi}(\hat{t}) \end{pmatrix}^T$

$$\mathbf{f} = \begin{bmatrix} \dot{z}(\hat{t}) \\ -2\xi\eta\dot{z} - \eta^2 z(\hat{t}) - \psi\delta(\hat{t}, \hat{\tau}) + \hat{W}_{\text{bf}} \\ \dot{\varphi}(\hat{t}) \\ -2\kappa\dot{\varphi}(\hat{t}) - \varphi(\hat{t}) - \delta(\hat{t}, \hat{\tau}) + \hat{T}_{\text{bf}} \end{bmatrix}$$

and $\mathbf{X}_t(s) = \mathbf{X}(t+s)$, $s \in$ [-r 0], $r \in R^+$. With these dimensionless variables, the state-dependent delay takes the form

$$\hat{\tau} = \hat{\tau}_0 - \frac{1}{\omega_0}\left(\varphi(\hat{t}) - \varphi(\hat{t} - \hat{\tau})\right) \tag{2.18}$$

The nonlinear systems developed in this chapter are used in the following chapters to carry out stability studies and numerical investigations.

Chapter 3: Linear stability analysis

3.1 Introduction

The nonlinearities of the system under investigation are the dry friction, loss of contact, and the state-dependent delay, which all arise from the cutting mechanism between the PDC drill bit and the rock. Due to the strong nonlinearities, a drill string system often suffers from the self-excited vibrations, and the corresponding cases are shown in Figures 2.4(a, b, c, d, e).

In this chapter, special attention will be paid to the local (linear) stability of the nominal motion cases (see Figure 2.4(a)). This case is the ideal scenario, since the penetration rate and spinning speed are in the direction of motions. Therefore, the friction components of weight and torque are present. Futhermore, in this case, the state-dependent delay is the only source of nonlinearity, and the original non-dimensional governing equations (Eq. (2.17)) will degenerate to

$$\dot{\mathbf{X}} = \bar{\mathbf{f}}\left(\mathbf{X}(\hat{t}), \mathbf{X}(\hat{t} - \hat{\tau}(\mathbf{X}_t)), \hat{\tau}(\mathbf{X}_t)\right) \tag{3.1}$$

where $\mathbf{X} = \begin{pmatrix} z(\hat{t}) & \dot{z}(\hat{t}) & \varphi(\hat{t}) & \dot{\varphi}(\hat{t}) \end{pmatrix}^T$

$$\bar{\mathbf{f}} = \begin{bmatrix} \dot{z}(\hat{t}) \\ -2\xi\eta\dot{z} - \eta^2 z(\hat{t}) - \psi\delta(\hat{t},\hat{\tau}) \\ \dot{\varphi}(\hat{t}) \\ -2\kappa\dot{\varphi}(\hat{t}) - \varphi(\hat{t}) - \delta(\hat{t},\hat{\tau}) \end{bmatrix}$$

and $\mathbf{X}_t(s) = \mathbf{X}(t+s)$, $s \in$ [-r 0], $r \in R^+$. With these dimensionless variables, the delay takes the form

$$\hat{\tau} = \hat{\tau}_0 - \frac{1}{\omega_0}\left(\varphi(\hat{t}) - \varphi(\hat{t} - \hat{\tau})\right) \tag{3.2}$$

For nonlinear systems, a standard approach for stability analysis contains two steps:

- Linearization of the nonlinear systems near the equilibrium points
- Investigation of the characteristic roots or characteristic multipliers of the linearized system

A state-dependent delay differential equation(SD-DDE) is always nonlinear, since the delay depends on it's state, while a linearized equation is a delay differential equation (DDE) with a constant or time varying delay. Therefore, the linearization of state-dependent delay differential equations is not as straight forward as ordinary differential equations(ODEs).

Linearization of SD-DDEs can be determined through perturbation analysis, with the linear DDE coming up as a perturbation to the original system with a

nominal solution. For example [41], consider the autonomous SD-DDE

$$\dot{x}(t) = x\left(t - (\tau_0 + x(t))\right) \tag{3.3}$$

Since the state-dependent time delay $\tau(x(t)) = \tau_0 + x(t)$, this equation is a nonlinear equation. Meanwhile, the DDE

$$\dot{y}(t) = y(t - \tau_0) \tag{3.4}$$

with constant delay τ_0 is a linear system which can be treated as a variation of Eq. (3.3) around it's equilibrium point $x = 0$. In this sense, linearization means that if the $y = 0$ solution of Eq. (3.4) is stable, then the $x = 0$ solution of Eq. (3.3) is stable as well.

With the goal of finding an appropriate linearization for the current systems, the remaining of the chapter is organized as follows. In the next section, utilizing the method developed by Huang and Turi [42, 43], and introduced to mechanical systems by Insperger, Stepan, and Turi [19], the linearized equation associated to the delay-differential equation with SD-DDE is carried out as a step towards stability analysis. For comparison, the linear delay-differential equation with constant time delay is also given. In the first part of Section 3.3, linear stability analysis methods for time delay systems are discussed. Following that, a brief introduction to the D-subdivision method is given. With the D-subdivsion method, the stability chart for the current system is obtained in the plane of non-dimensional axial and

rotational speed with different axial-torsional damping ratios. Finally, case studies with numerical simulations are provided in Section 3.4 and discussed.

3.2 Construction of associated linear system

3.2.1 State-dependent time delay case

After substituting Eq. (3.2) into the non-dimensional governing equations for the nominal motion case, one has

$$\bar{\mathbf{f}} = \begin{bmatrix} \dot{z}(\hat{t}) \\ -2\xi\eta\dot{z} - \eta^2 z(\hat{t}) - N\psi\left(z(\hat{t}) - z(\hat{t}-\hat{\tau})\right) + N\psi v_0(\hat{\tau}_0 - \hat{\tau}) \\ \dot{\varphi}(\hat{t}) \\ -2\kappa\dot{\varphi}(\hat{t}) - \varphi(\hat{t}) - N\left(z(\hat{t}) - z(\hat{t}-\hat{\tau})\right) + Nv_0(\hat{\tau}_0 - \hat{\tau}) \end{bmatrix} \tag{3.5}$$

According to the work of Hartung [44], the true linearization of system with state-dependent delay is not possible due to the fact that the solution of the system is not differentiable with respect to state-dependent delay. Hence, one needs to find a constant delay model, which has the same local stability properties as the original system. Introduced by Hartung, the linear system associated with the constant solution $\mathbf{X}(\hat{t}) \equiv \bar{\mathbf{X}}$ is written as

$$\begin{aligned} \dot{\tilde{\mathbf{X}}} = D_1\bar{\mathbf{f}}\left(\bar{\mathbf{X}}, \bar{\mathbf{X}}, \hat{\tau}(\bar{\mathbf{X}}_t)\right)\tilde{\mathbf{X}}(\hat{t}) + D_2\bar{\mathbf{f}}\left(\bar{\mathbf{X}}, \bar{\mathbf{X}}, \hat{\tau}(\bar{\mathbf{X}}_t)\right)\tilde{\mathbf{X}}(\hat{t} - \hat{\tau}(\bar{\mathbf{X}})) \\ + D_3\bar{\mathbf{f}}\left(\bar{\mathbf{X}}, \bar{\mathbf{X}}, \hat{\tau}(\bar{\mathbf{X}}_t)\right) D\hat{\tau}(\bar{\mathbf{X}}_t)\tilde{\mathbf{X}}_t \end{aligned} \tag{3.6}$$

where, D_1, D_2, and D_3 are the derivatives with respect to the 1st, 2nd, and 3rd, arguments of $\bar{\mathbf{f}}$, and $D\hat{\tau}$ denotes the Fréchet derivative of time delay $\hat{\tau}$ with respect to $\tilde{\mathbf{y}}_t$. The $\tilde{\mathbf{X}}$ vector is defined as

$$\tilde{\mathbf{X}}(\hat{t}) = \begin{bmatrix} \tilde{z}(\hat{t}) \\ \dot{\tilde{z}}(\hat{t}) \\ \tilde{\varphi}(\hat{t}) \\ \dot{\tilde{\varphi}}(\hat{t}) \end{bmatrix} \tag{3.7}$$

where $\tilde{z} = z - \bar{z}$ and $\tilde{\varphi} = \varphi - \bar{\varphi}$ are the perturbations around the constant solution $z(\hat{t}) \equiv \bar{z}$, and $\varphi(\hat{t}) \equiv \bar{\varphi}$ (case of no vibrations).

According to Hartung and Turi [41], the linearized system given in Eq.(3.6) is the variation of SD-DDE (3.5), if it preserves local stability properties. Otherwise stated, if the trivial solution $\tilde{\mathbf{X}} \equiv \mathbf{0}$ of Eq.(3.6) is stable, then, it follows that the constant solution $\mathbf{X}(\hat{t}) \equiv \bar{\mathbf{X}}$ is stable as well.

First, the constant solution is associated with the stationary cutting process $\bar{z} = 0$, and $\bar{\varphi} = 0$. On substituting the solutions into Eq.(3.2), one obtains the constant delay

$$\hat{\tau}(\bar{\mathbf{X}}_t) = \hat{\tau}_0 = \frac{2\pi}{N\omega_0} \tag{3.8}$$

Now, the derivative terms in equation are in the form

$$D_1\bar{\mathbf{f}}\left(\bar{\mathbf{X}},\bar{\mathbf{X}},\hat{\tau}(\bar{\mathbf{X}}_t)\right)=\begin{bmatrix}0 & 1 & 0 & 0\\ -\eta^2-N\psi & -2\xi\eta & 0 & 0\\ 0 & 0 & 0 & 1\\ -N & 0 & -1 & -2\kappa\end{bmatrix} \tag{3.9}$$

$$D_2\bar{\mathbf{f}}\left(\bar{\mathbf{X}},\bar{\mathbf{X}},\hat{\tau}(\bar{\mathbf{X}}_t)\right)=\begin{bmatrix}0 & 0 & 0 & 0\\ N\psi & 0 & 0 & 0\\ 0 & 0 & 0 & 0\\ N & 0 & 0 & 0\end{bmatrix} \tag{3.10}$$

and,

$$D_3\bar{\mathbf{f}}\left(\bar{\mathbf{X}},\bar{\mathbf{X}},\hat{\tau}(\bar{\mathbf{X}}_t)\right)=\begin{bmatrix}0\\ -N\psi v_0\omega_0\\ 0\\ -Nv_0\omega_0\end{bmatrix} \tag{3.11}$$

The term $D\hat{\tau}(\bar{\mathbf{X}}_t)\tilde{\mathbf{X}}_t$ can be determined as

$$D\hat{\tau}(\bar{\mathbf{X}}_t)\tilde{\mathbf{X}}_t=\begin{bmatrix}D_z\hat{\tau}(\bar{\mathbf{X}}_t)\\ D_{\dot{z}}\hat{\tau}(\bar{\mathbf{X}}_t)\\ D_{\varphi}\hat{\tau}(\bar{\mathbf{X}}_t)\\ D_{\dot{\varphi}}\hat{\tau}(\bar{\mathbf{X}}_t)\end{bmatrix}^T\begin{bmatrix}\tilde{z}(\hat{t})\\ \dot{\tilde{z}}(\hat{t})\\ \tilde{\varphi}(\hat{t})\\ \dot{\tilde{\varphi}}(\hat{t})\end{bmatrix} \tag{3.12}$$

where $D_z\hat{\tau}$, $D_{\dot{z}}\hat{\tau}$, $D_{\varphi}\hat{\tau}$, and $D_{\dot{\varphi}}\hat{\tau}$ denote the Fréchet derivatives of $\hat{\tau}$ with respect to

the 1st, 2nd, 3rd, and 4th elements of $\mathbf{X}_t$. As shown in Eq.(3.2), the state-dependent time delay depends only on the third element φ; consequently, $D_z\hat{\tau} = 0$, $D_{\dot{z}}\hat{\tau} = 0$, $D_{\dot{\varphi}}\hat{\tau} = 0$. As a result,

$$D\hat{\tau}(\bar{\mathbf{X}}_t)\tilde{\mathbf{X}}_t = D_{\varphi}\hat{\tau}(\bar{\mathbf{X}}_t)\tilde{\varphi}(\hat{t}) = -\frac{\varphi(\hat{t}) - \varphi(\hat{t} - \hat{\tau}_0)}{\omega_0} \tag{3.13}$$

After substitution of Eq.(3.9), (3.10), (3.11), and(3.13) into Eq.(3.6), the resulting linearized system is

$$\dot{\tilde{\mathbf{X}}}(\hat{t}) = \tilde{\mathbf{f}}\left(\tilde{\mathbf{X}}(\hat{t})\right) \tag{3.14}$$

where

$$\tilde{\mathbf{f}} = \begin{bmatrix} \dot{z}(\hat{t}) \\ -2\xi\eta\dot{z} - \eta^2 z(\hat{t}) - N\psi\left(z(\hat{t}) - z(\hat{t} - \hat{\tau})\right) + N\psi v_0 \frac{\varphi(\hat{t}) - \varphi(\hat{t} - \hat{\tau}_0)}{\omega_0} \\ \dot{\varphi}(\hat{t}) \\ -2\kappa\dot{\varphi}(\hat{t}) - \varphi(\hat{t}) - N\left(z(\hat{t}) - z(\hat{t} - \hat{\tau})\right) + N v_0 \frac{\varphi(\hat{t}) - \varphi(\hat{t} - \hat{\tau}_0)}{\omega_0} \end{bmatrix} \tag{3.15}$$

In addition, if one defines the dimensionless nominal depth of cut $\delta_0 = v_0/\omega_0$, and drop the tilde sign, then, the linearized governing equations can be rewritten into the state-space form as

$$\dot{\mathbf{X}}(\hat{t}) = \mathbf{A}_0\mathbf{X}(\hat{t}) + \mathbf{A}_1\mathbf{X}(\hat{t} - \hat{\tau}_0) \tag{3.16}$$

Here, $\mathbf{A}_0$ and $\mathbf{A}_1$ are the coefficient matrix of current and delayed state, which are

given by

$$\mathbf{A_0} = \begin{bmatrix} 0 & 1 & 0 & 0 \\ -\eta^2 - N\psi & -2\xi\eta & N\psi\delta_0 & 0 \\ 0 & 0 & 0 & 1 \\ -N & 0 & N\delta_0 - 1 & -2\kappa \end{bmatrix} \tag{3.17}$$

$$\mathbf{A_1} = \begin{bmatrix} 0 & 0 & 0 & 0 \\ N\psi & 0 & -N\psi\delta_0 & 0 \\ 0 & 0 & 0 & 0 \\ N & 0 & -N\delta_0 & 0 \end{bmatrix} \tag{3.18}$$

Then, the corresponding characteristic equation $\det(s\mathbf{I} - \mathbf{A_0} - \mathbf{A_1}e^{-st}) = 0$ can be written in the form

$$P_0(s) + P_1(s)(1 - e^{-\hat{\tau}_0 s}) = 0 \tag{3.19}$$

Here, P_0 and P_1 are polynomials in the eigenvalue s, and they are defined as

$$P_0(s) = s^4 + (2\xi\eta + 2\kappa)s^3 + (\eta^2 + 4\kappa\xi\eta + 1)s^2 + (2\xi\eta + 2\kappa\eta^2)s + \eta^2 \tag{3.20}$$

$$P_1(s) = (N\psi - N\delta_0)s^2 + (2\kappa N\psi - 2\xi\eta N\delta_0)s + (N\psi - N\eta^2\delta_0) \tag{3.21}$$

3.2.2 Constant time delay case

For Eq. (3.5), without using the linearization method discussed in previous section, and considering the state-dependent delay $\hat{\tau} = \hat{\tau}_0$, the governing system will

degenerate to

$$\dot{\mathbf{X}}(\hat{t}) = \mathbf{g}\left(\mathbf{X}(\hat{t})\right) \tag{3.22}$$

where

$$\mathbf{g} = \begin{bmatrix} \dot{z}(\hat{t}) \\ -2\xi\eta\dot{z} - \eta^2 z(\hat{t}) - N\psi\delta_0\left(z(\hat{t}) - z(\hat{t}-\hat{\tau})\right) \\ \dot{\varphi}(\hat{t}) \\ -2\kappa\dot{\varphi}(\hat{t}) - \varphi(\hat{t}) - N\delta_0\left(z(\hat{t}) - z(\hat{t}-\hat{\tau})\right) \end{bmatrix} \tag{3.23}$$

In the state-space form, one has

$$\dot{\mathbf{X}}(\hat{t}) = \mathbf{A}_0\mathbf{X}(\hat{t}) + \mathbf{A}_2\mathbf{X}(\hat{t}-\hat{\tau}_0) \tag{3.24}$$

the delayed coefficient matrix $\mathbf{A}_2$ can be expresses as

$$\mathbf{A_2} = \begin{bmatrix} 0 & 0 & 0 & 0 \\ N\psi & 0 & 0 & 0 \\ 0 & 0 & 0 & 0 \\ N & 0 & 0 & 0 \end{bmatrix} \tag{3.25}$$

Similarly, the corresponding characteristic equation $\det(s\mathbf{I} - \mathbf{A_0} - \mathbf{A_2}e^{-st}) = 0$ can be written in the form

$$P_0(s) + P_2(s)(1 - e^{-\hat{\tau}_0 s}) = 0 \tag{3.26}$$

where P_2 is defined as

$$P_2(s) = N\psi(s^2 + 2\kappa s + 1) \tag{3.27}$$

3.3 Stability crossing set and stability charts

3.3.1 D-subdivision method

It is quite obvious that Eq. (3.19) has infinite number of roots $s \in C$, which determine the stability of the trivial solution. The trivial solution is (asymptotically) stable provided all roots of the characteristic Eq. (3.19) have negative real parts; this solution is unstable if there exists a root with a positive real part. Therefore, the stability problem for time delay problem is not as straightforward as that for a system without a delay. Generally speaking, the stability analysis of time delayed systems may be roughly divided to time-domain methods and frequency-domain methods. In this work, the author has focused on the frequency-domain methods.

Direct stability analysis of time-delay systems in frequency domain, such as Pontryagin's Theorem [45] (also known as the generalized Hermite-Biehler Theorem), are usually difficult to implement in practice. A more commonly used approach is the D-subdivision method (also known as the D-partitioning method).

A comprehensive overview of D-subdivision method, mainly for systems without delays, may be found in reference [46]. The first known D-subdivision method applied to time-delay systems in the literature is in reference [47]. A rich collection of examples of stability charts, mostly for two parameters that may include one delay parameter, obtained by using the D-subdivision method, may be found in [48, 49]. An example of D-subdivision method used to study three-parameter time-delay system is the identification of stabilizing PID control regions [50].

The main idea behind the D-subdivision method may be described as follows: In the parameter space, let $\mathcal{T}$ be the set of parameter values for which the characteristic equation has imaginary roots. This set is generally a co-dimension 1 hypersurface in the parameter space, and is known as the stability crossing set. For systems of retarded type, or systems of neutral type under certain mild restrictions, with $\mathcal{T}$ one divides the parameter space into regions with fixed amount of right-half-plane(RHP) roots, and the difference of the numbers of RHP roots between two neightboring regions can be obtained by studying the crossing direction of imaginary roots at $\mathcal{T}$.

3.3.2 Stability crossing set and stability charts

Follow the procedure of D-subdivision method, after substituting $s = i\omega$ and $\hat{\tau}_0 = 2\pi/N\omega_0$ into Eq. (3.19) and separating the real and imaginary parts, one obtains the stability crossing set in the $\omega_0 - \psi$ domain:

$$\begin{aligned} \psi_{SDD} &= \frac{1}{N[\alpha(\omega^2-1)-2\beta\kappa\omega]}[\frac{\alpha^2+\beta^2}{2}+(\alpha(\omega^2-\eta^2)+2\beta\xi\eta\omega)Nv_0] \\ \omega_{0SDD} &= \frac{2\pi\omega}{N(\Theta_1+(2k-1)\pi)}, \qquad k=1,2,..., \end{aligned} \tag{3.28}$$

Here,

$$\alpha = Re(P_0) \qquad \beta = Im(P_0) \qquad \Theta_1 = \angle\frac{-P_1}{P_0+P_1} \tag{3.29}$$

Following the same procedure as before, the stability boundary for constant

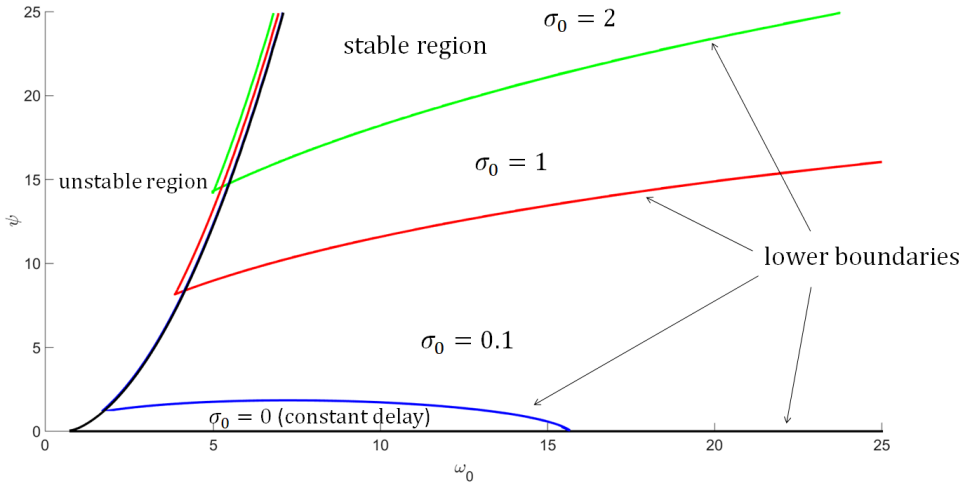

Figure 3.1: Stability charts in the plane of drive speed ω_0 and coefficient ψ for different penetration speeds δ_0.

delay model is given by

$$\begin{aligned} \psi_{CD} &= \frac{1}{N[\alpha(\omega^2-1)-2\beta\kappa\omega]}\frac{\alpha^2+\beta^2}{2} \\ \omega_{0CD} &= \frac{2\pi\omega}{N(\Theta_2+(2k-1)\pi)}, \qquad k=1,2,..., \end{aligned} \tag{3.30}$$

and

$$\Theta_2 = \angle\frac{-P_2}{P_0+P_2} \tag{3.31}$$

For the parameters listed in Table 1, the stability chart generated in the $\omega_0-\psi$ plane is shown in Figure 3.1. In this chart, the stability boundaries obtained for $v_0 =$ 0, 0.1, 1, and 2 are given, respectively. The stability chart for $v_0 = 0$ is equivalent to that for the constant delay case. It can be seen that the left boundaries for both the constant delay ($v_0 = 0$) and state-dependent delay cases are almost identical to each other. With an increase in v_0, the right boundary for the chart of the state-dependent

delay model is shifted upwards. By contrast, the right boundary of the stability chart for the constant delay remains the same and independent of the penetration rate v_0. It is clear that the consideration of the state-dependent delay is important to capture the reduction in the stability region in the considered $\omega_0 - \psi$ plane. Furthermore, from these results, it can be discerned that for stability purposes, a higher cutting coefficient ψ is preferrable. The obtained results are consistent with those obtained in prior work conducted in the author's group [5, 16]. Here, the linearization construction and analytical construction of the stability boundaries allows for more convenient generation of the stability charts.

Next, another stability chart is provided in the parameter space of penetration rate v_0 and drive speed ω_0, which are two critical control parameters for drill operations. By using the same approach as before, the stability boundary for state-dependent delay model can be derived as the following:

$$\begin{aligned} \delta_{0SDD} &= \frac{1}{N[\alpha(\omega^2-\eta^2)+2\beta\xi\eta\omega]}[\frac{\alpha^2+\beta^2}{2}+(\alpha(1-\omega^2)+2\beta\kappa\omega)N\psi] \\ \omega_{0SDD} &= \frac{2\pi\omega}{N(\Theta_1+(2k-1)\pi)}, \qquad k=1,2,..., \end{aligned} \tag{3.32}$$

Unlike the state-dependent delay case, for the constant delay case, one can only get the stability boundary in terms of spin rate ω_0, which is a function of the crossing frequency ω_c. The boundary is determined from

$$\omega_{0CD} = \frac{2\pi\omega_c}{N(\Theta_2+(2k-1)\pi)} \tag{3.33}$$

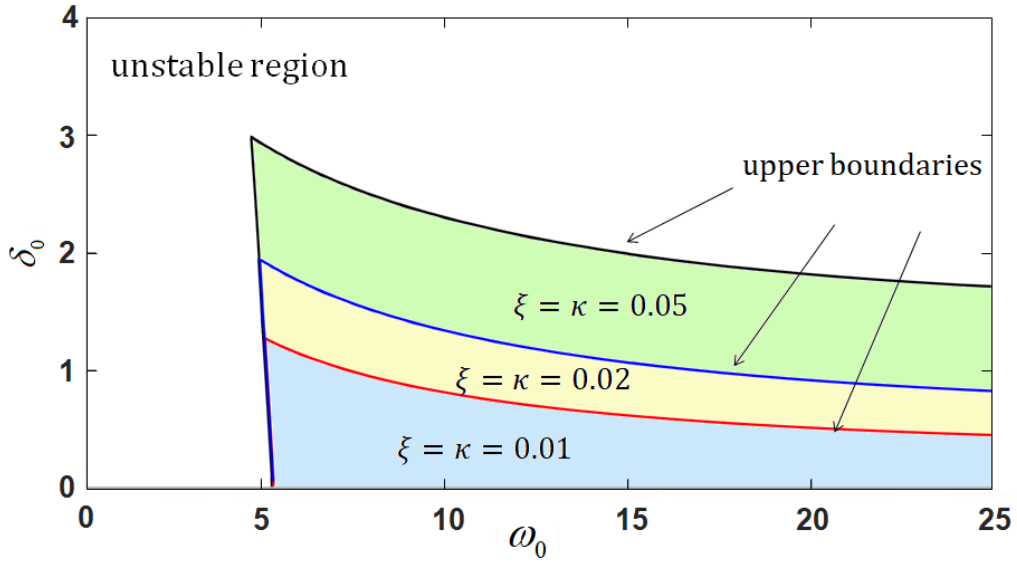

Figure 3.2: Stability charts in the plane of drive speed ω_0 and the penetration speed δ_0 for different values of ξ and κ.

For the crossing frequency, the obtained expression is

$$\omega_c = \frac{\kappa\beta + \sqrt{\kappa^2\beta^2 - \alpha(\alpha + \frac{\alpha^2+\beta^2}{2N\psi})}}{\alpha} \tag{3.34}$$

Based on the expressions obtained, the stability charts obtained for the state-dependent delay model in the space of the drive speed ω_0 and the axial penetration speed v_0 are shown in Figure 3.2, for different damping ratios and stiffness values. The damping parameter is meant to capture the influence of drill mud, which is used in drilling operations to control drill-string dynamics. The top boundary of the stability crossing set, is generated when the crossing frequency ω is small (typically $\omega < 1$) and this boundary shifts upwards as the damping is increased. As previously noted in the context of the results presented in the ω_0-ψ plane, the left boundaries

do not shift with respect to the increase in damping. In fact, the left boundary can be represented by Eq. (3.33), which corresponds to the constant delay and is associated with a large crossing frequency ω. The results indicate that damping can be influential in addressing instabilities associated with the state-dependent delay.

3.4 Case study

Although, there are infinite number of poles for the characteristic equations of the time delayed system, the number of roots in any right half plane $\mathrm{Re}(s) > n, n \in R$ is finite; hence, the stability is always determined by a finite number of roots. Two commonly approaches to address this are called D-subdivision method (also known as the D-partitioning or D-decomposition) previously presented in this chapter, and the semi-discretization method [35]. Semi-discretization method is a numerical method, which is widely used in computational fluid mechanics, and is first introduced by Insperger and Stepan for time-delay systems. By using semi-diescretization method, Xianbo Liu [5] presented stability studies for drilling system with time delay. Compared to Liu's work, with the stability analysis carried out by using the D-subdivision method presented in last section, not only the stability region is found, but the unstable regions are also classified; this can be beneficial for further nonlinear analysis.

Generally speaking, the procedure of the D-subdivision method may be described as follows: first, one defines the stability crossing set in the parameter space where characteristic equation has imaginary roots. Then, by studying the cross-

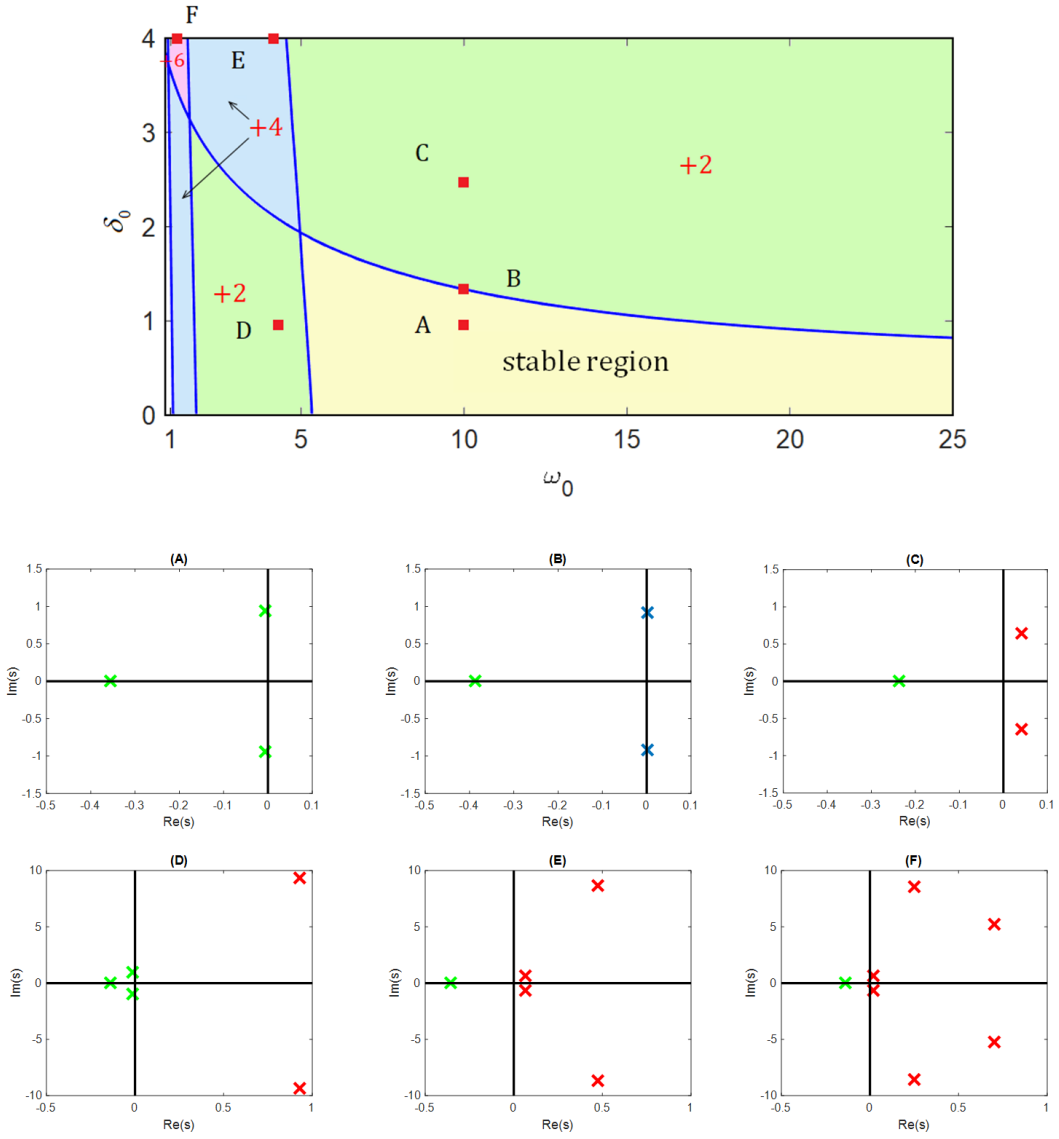

Figure 3.3: Stability charts in the plane of drive speed ω_0 and the penetration speed δ_0, with parameters $\zeta = \kappa = 0.02$, $\psi = 14$; pole positions for cases A, B, C, D, E, and F.

ing direction of imaginary roots of the crossing set, the number of right-half-plane (RHP) roots are determined. Following this procedure, one can get the stability crossing set that is parameterized by ω_0, δ_0 given in Eq.(3.32). Let k vary from 0, 1, ...m; then, one will get a set of curves, which are also known as stability crossing curves in the plane of drive speed and penetration speed. Next, by studying the direction of crossing the imaginary axis, the number of poles on the RHP can be determined. Finally, the stability chart with the number of poles in the RHP in the plane of drive speed ω_0 and depth of cut δ_0, and the obtained pole positions for the six different cases marked as A, B, C, D, E, and F are given in Figure 3.3.

In order to verify the effectiveness of the linear stability analysis presented in last section, both the linear and nonlinear simulations of non-dimensional angular speed $\omega_0+\dot{\varphi}(\hat{t})$ and non-dimensional penetration rate v_0, are also given and discussed as follow:

- Case A: $\zeta = \kappa = 0.02, \eta = 1.6, \psi = 14, \omega_0 = 10, \delta_0 = 1$. According to the stability charts, there are no poles in the RHP, and the linearized system is stable. For the linearized system simulations given in Figure 3.4, with a initial disturbance: $\dot{\varphi}(0) = 0.1$, the system gradually goes back to a stable state. Furthermore, the nonlinear simulations are based on the original governing equations Eq.(2.17)

- Case B: $\zeta = \kappa = 0.02, \eta = 1.6, \psi = 14, \omega_0 = 10, \delta_0 = 1.33$. Point B is on the stability crossing curve, and therefore, this location belongs to the stability crossing set. Specifically, there are no poles in the RHP, and the linearized system is marginally stable. With a initial disturbance: $\dot{\varphi}(0) = 0.1$, the linearized system and original nonlinear system stay in a motion state of constant magnitude vibration;

therefore, verifying the effectiveness of the linear analysis.

• Case C: $\zeta = \kappa = 0.02, \eta = 1.6, \psi = 14, \omega_0 = 10, \delta_0 = 2.4$. As shown in the stability chart, point C is in the unstable region, and there are two poles on the right half plane. Similar to case A and B, torsional perturbation $\dot{\varphi}(0) = 0.1$ is used as the initial condition. Both the linear and nonlinear system are excited by this perturbation, and become unstable, with an increasing amplitude. However, in this case, the linearized system simulation is not a reasonable approximation of the original nonlinear system, due to the fact that amplitude of the vibrations approaches to infinity as time increases. As shown in Figure 3.5(a)(b), the torsional motion is in a state of stick-slip vibrations, where the angular speed equals zero stop during the stick phase, and reaches a value about two times the drive rotation speed during the slip phase. Meanwhile, for the axial motions, the linearized system does not match with the original nonlinear system. The lienarized system rapidly goes to an unstable state with a large magnitude. However, the true nonlinear system is experiencing bit-bounce vibrations. As shown in Figure 3.5(c)(d), the axial velocity became negative during bit bounce vibrations.

Finally, the contribution of the chapter are summarised and given as follows:

• Local stability analysis has been carried out to obtain the stability region of the operation. Moreover, compared to previous approaches, with the D-subdivision method used in this chapter, one can obtain more information about the severeness of the instability by giving the number of poles in the RHP.

• For simulations, the linearized system can only match well with the original system when is one near around the local stable equilibrium $\mathbf{X} = (0 \quad 0 \quad 0 \quad 0)^T$.

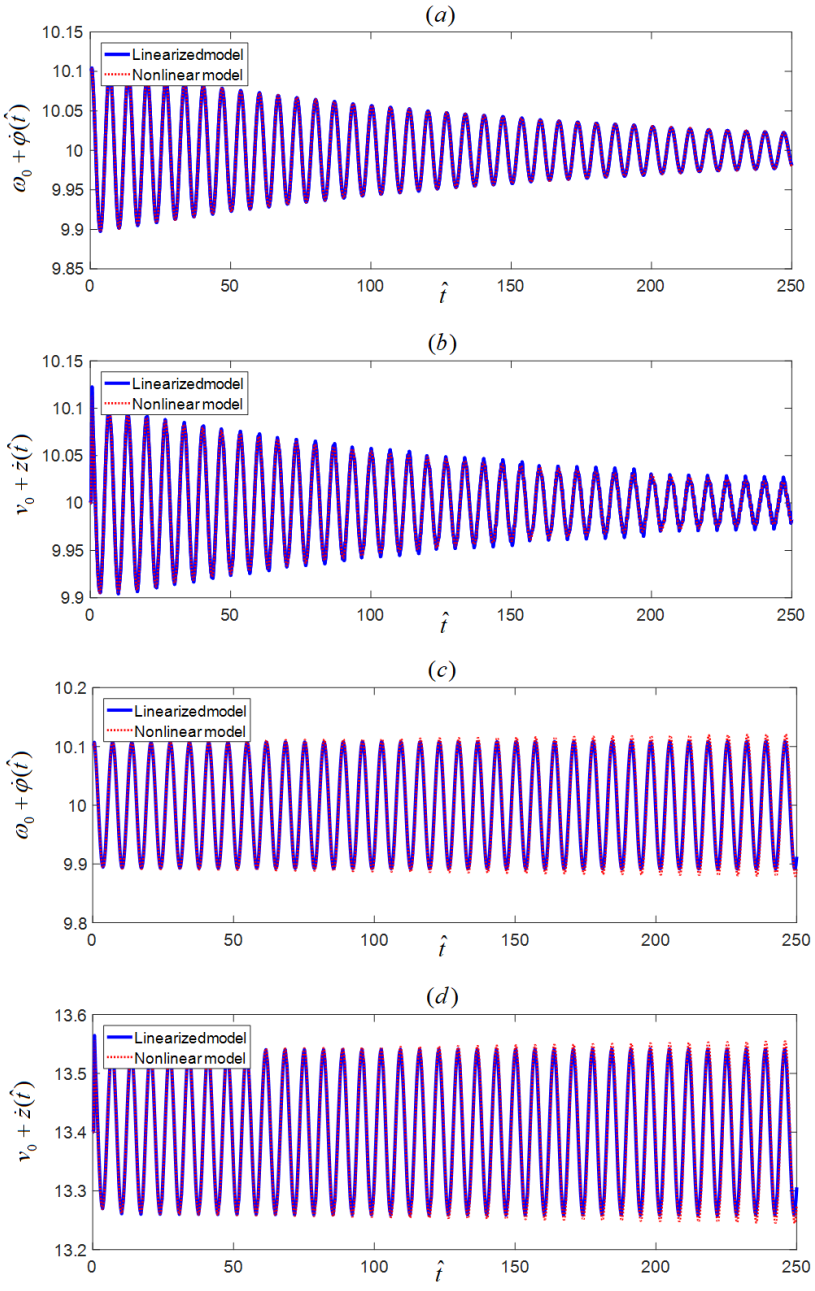

Figure 3.4: Simulations with linearized and nonlinear systems. For Case A: (a) time histories of non-dimensional angular speed $\omega_0 + \dot{\varphi}(\hat{t})$ with drive speed $\omega_0 = 10$ and (b) time histories of non-dimensional axial speed $v_0 + \dot{z}(\hat{t})$ with drive speed $v_0 = 10$. For case B: (c) time histories of non-dimensional angular speed $\omega_0 + \dot{\varphi}(\hat{t})$ with drive speed $\omega_0 = 10$ and (d) time histories of non-dimensional axial speed $v_0 + \dot{z}(\hat{t})$ with drive speed $v_0 = 13.3$.

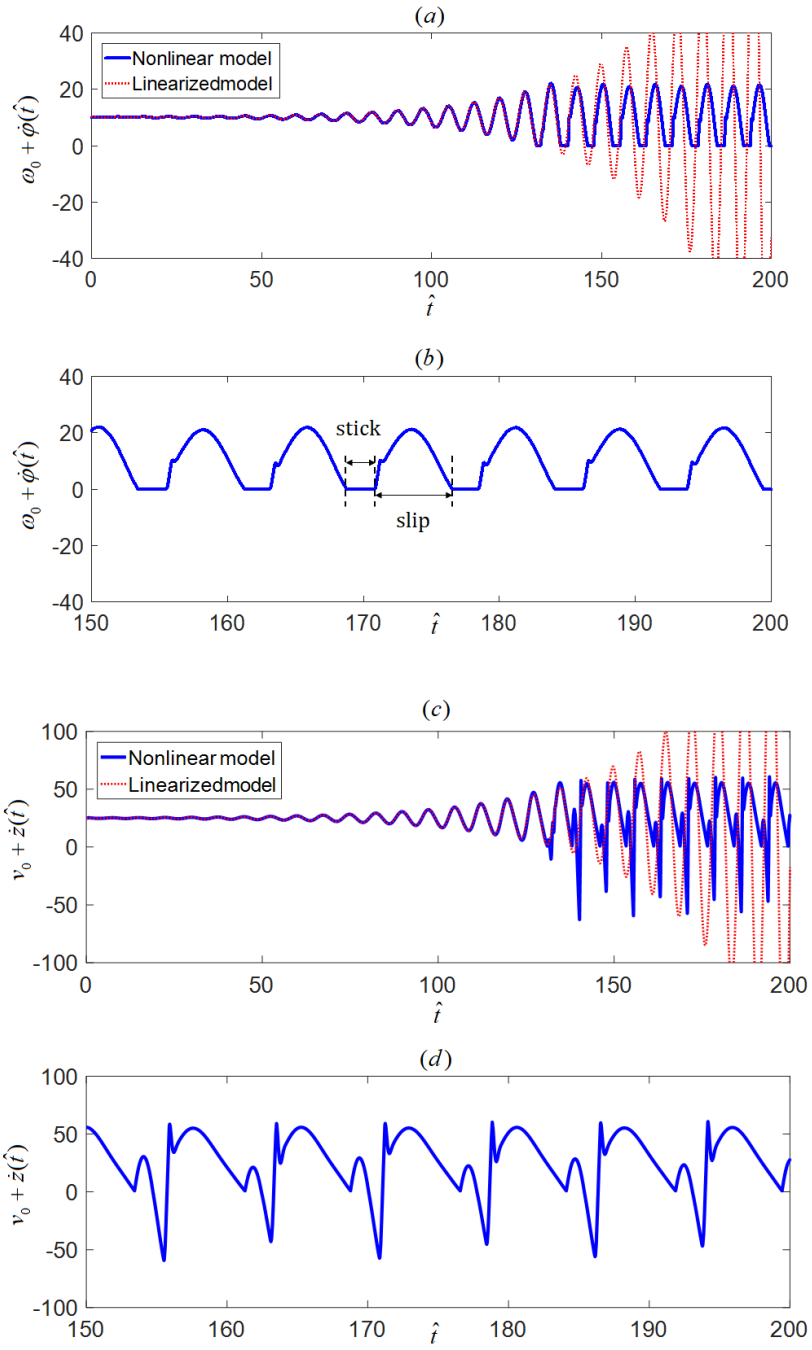

Figure 3.5: Simulations with linearized and nonlinear system for Case C: (a) time histories of non-dimensional angular speed $\omega_0 + \dot{\varphi}(\hat{t})$ with drive speed $\omega_0 = 10$; (b) stick-slip phenomenon in torsion response; (c) time histories of non-dimensional axial speed $v_0 + \dot{z}(\hat{t})$ with drive speed $v_0 = 24$; and (d) bit bounce phenomenon in axial response.

Otherwise, the linearization is not a suitable approximation and can out capture all of the nonlinear phenomenona (e.g., bit bounce, stick-slip). Therefore, it is necessary to do the nonlinear analysis to describe and study the root cause, and the path leading the drill-string system from a stable motion state to an unstable motion state.

Chapter 4: Nonlinear analysis

4.1 Overview

Through the linear stability analysis presented in the previous section, one can investigate the operations near a norminal state wherein friction and loss of contact have no impact on the dynamics. The state-dependent delay and its effect were studied by using an equivalent constant time delay. In this section, to further the knowledge of what may lead the system from a stable equilibrium state to a stable or unstable limit cycle motion and finally to a stick-slip vibration, the non-dimensional nonlinear governing equations are considered. For the system considered here, loss of contact, friction, and state-dependent delay are the sources of nonlinerity. SD-DDEs are always nonlinear, since the state itself arises in its own argument through the delay. Despite the fact that nonlinear analysis of SD-DDE is an actively developing area in mathematics, there is no analytical method that can be applied directly to the considered system. The numerical continuation method approach for the nonlinear analysis of DDE is developed by Engelborghs, Luzyanina, and Roose in reference [51]. Furthermore, using MATLAB they build a toolbox named DDE-BIFTOOL [52, 53] which can be used to study the bifurcation for nonlinear system with constant and state-dependent delay. As example of a turning

operation is given by Insperger, Barton, and Stepan in [21]. Their research revealed that compared to traditional constant delay model, a state-dependent delay model has more sophisticated nonlinear behaviors. The criticality of the bifurcation can alternate from subcritical to supercritical by varying turning operation parameters.

For the considered drill-string system, the nonlinear analysis for the system is organized as follows:

• In the first part, the motion near equilibrium points will be considered. The Eq.(3.1) where the state-dependent term is the only source for nonlinearity in the considered nondimensioinalized system will be used. The state-dependent delay is transformed from implicit form to explicit by Taylor expansion. The criticality of the bifurcation will be studied with the consideration of different damping ratios. The bifurcation diagram in the plane of penetration speed v_0 and maximum dimensionless angle φ will be presented, and Floquet multipliers will be given to justify the results.

• In the second part, state-dependent delay together with friction and loss of contract will be considered, and Eq.(2.17) will be used for the analysis. However, to take advantage of the DDE-BIFTOOL, all functions need to be differentiable and the state-dependent delay must be in the explicit form. To address these issues, the Heaviside step function and ramp function, which used to represent the loss of contact and friction, will be replaced by hyperbolic tangent function and sigmoid function. The result will be presented in the bifurcation diagram in the plane of penetration speed v_0 and maximum dimensionless angle φ as well. The numerical simulation will be provided to justify the results.

4.2 Nonlinear analysis with the state-dependent model

As mentioned in last section, to take advantage of this tool, all functions need to be differentiable and the state-dependent delay must be in explicit form. In order to overcome this difficulty, state-dependent delay from Eq. (3.2) will be rewritten as three level of nested constant delay as,

$$\varphi(\hat{t}-\hat{\tau}) = \varphi(\hat{t}-(\hat{\tau}_0 - \frac{\varphi(\hat{t}) - \varphi(\hat{t}-\hat{\tau}_0)}{\omega_0}))) \tag{4.1}$$

By using a Taylor expansion at $\hat{t}-\hat{\tau}_0$, we will have

$$\varphi(\hat{t}-(\hat{\tau}_0 - \frac{\varphi(\hat{t}) - \varphi(\hat{t}-\hat{\tau}_0)}{\omega_0}))) = \varphi(\hat{t}-\hat{\tau}_0) + \frac{\varphi(\hat{t}) - \varphi(\hat{t}-\hat{\tau}_0)}{\omega_0}\dot{\varphi}(\hat{t}-\hat{\tau}_0) + h.o.t \tag{4.2}$$

Keeping the first two terms only, and substituting them into Eq. (2.18), the explicit form of state dependent delay is determined as

$$\hat{\tau} = \hat{\tau}_0 - \frac{1}{\omega_0}(\varphi(\hat{t}) - \varphi(\hat{t}-\hat{\tau}_0)) + \frac{1}{\omega_0^2}(\varphi(\hat{t}) - \varphi(\hat{t}-\hat{\tau}_0))\dot{\varphi}(\hat{t}-\hat{\tau}_0) \tag{4.3}$$

After combining the non-dimensionalized governing system Eq. (3.1) together with the explicit state-dependent delay function Eq. (4.3) and using the DDE-BIFTOOL, we can generate the bifurcation diagram with different dimensionless damping ratios as given in Figure 4.1. The continuation of the periodic orbit is stopped, when the state-dependent delay $\hat{\tau} < 0$. Along the y axis, the maximum value of the dimensionless angle φ is shown. Similarly to the turning case from Insperger, Barton, and

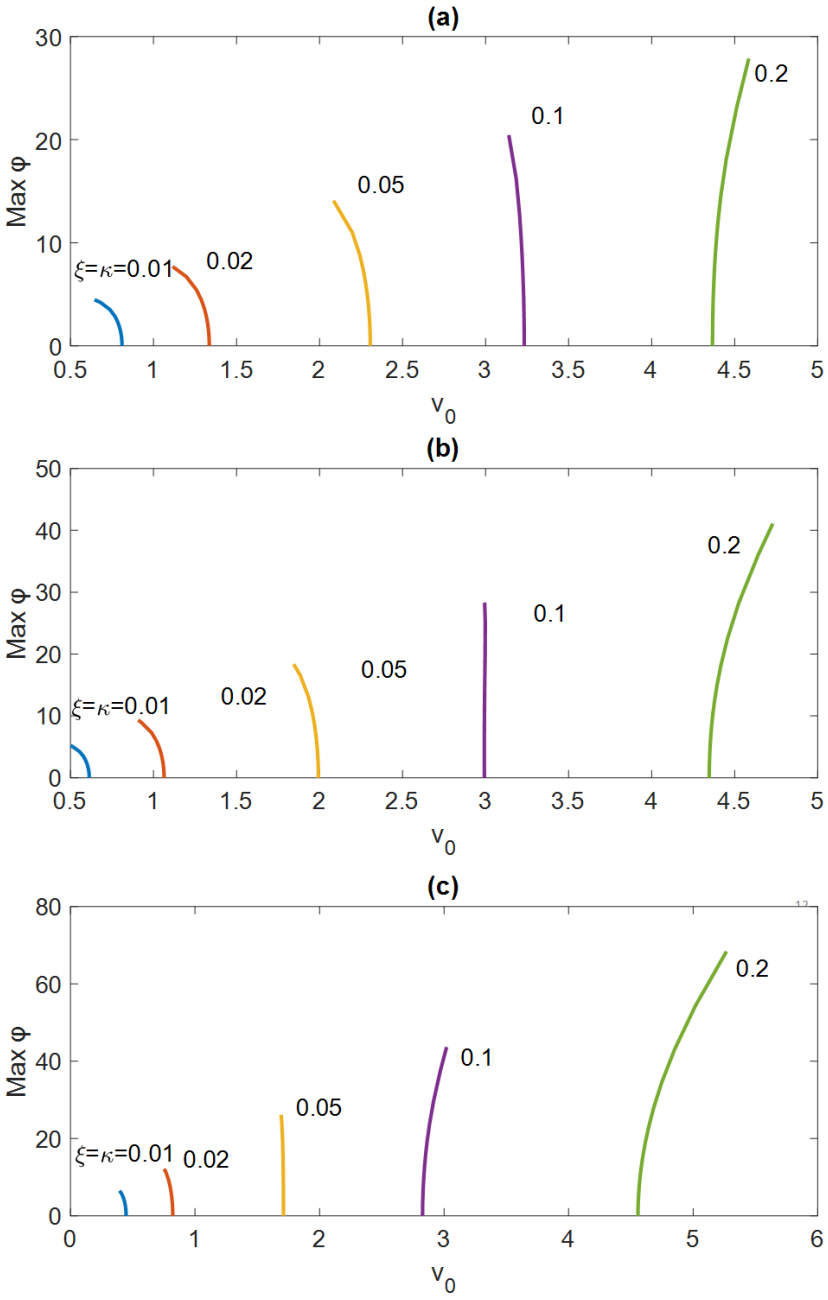

Figure 4.1: Bifurcation diagram in the plane of penetration speed v_0 and maximum dimensionless angle φ, for different values of ζ and κ, (a) $\omega_0 = 10$, (b) $\omega_0 = 15$, and (c) $\omega_0 = 25$.

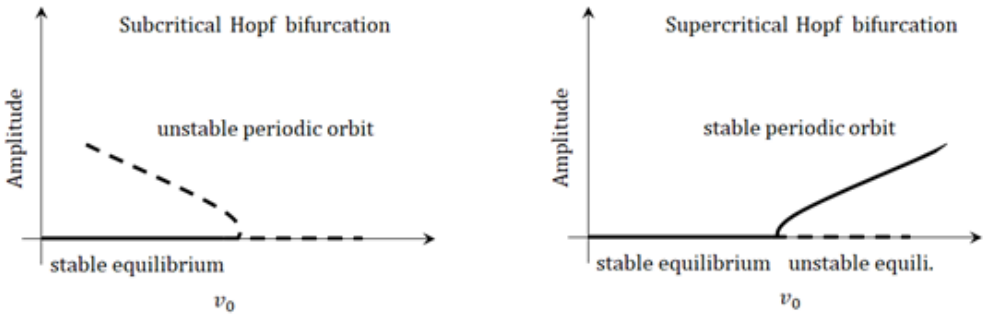

Figure 4.2: Sketches of subcritical and supercritical Hopf bifurcations.

Stepan [21], when subcritical bifurcation happens, an unstable limit cycle (periodic orbit) coexists with the stable equilibrium, and for supercritical bifurcation, an stable limit cycle (periodic orbit) coexists with unstable equilibrium(shown in Figure 4.1). From the diagram, we can draw two conclusions as follow,

First, when the dimensionless drive speed ω_0 is small, branches of periodic motions tend to bend to the left, which indicate these are unstable periodic motion (subcritical bifurcation). As ω_0 increase, those brunches start to bend to the right, the periodic motion changes from unstable to stable (supercritical bifurcation). For example, when $\omega_0 = 10$, and $\xi = \kappa = 0.1$ the curve bend to the left, which means it is unstable(see Figure 4.1b). However, when $\omega_0 = 25$, and $\xi = \kappa = 0.1$, the curve bends to right, and it becomes stable orbit(see Figure 4.1c).

Second, with a small value of dimensionless axial and torsional damping ratio, branches of periodic motions bends to the left, which indicate these are subcritical bifurcation. As damping ratio increases, those brunches start to bend to the right, the Hopf bifurcation changes from subcritical to supercritical. One of those example can be found in Figure 4.1a. When the damping ratios are small i.e. $\xi = \kappa = 0.02$,

$\xi = \kappa = 0.1$, the bifurcation curve bends to the left which imply these are subcritical bifurcation. When the damping ratio are larger i.e. $\xi = \kappa = 0.2$, the curve bend to the right, the bifurcation become supercritical. The corresponding stability information is provided in Figure(4.3). In practical, supercritical bifurcation is more favorable compare with subcritical bifurcation, due to the fact that vibration can not occur below the stability lobes. Therefore, larger axial and torsion damping ratio are more preferable.

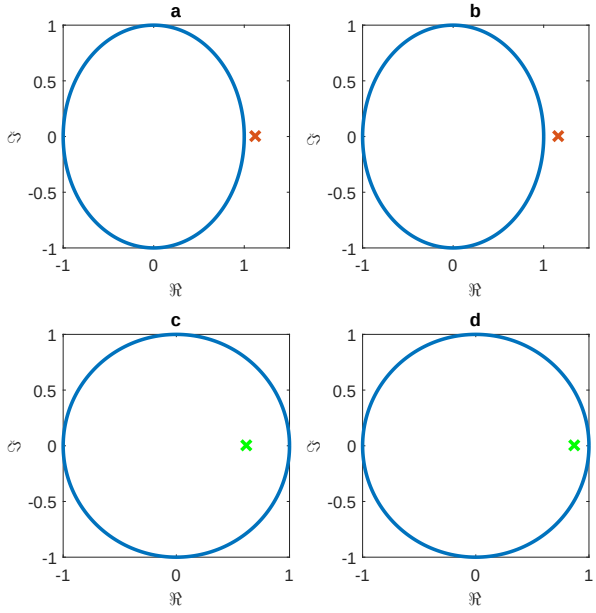

Figure 4.3: Floquet multipliers (a) $\xi = \kappa = 0.02$, $\omega_0 = 10$, $v_0 = 1.3$; (b) $\xi = \kappa = 0.1$, $\omega_0 = 10$, $v_0 = 3.2$; (c) $\xi = \kappa = 0.1$, $\omega_0 = 25$, $v_0 = 2.8$; and (d) $\xi = \kappa = 0.2$, $\omega_0 = 10$, $v_0 = 4.5$.

Based on those results, it can be inferred that both the axial damping ratio and torsion damping ratio play a significant role in determining the linear stability of the equilibrium solution and the nature of the Hopf bifurcation of the equilibrium solution.

4.3 Nonlinear analysis with the generalized model

In this section, to further the knowledge of what may lead the system from a stable equilibrium state to a stable or unstable limit cycle motion and finally to a stick-slip vibration, the original non-dimensional nonlinear governing equation which combined loss of contact and friction, Eq. (2.17) is adopted here. Furthermore, in order to use the tool, all function need to be differentiable. Therefore, the Heaviside step function can be replaced by a sigmoid function defined as

$$S(x) = \frac{1}{1 + e^{-\lambda x}} \tag{4.4}$$

and the sgn(·) function can be replaced by a Hyperbolic tangent function defined as

$$T(x) = \tanh(\lambda x) \tag{4.5}$$

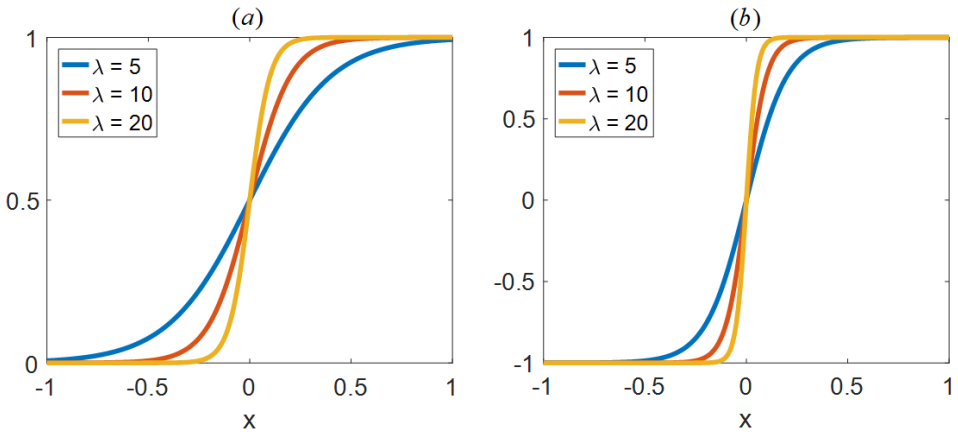

Figure 4.4: (a) Sigmoid functions and (b) tanh function.

In addition, after substituting the first-order Taylor approximation $\varphi(\hat{t}-\hat{\tau}) \approx \varphi\left(\hat{t}\right) - \dot{\varphi}\left(\hat{t}\right) \cdot \hat{\tau}$ into Eq.(2.18), the explicit form of the state dependent delay is determined as

$$\hat{\tau}(\hat{t}) = \frac{2\pi}{N\left(\omega_0 + \dot{\varphi}(\hat{t})\right)} \tag{4.6}$$

By comparing with the original nonlinear model, it is believed that $\lambda = 20$ is an appropriate choice for the current work. After combining the sigmoid function, the hyperbolic tangent function, and explicit state-dependent delay function together with the governing equation and using DDE-BIFTOOL, the authors generate the bifurcation diagrams for different fixed dimensionless drive speed ω_0 as shown in Figure 4.5. These bifurcation diagrams are shown in the plane of non-dimensional depth of cut δ_0, and the maximum value of the perturbation speed $\varphi(\hat{t})$ over the orbit. To verify the information in a bifurcation diagram, simulation results are obtained for different cases, as shown in Figure 4.6. These results are based on the untransformed original governing equations (11), wherein the Heaviside step function and sign function are used and the implicit state-dependent delay is numerically determined. From the diagrams generated by ($\zeta = \kappa = 0.02, \eta = 1.6, \psi = 14$), one can draw the following conclusions:

- Case 1 ($\omega_0 = 10,\ 0 < \delta_0 < A$; $\omega_0 = 20,\ 0 < \delta_0 < E$): As shown in the stability chart, it is within the stable region. The stable equilibrium branch is the only branch.

- Case 2 ($\omega_0 = 10,\ A < \delta_0 < B$; $\omega_0 = 20,\ E < \delta_0 < F$): It is inside of the stability region and near the stability boundaries, the equilibrium branch is

coexist with the stick-slip branch. This indicates that with a small amplitude of perturbation, the system can back to the equilibrium branch. However, with a large amplitude of perturbation, the system can jump from stable branch to the stick-slip branch. This occurrence is illustrated in Figures 4.6(a-b). Meanwhile, there is an unstable branch between the stable branch and the stick-slip branch. Similar to the result in previous section, the unstable branch bend to the left and it is a subcritical bifurcation.

- Case 3 ($\omega_0 = 10$, $B < \delta_0 < C$; $\omega_0 = 20$, $F < \delta_0 < G$): This is the most complex case. There are three stable branch which are the equilibrium branch, the stable limit cycle branch without stick-slip, and the stick-slip branch. With different perturbation, the system can jump from one to another. Meanwhile, there are coexist two unstable branch which is represented by the dash line in the bifurcation diagram.

- Case 4 ($\omega_0 = 10$, $C < \delta_0 < D$): For this case, due to the nature of the instabilities, when the depth of cut is in certain region, a portion of the stick-slip limit cycle branch coexists with a stable limit cycle branch without stick slip; this occurrence is illustrated in Figures 4.6(c-e). Also, there exist one unstable branch which bend to the left, which is a indication of sub critical bifurcation.

- Case 5 ($\omega_0 = 10$, $\delta_0 > D$; $\omega_0 = 20$, $F < \delta_0 > H$): The bifurcation diagrams imply that, there is only one stable stick-slip branch exist. With any kind initial conditions, the system will end up with stick-slip vibrations.

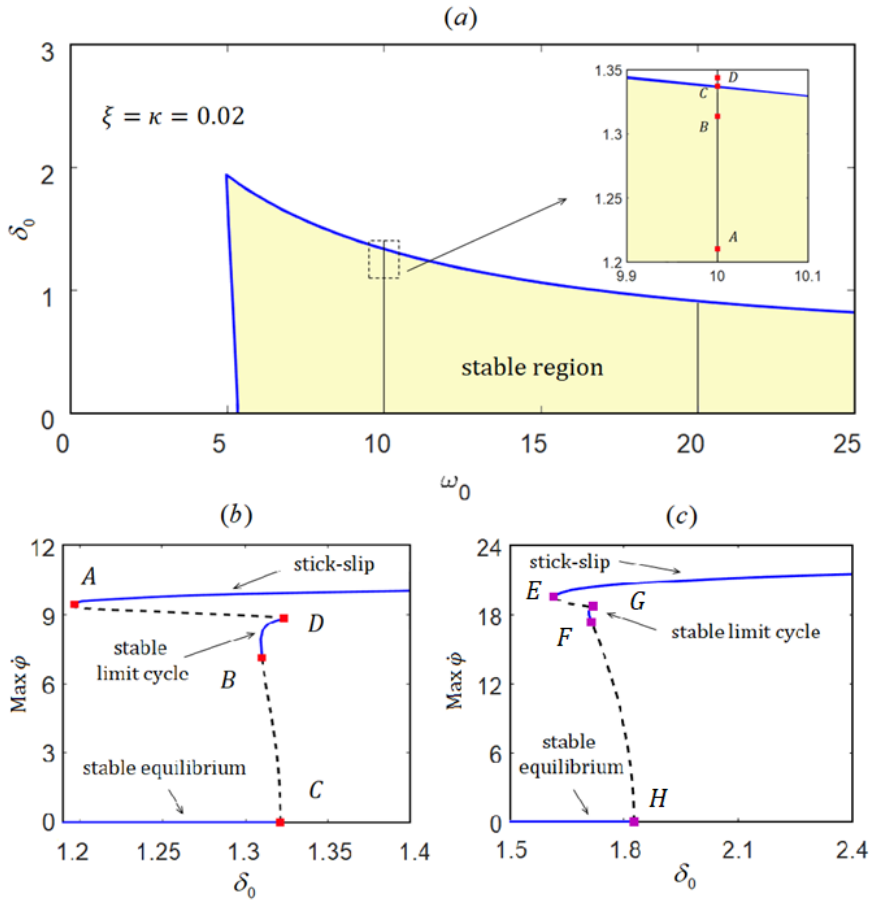

Figure 4.5: (a) Stability chart. Bifurcation diagram with fixed non-dimensional drive speed: (b) $\omega_0 = 10$ and (c) $\omega_0 = 20$. Solid lines are used for stable branches and dashed lines are used for unstable branches. A subcritical Hopf instability and cyclic fold instabilities are noticeable for cases (b) and (c).

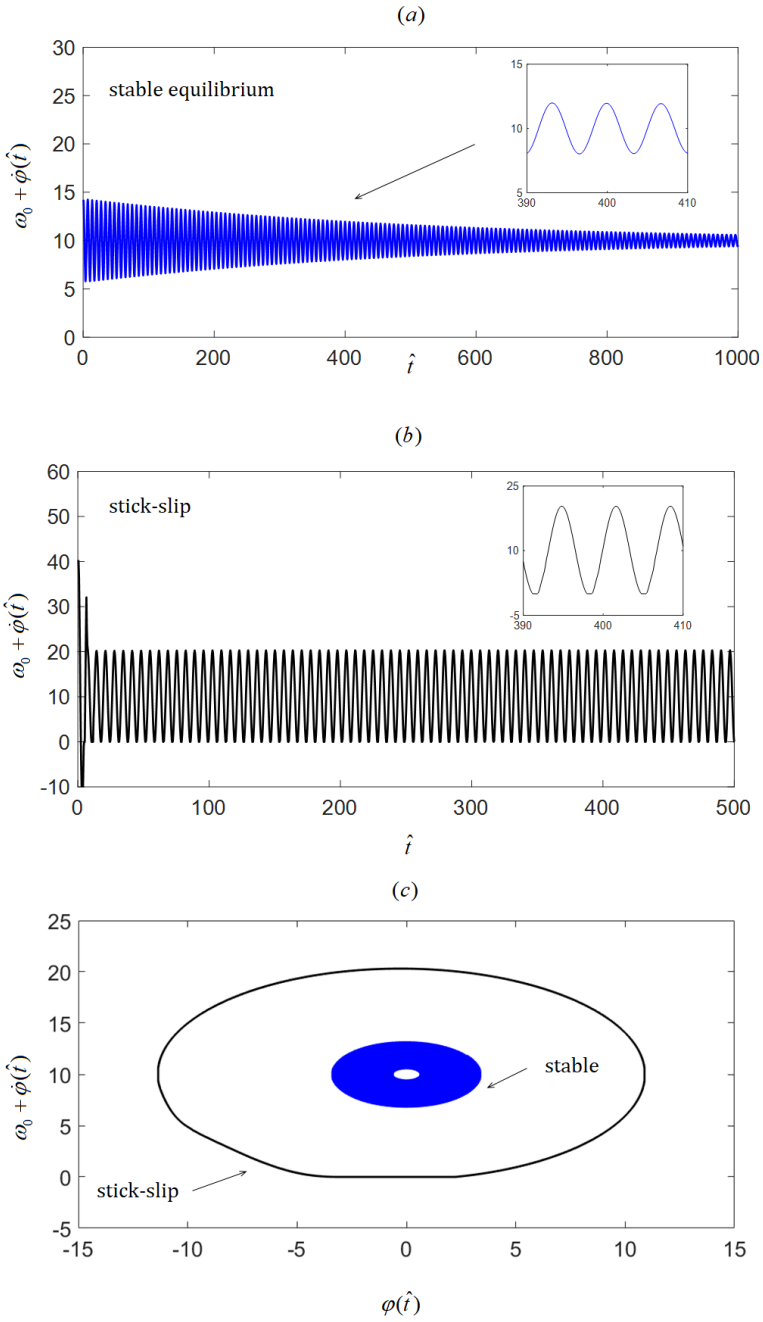

Figure 4.6: Time histories of non-dimensional angular speed $\omega_0 + \dot{\varphi}(\hat{t})$ with drive speed $\omega_0 = 10$: (a) solution from stable equilibrium branch for depth of cut $\delta_0 = 1.23$, (b) solution from stick-slip branch for depth of cut $\delta_0 = 1.23$, and (c) phase portraits for motions shown in (a) and (b).

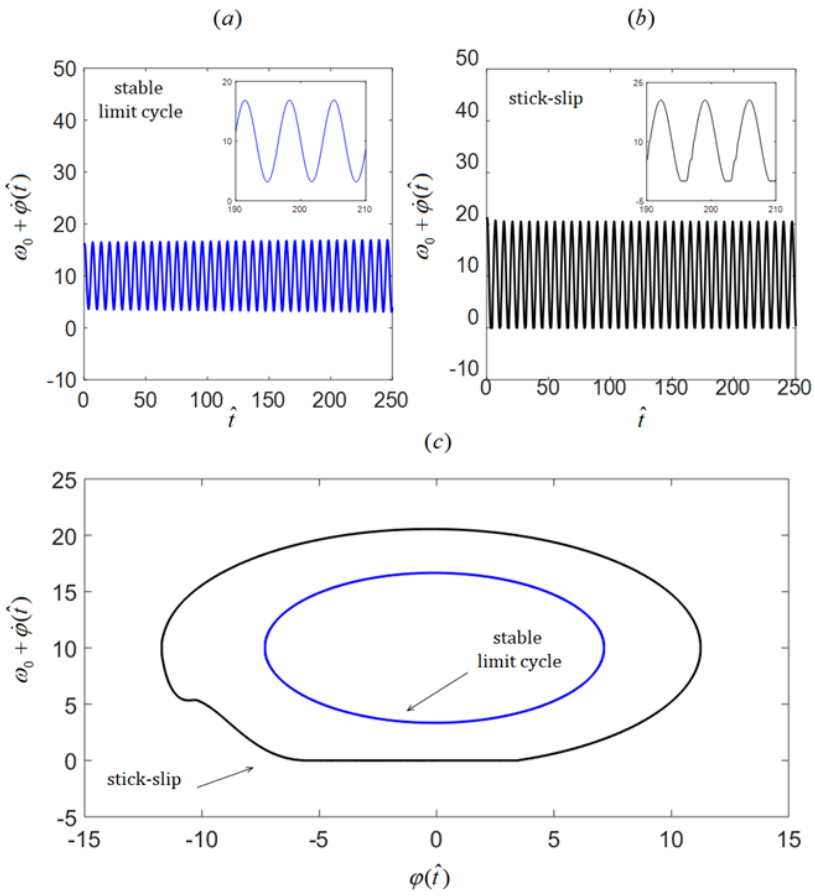

Figure 4.7: Time histories of non-dimensional angular speed $\omega_0 + \dot{\varphi}(\hat{t})$ with drive speed $\omega_0 = 10$: (a) solution from stable limit cycle branch for depth of cut $\delta_0 = 1.33$, (b) solution from stick-slip branch for depth of cut $\delta_0 = 1.33$, and (c) phase portraits for motions shown in (a) and (b).

4.4 Observations

In this section, the nonlinear analysis of the drill-string system is given. The motion near the equilibrium point is first studied. In this case, the state-dependent delay is the only source of nonlinearity. The bifurcation diagram with different damping ratio is generated. The results show that axial damping and torsion damping which are representative of effects from drill mud play a significant role in determining the linear stability of the equilibrium solution and the nature of the Hopf bifurcation of the solution. Following by that, the motions including loss of contact and friction are considered. The bifurcation diagram are developed and presented. The results indicated the system has strong nonlinearities. Even within the stable region near the boundaries, the system can suffer from stick-slip vibrations with a large amplitude perturbation. In addition, due to the influence of the state-dependent delay, there is a stable limit cycle without stick-slip coexist with the stick-slip vibration.

Chapter 5: Controller design

5.1 Overview

The control of system with time delay has been studied in network control system [54], biological systems [55], speed control of combustion engines [56], and metal cutting systems [57, 58]. Different control strategies such as PID control [59], optimal control [60], adaptive control [61], and Robust control [62] have been developed and implemented successfully on those areas. For drilling system, the soft torque controller, which was patented by Shell in 1992, is widely used in industry. With a goal of damping the first mode of torsional motion, this controller was essentially a PI controller based on the error between the measured top drive speed and a reference speed. Following this approach, soft speed as well as Z-torque controller have been designed. However, as pointed out in the work of Kyllingstad, these controller are very sensitive to time delay, and even a small amount of time delay can cause the control scheme to fail in the treatment of stick-slip vibrations. For drill system with time delay, X.Liu, N. Vlajic, X. Long, G. Meng, and B. Balachandran [5], proposed a PID controller with optimal feedback gain using semi-discretization method. This method requires real time information of angle and axial displacement from the down-hole. In practice, it is not always available due to limitations on the

sampling rate, time delay of the measurements, and/or the high cost involved. In the work of B. Besselink, T. Vromen, N. Kremers, and N. Wouw [36], an observer based controller is developed by using continuous pole placement method for time delay system, which originally introduced by The optimal feedback gain is obtained by a numerical gradient based optimization method. However, in their model the torsion dynamics is only considered, the effect of axial dynamics is simplified as a velocity-weakening term. In order to overcome those disadvantages, this chapter is organized as follows:

• In the first part, a controller design that is based on current and delayed feedback of the torsional displacement and velocity, which essentially is a PD controller, is given. This method is first introduced by by Elbeyli and Sun [63] for discretized system with time delay. Here, the method will be modified and applied to continuous system, the gains of P and D will be determined by a numerical optimal method.

• In the second part, since only the torsional states can be measured directly in practice, an observer for time delay system will be developed here to estimate axial states. Then a revised continuous pole placement method for time delay system introduced by Michiels and Niculescu [27] will be adopted here. The feedback gain for the controller and observer will be determined by a numerical optimization method. Finally, the controller will be applied to the original nonlinear system to justify the effectiveness.

5.2 PD controller design and application

5.2.1 Controller design for the linearized model

As shown in last section, if the drill systems are operated within the stable region but near the boundaries, the system is still susceptible to stick-slip vibrations. Therefore, a control strategy that can be used to mitigate the stick-slip behavior is essential in practice. However, control methods that can be directly applied to state-dependent delay are still under investigate, the linearized state-dependent model holding the same local stability properties, will be used in this section. The control input will be the torque which is provided by the drive motor on the top of the drill string, and it is the most common approach in practice. The output here is chosen to the dimensionless angle and angular speed of the BHA, since the main goal is to mitigate the torsion vibration. With those assumption, the system with controller can be written as,

$$\begin{aligned} \ddot{z}(\hat{t}) + 2\xi\eta\dot{z} + \eta^2 z(\hat{t}) &= -N\psi\left(z(\hat{t}) - z(\hat{t}-\hat{\tau}_0)\right) + N\psi\delta_0\left(\varphi(\hat{t}) - \varphi(\hat{t}-\hat{\tau}_0)\right) \\ \ddot{\varphi}(\hat{t}) + 2\kappa\dot{\varphi}(\hat{t}) + \varphi(\hat{t}) &= -N\left(z(\hat{t}) - z(\hat{t}-\hat{\tau}_0)\right) + N\delta_0\left(\varphi(\hat{t}) - \varphi(\hat{t}-\hat{\tau}_0)\right) + u(\hat{t}, \hat{t}-\hat{\tau}_0) \end{aligned} \tag{5.1}$$

where $u(\hat{t}, \hat{t}-\hat{\tau}_0)$ is the feedback of the state variables that also includes delayed states. With this feedback signal, the matrix form can be written as

$$\dot{\mathbf{X}}(\hat{t}) = \mathbf{A}_0\mathbf{X}(\hat{t}) + \mathbf{A}_1\mathbf{X}(\hat{t}-\hat{\tau}_0) + \mathbf{B}u(\hat{t}, \hat{t}-\hat{\tau}_0) \tag{5.2}$$

where $\mathbf{A}_0$ and $\mathbf{A}_1$ are same as in Eq.(3.18), the control matrix $\mathbf{B}$ is given as

$$\mathbf{B} = \begin{bmatrix} 0 & 0 & 0 & 1 \end{bmatrix}^T$$

The block diagram for the system with control is given in Figure 5.1. The elements within the dashed rectangle represent the original system and the matrices $\mathbf{A}_0$, $\mathbf{A}_1$, and state vector $\mathbf{X}$ are defined in Eq.(5.2). Typically, for a drill-string system, the torque on top can be monitored and the torsional vibrations can be observed indirectly from the torque or directly from a down-hole measurement [64]. Therefore, the system output $\mathbf{Y}$ can be expressed as

$$\mathbf{Y}(\hat{t}) = \mathbf{C}\mathbf{X}(\hat{t}) \tag{5.3}$$

the output matrix $\mathbf{C}$ is in the form of

$$\mathbf{C} = \begin{bmatrix} 0 & 0 & 1 & 0 \\ \\ 0 & 0 & 0 & 1 \end{bmatrix}$$

it denotes that angular displacement $\varphi(\hat{t})$, and rotary speed $\dot{\varphi}(\hat{t})$ are the physical measurement of the system. Follow by that, the feedback control law based on the measurement is constructed as

$$u(\hat{t}, \hat{t} - \hat{\tau}_0) = \mathbf{K}_1\mathbf{Y}(\hat{t}) + \mathbf{K}_2\mathbf{Y}(\hat{t} - \hat{\tau}_0) \tag{5.4}$$

where K_1 and K_2 are the feedback gains for the states and the delayed states, respectively. They are defined as

$$K_1 = (p_1, d_1)$$

$$K_2 = (p_2, d_2)$$

The control law Eq.(5.4) includes feedback of both the current output and the delayed output. On substituting it into the governing equation Eq.(5.2), the system takes the form,

$$\dot{\mathbf{X}}(\hat{t}) = (\mathbf{A}_0 + \mathbf{B}\mathbf{K}_1\mathbf{C})\,\mathbf{X}(\hat{t}) + (\mathbf{A}_1 + \mathbf{B}\mathbf{K}_2\mathbf{C})\,\mathbf{X}(\hat{t} - \hat{\tau}_0) \tag{5.5}$$

As presented in the previous chapter, the stability of the system with controlled feedback can be determined using D-subdivision method. The feedback gains K_1 and K_2 are design parameters that can be determined through an optimization procedure. Moreover, the relative stability of the linearized system depends on the position of the rightmost pole. Specifically, the system is more stable, if the rightmost pole is with larger distance from the imaginary axis. Therefore the objective function can be defined as follows:

$$J(\mathbf{K}_1, \mathbf{K}_2) = \sup_s \left\{ \mathrm{Re}(s) | \det \left(s\mathbf{I} - (\mathbf{A_0} + \mathbf{B}\mathbf{K}_1\mathbf{C}) - (\mathbf{A_1} + \mathbf{B}\mathbf{K}_2\mathbf{C}) e^{-\hat{\tau}_0 s} \right) = 0 \right\} \tag{5.6}$$

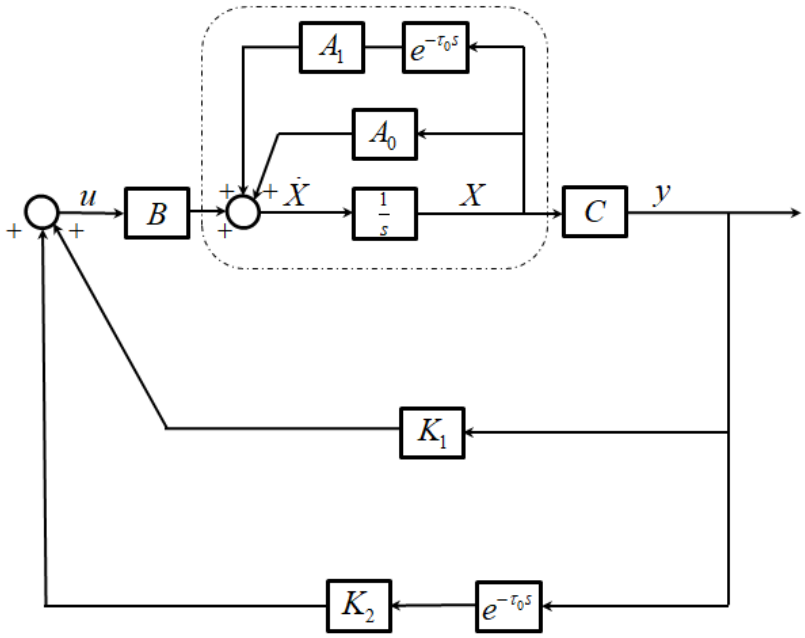

Figure 5.1: Block diagram for the time-delay system with feedback control. The elements in the dashed rectangle represent the uncontrolled original system.

Here, $J(\cdot)$ represents the rightmost pole of the drill-string dynamics. when objective function is negative, asymptotic stability is guaranteed.

$$J(\mathbf{K}_1, \mathbf{K}_2) < 0 \tag{5.7}$$

5.2.2 Optimal feedback gain design

The system is more stable with a smaller value of $J(\mathbf{K}_1, \mathbf{K}_2)$. One way to determine the feedback gain $\mathbf{K}_1$ and $\mathbf{K}_2$ is to solve the optimization problems

$$\min_{\mathbf{K}_1, \mathbf{K}_2} J(\mathbf{K}_1, \mathbf{K}_2) \tag{5.8}$$

so that the right most pole of the drill-string dynamics has the minimum values. However, the objective function is not differentiable. The discontinuity may occur when the rightmost poles change, or some rightmost poles have a multiplicity larger than one. One example can be found in the root locus plot of Figure(5.2). where a multiplicity 3, and a multiplicity 2 root rise respectively with continuously increasing K_{11}. After the multiplicity 3 root rises, the rightmost pole jump from branch 3 to complex conjugate branch 1 and 2. Similarly, after the multiplicity 2 root rises, the complex conjugate branch 1 and 2 split, and branch 2 becomes the only rightmost pole branch.

To address these issues, a robust gradient sampling method(stabilized steepest descent algorithm) based on optimization (by Burke, Lewis, and Overton [65]) is employed here to get the optimal pole placement position. The steps of this method can be briefly stated as follows:

1. Approximate the Clarke subdifferential by gradient sampling.
2. Compute a search direction.
3. Compute a step length.

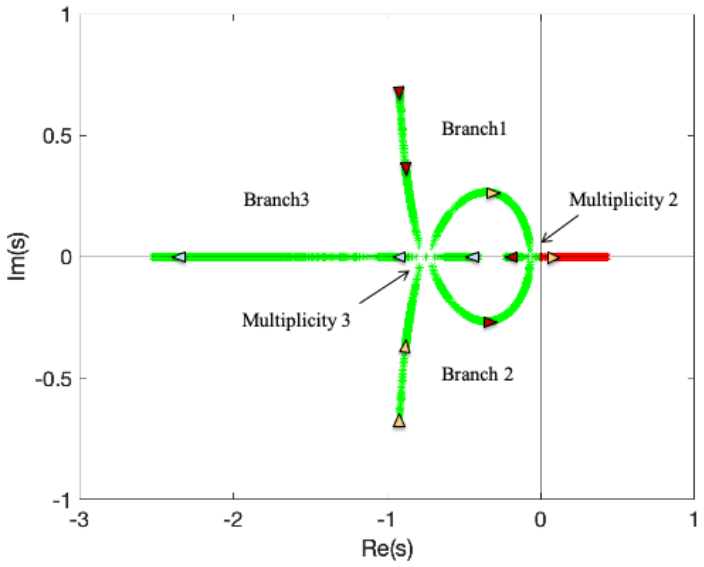

Figure 5.2: Root Locus of the 3 rightmost poles for system($\omega_0 = 10, \delta_0 = 1.23, \psi = 14, \zeta = \kappa = 0.02$) with feedback gain $\mathbf{K}_1 = [(0 \sim 2), \quad -0.6626], \mathbf{K}_2 = [-0.3432, \quad -0.7918]$.

4. Update.

Based on the procedures, with the MATLAB codes offered in reference, consider the case for which the drill-string parameters are ($\psi = 14, \eta = 1.6, \zeta = \kappa = 0.02, \omega_0 = 10, \delta_0 = 1.23$). The bifurcation diagram and the system simulations (see Figure(4.6)) show that the system is stable and there is a stick-slip limit cycle branch coexist with the stable equilibrium. After applying the optimization technique, the optimal values of K_1 and K_2 are listed as follow,

$$\mathbf{K}_1 = \begin{bmatrix} 0.2658 & -0.6626 \end{bmatrix}$$

$$\mathbf{K}_2 = \begin{bmatrix} -0.3432 & -0.7918 \end{bmatrix} \tag{5.9}$$

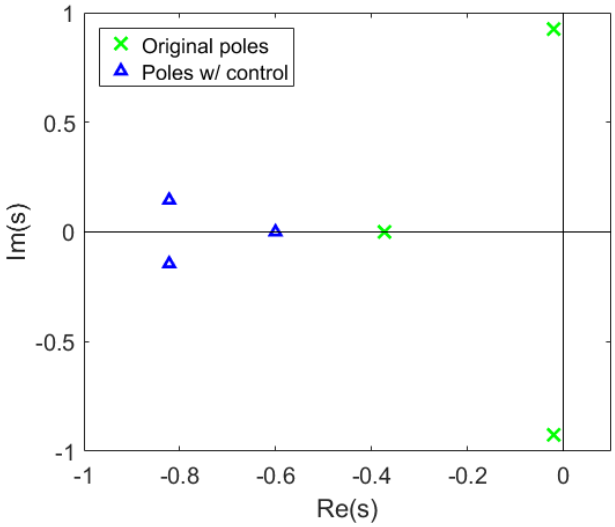

Figure 5.3: Position of the 3 rightmost poles of original system($\omega_0 = 10, \delta_0 = 1.23, \psi = 14, \zeta = \kappa = 0.02$) and system optimal feedback gain($\mathbf{K}_1, \mathbf{K}_2$).

The corresponding optimal objective function satisfies

$$J(\mathbf{K}_1, \mathbf{K}_2) = -0.6003 \tag{5.10}$$

For the original system the rightmost pole is $J(\cdot) = -0.02$. Therefore, the system with control is much more stable compared to the original system. For more information, the comparison of the poles position of original system and system with PI control is given in Figure 5.3.

The control strategy presented in this section is developed according to the linearized system given by Eq. (5.2). However, The ultimate goal of current research is to mitigate the stick-slip vibration of the drill-system which is nonlinear in practice. Therefore, author will investigate the effectiveness of the controller on the motions of the dimensionless nonlinear system governed by Eq. (2.17), wherein the

state-dependent delay, friction, and loss of contact are taken into account as sources of nonlinearity. For parameter values of $\omega_0 = 10$ and $\delta_0 = 1.23$, the system response can either be stable equilibrium or stick-slip limit cycle, as depicted in Figure 4.6. It is noted that in both instances, the controller can be used to stabilize the system to an equilibrium state, thus showing that the controller is viable for the nonlinear system.

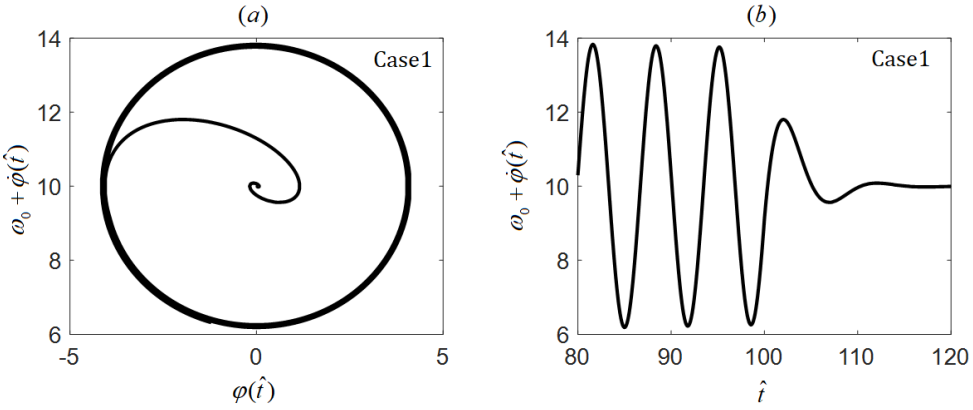

Figure 5.4: Simulation of nonlinear system($\omega_0 = 10, \delta_0 = 1.23, \psi = 14, \zeta = \kappa = 0.02$) with control at $\hat{t} = 100$. Case 1 - stable equilibrium (a) phase portrait projection and (b) torsional motion response.

5.3 Observer based controller design

5.3.1 Observer design

The PD controller design presented in last section is based on the information of current torsional states $\varphi(\hat{t})$, $\dot{\varphi}(\hat{t})$ and the delayed torsional states $\varphi(\hat{t} - \hat{\tau}_0)$, $\dot{\varphi}(\hat{t} - \hat{\tau}_0)$. However, the axial information has neglected and did not play a role

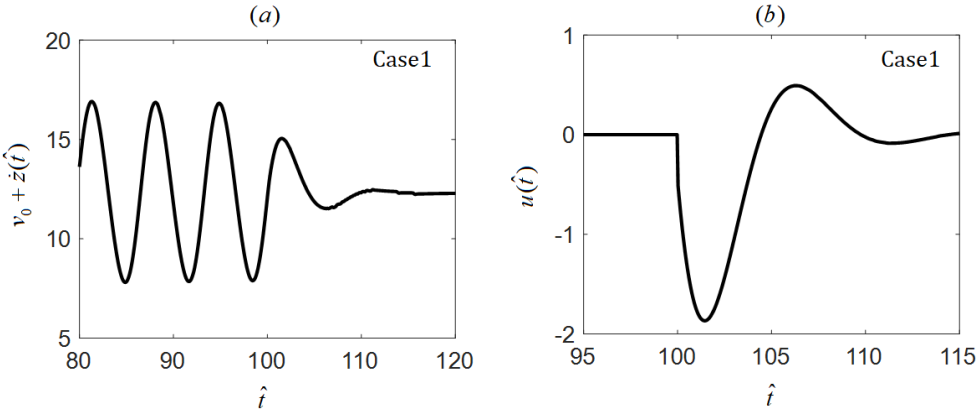

Figure 5.5: Simulation of nonlinear system($\omega_0 = 10, \delta_0 = 1.23, \psi = 14, \zeta = \kappa = 0.02$) with control at $\hat{t} = 100$. Case 1 - stable equilibrium (a) axial motion response and (b) control signal.

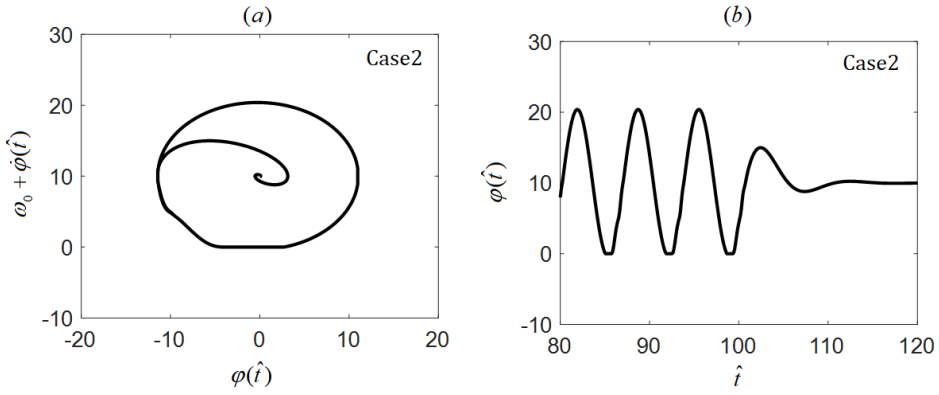

Figure 5.6: Simulation of nonlinear system($\omega_0 = 10, \delta_0 = 1.23, \psi = 14, \zeta = \kappa = 0.02$) with control at $\hat{t} = 100$. Case 2 - stick-slip limit cycle (a) phase portrait projection and (b) torsional motion response.

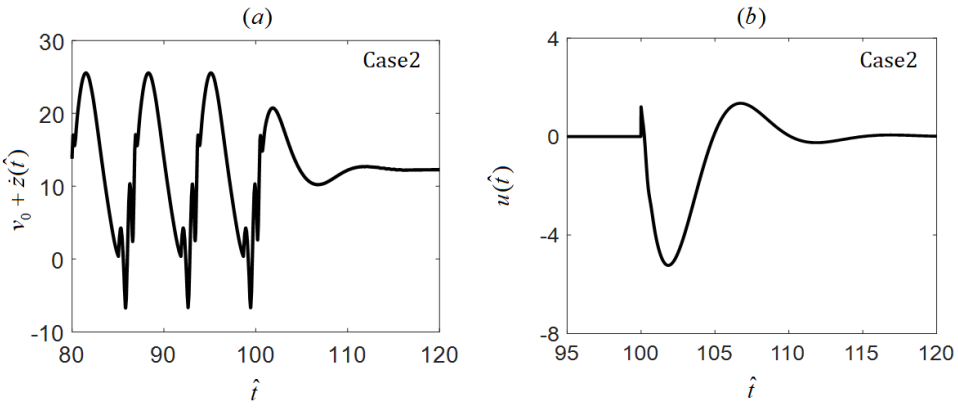

Figure 5.7: Simulation of nonlinear system($\omega_0 = 10, \delta_0 = 1.23, \psi = 14, \zeta = \kappa = 0.02$) with control at $\hat{t} = 100$. Case 2 - stick-slip limit cycle (a) axial motion response and (b) control signal.

in the controller design. In this section, by using the pole placement technique based on the numerical optimization method for time delay intorduced by Michiels and Niculescu [27], and extending the work of Besselink, Vromen, Kremers, and Wouw [36], where only the torsional dynamics is included in the controller design, the author purposes a control scheme for coupled axial-torsional dynamics. Similar to the PD controller design in last section, the linearized model governed by Eq.(3.15) which has the same local stability properties as original system, is used in this work. The control signal $r(\hat{t})$ is the dimensionless torque, which can be provided by the drive motor on the top, and this is one of the most common implementation in practice. As the PD controller, the outputs are the non-dimensional angular position $\varphi(\hat{t})$ and the non-dimensional angular velocity $\dot{\varphi}(\hat{t})$, which can be obtained by downhole measurements. With these assumptions, the system with the controller

can be written as,

$$\begin{aligned} \dot{\mathbf{X}}(\hat{t}) &= \mathbf{A_0}\mathbf{X}(\hat{t}) + \mathbf{A_1}\mathbf{X}(\hat{t} - \hat{\tau}_0) + \mathbf{B}r(\hat{t}) \\ \mathbf{Y}(\hat{t}) &= \mathbf{C}\mathbf{X}(\hat{t}) \end{aligned} \tag{5.11}$$

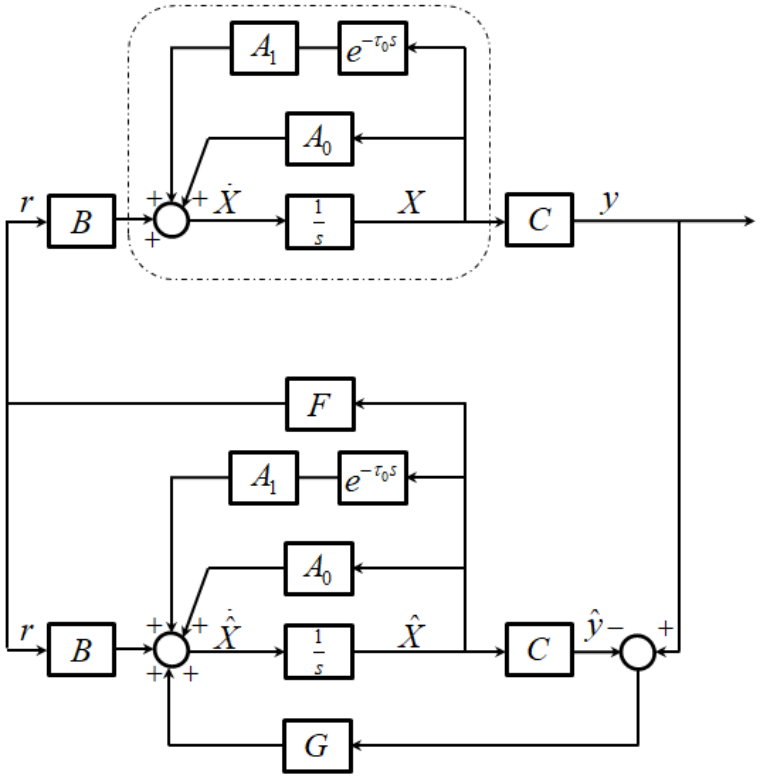

Figure 5.8: Block diagram of the system with time delay and observer based controller

Here, coefficient matrices $\mathbf{A_0}$, $\mathbf{A_1}$, control matrix $\mathbf{B}$, output matirx $\mathbf{C}$ are same as in the PD controller design. The original linearized system lies inside the dashed rectangle, and the observer based controller is at the bottom portion of the block diagram which given in Figure(5.8). Now, the observer-based state-feedback

controller can be proposed in the form as follows:

$$\begin{aligned}
\dot{\tilde{\mathbf{X}}}(t) &= \mathbf{A_0}\tilde{\mathbf{X}}(\hat{t}) + \mathbf{A_1}\tilde{\mathbf{X}}(\hat{t}-\hat{\tau}_0) + \mathbf{B}r(\hat{t}) + \mathbf{L}(\mathbf{Y}(\hat{t}) - \tilde{\mathbf{Y}}(\hat{t})) \\
\tilde{\mathbf{Y}}(\hat{t}) &= \mathbf{C}\tilde{\mathbf{X}}(\hat{t}) \\
r(\hat{t}) &= \mathbf{K}\tilde{\mathbf{X}}(\hat{t})
\end{aligned} \tag{5.12}$$

$\mathbf{K}$ and $\mathbf{L}$ are the controller and observer gains to be determined, respectively. Moreover, the error dynamics in terms of the state $\mathbf{X}$ and observer error $\mathbf{E} = \tilde{\mathbf{X}} - \mathbf{X}$ can be formulated as,

$$\begin{bmatrix} \dot{\mathbf{X}}(\hat{t}) \\ \dot{\mathbf{E}}(\hat{t}) \end{bmatrix} = \begin{bmatrix} \mathbf{A_0} + \mathbf{BK} & \mathbf{BK} \\ 0 & \mathbf{A_0} - \mathbf{LC} \end{bmatrix} \begin{bmatrix} \mathbf{X}(\hat{t}) \\ \mathbf{E}(\hat{t}) \end{bmatrix} + \begin{bmatrix} \mathbf{A_1} & 0 \\ 0 & \mathbf{A_1} \end{bmatrix} \begin{bmatrix} \mathbf{X}(\hat{t}-\hat{\tau}_0) \\ \mathbf{E}(\hat{t}-\hat{\tau}_0) \end{bmatrix} \tag{5.13}$$

Next, the continuous pole placement technique developed in reference [27] can be applied to determine $\mathbf{K}$ and $\mathbf{L}$. Since the separation principle holds for the dynamics of the drill string and the error, one can have the drill-string dynamics (zero observer error)

$$\dot{\mathbf{X}}(\hat{t}) = (\mathbf{A_0} + \mathbf{BK})\mathbf{X}(\hat{t}) + \mathbf{A_1}\mathbf{X}(\hat{t}-\hat{\tau}_0) \tag{5.14}$$

and the observer error dynamics

$$\dot{\mathbf{E}}(\hat{t}) = (\mathbf{A_0} - \mathbf{LC})\mathbf{E}(\hat{t}) + \mathbf{A_1}\mathbf{E}(\hat{t}-\hat{\tau}_0) \tag{5.15}$$

In order to mitigate the vibrations, Eq. (5.14) and Eq. (5.15) need to be globally

exponentially stable, respectively. Then, the objective function can be formulated as

$$J(\mathbf{K}) = \sup_s \{\mathrm{Re}(s) | \det(s\mathbf{I} - (\mathbf{A_0} + \mathbf{BK}) - \mathbf{A_1} e^{-\hat{\tau}_0 s}) = 0\} \tag{5.16}$$

and

$$Q(\mathbf{L}) = \sup_s \{\mathrm{Re}(s) | \det(s\mathbf{I} - (\mathbf{A_0} - \mathbf{LC}) - \mathbf{A_1} e^{-\hat{\tau}_0 s}) = 0\} \tag{5.17}$$

Here, $J(\cdot)$ and $Q(\cdot)$ represent the rightmost pole of the drill-string dynamics Eq. (5.14) and observer error dynamics Eq. (5.15), respectively. When these objective functions are negative, asymptotic stability is guaranteed.

5.3.2 Optimal feedback gain design

One way to design control gain matrix $\mathbf{K}$ and observer gain $\mathbf{L}$ is to respectively solve the optimization problems

$$\min_{\mathbf{K}} J(\mathbf{K}) \tag{5.18}$$

and

$$\min_{\mathbf{L}} Q(\mathbf{L}) \tag{5.19}$$

so that the rightmost pole of the drill-string dynamics and observer error dynamics have the minimum values. However, the objective functions are not differentiable. To address this issue, the optimization method used in last section will be adopted here. Procedures listing below will be used to calculate the optimized gains.

1. Approximate the Clarke subdifferential by gradient sampling.

2. Compute a search direction.

3. Compute a step length.

4. Update.

First, let's reconsider the case shown in Figure(4.6) where a stable equilibrium co-exists with a limit cycle with stick-slip: $(\psi = 14, \eta = 1.6, \zeta = \kappa = 0.02, \delta_0 = 1.23, \omega_0 = 10)$, the optimal values for $\mathbf{K}$ and $\mathbf{L}$ obtained are listed below:

$$\mathbf{K}_{\text{opt}} = \begin{bmatrix} 1.9999 & 2.2378 & -4.1001 & -6.0341 \end{bmatrix} \tag{5.20}$$

$$\mathbf{L}_{\text{opt}} = \begin{bmatrix} 0.6072 & 0.0788 & 0.2359 & 0.2319 \\ 0.1838 & -0.2581 & -0.0612 & -0.9894 \end{bmatrix}^T \tag{5.21}$$

The corresponding optimal objective functions satisfy

$$J(\mathbf{K}_{\text{opt}}) = -1.0739 \tag{5.22}$$

and

$$Q(\mathbf{L}_{\text{opt}}) = -0.9638 \tag{5.23}$$

For the original linearized system the rightmost pole is $J(\cdot) - 0.02$, the system with optimal PD control with the rightmost pole located at $J(\mathbf{K}_1, \mathbf{K}_2) = -0.6003$. The plot of the rightmost poles for each case is given in Figure(5.9). Similar to the PD control presented in previous section, the observer based controller is also

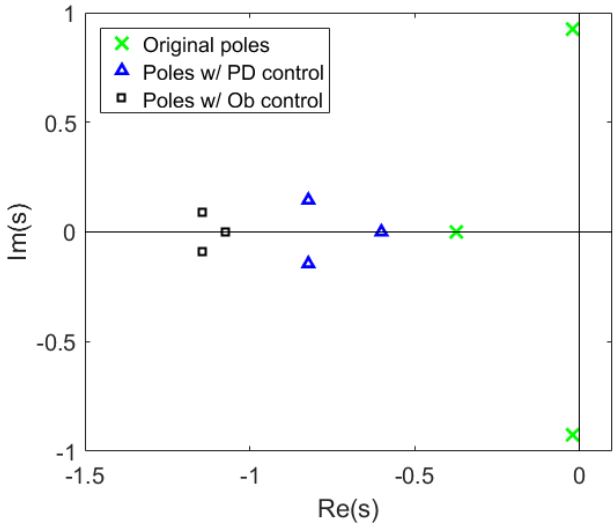

Figure 5.9: Position of the 3 rightmost poles of original system($\omega_0 = 10, \delta_0 = 1.23, \psi = 14, \zeta = \kappa = 0.02$), system with PD control ($\mathbf{K}_1, \mathbf{K}_2$), and system with observer-based control.

based on the lienarized system. With the ultimate goal to be the mitigation of the undesired nonlinear vibrations, the observer based controller will be applied to original nonlinear system where the state-dependent delay, friction, and loss of contact will be considered.

As stated, for parameter values of $\omega_0 = 10$ and $\delta_0 = 1.23$, the system response can either be stable equilibrium or stick-slip limit cycle, as depicted in Figure(4.6). It is noted that in both instances, the controller can be used to stabilize the system to an equilibrium state, thus showing that the controller is viable for the nonlinear system.

Next, let's consider the more complex case shown in Figure(4.7)(a, b) where a stable limit cycle without stick slip co-exists with a limit cycle with stick-slip: ($\psi = 14, \eta = 1.6, \zeta = \kappa = 0.02, \delta_0 = 1.33, \omega_0 = 10$), the optimal values for $\mathbf{K}$ and $\mathbf{L}$

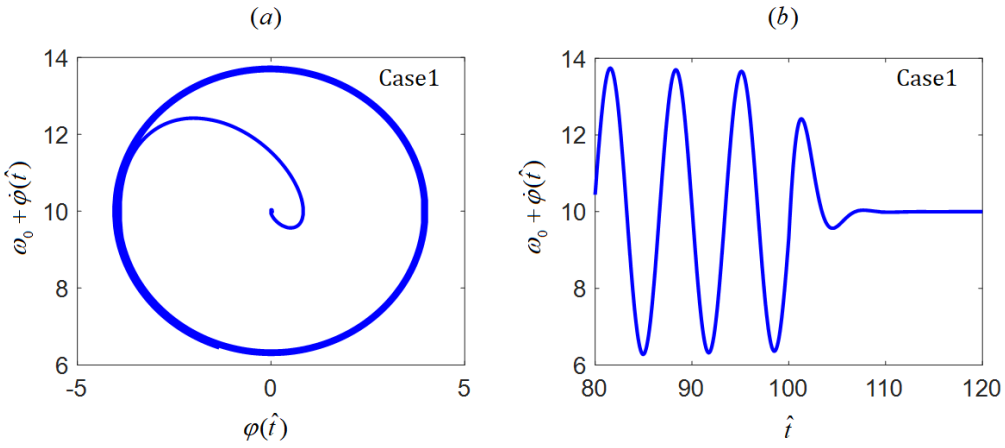

Figure 5.10: Simulation of nonlinear system($\omega_0 = 10, \delta_0 = 1.23, \psi = 14, \zeta = \kappa = 0.02$) with control at $\hat{t} = 100$. Case 1 - slowly stable equilibrium (a) phase portrait projection, (b) torsional motion response.

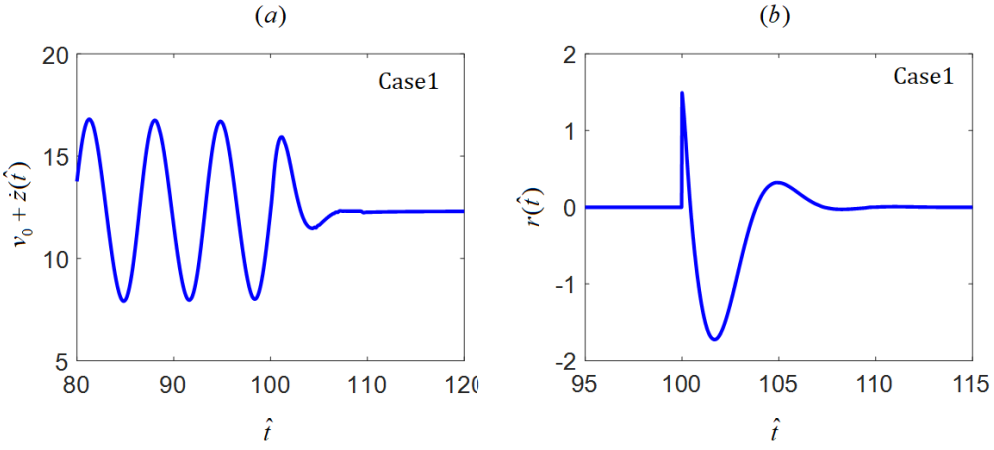

Figure 5.11: Simulation of nonlinear system($\omega_0 = 10, \delta_0 = 1.23, \psi = 14, \zeta = \kappa = 0.02$) with control at $\hat{t} = 100$. Case 1 - slowly stable equilibrium (a) axial motion response and (b) control signal.

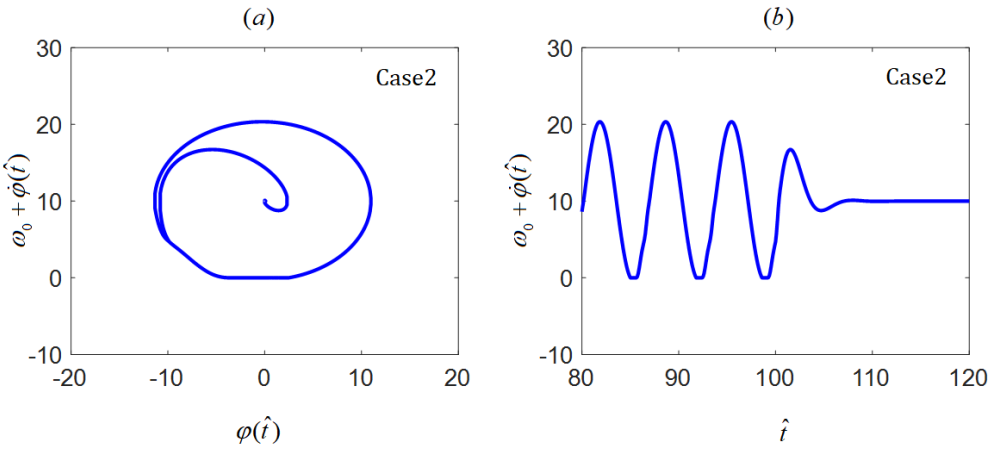

Figure 5.12: Simulation of nonlinear system($\omega_0 = 10, \delta_0 = 1.23, \psi = 14, \zeta = \kappa = 0.02$) with control at $\hat{t} = 100$. Case 2 - stick-slip limit cycle (a) phase portrait projection and (b) torsional motion response.

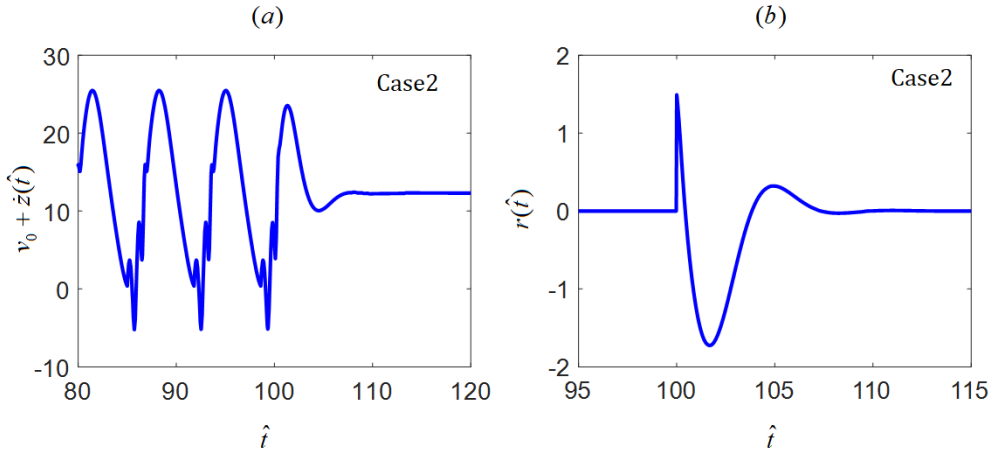

Figure 5.13: Simulation of nonlinear system($\omega_0 = 10, \delta_0 = 1.23, \psi = 14, \zeta = \kappa = 0.02$) with control at $\hat{t} = 100$. Case 2 - stick-slip limit cycle (a) axial motion response and (b) control signal.

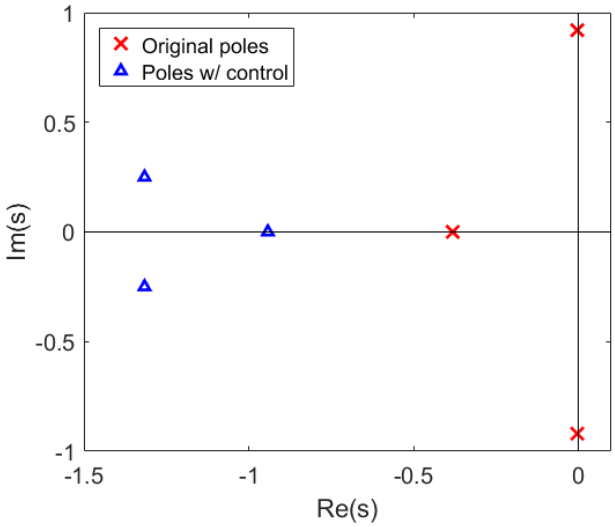

Figure 5.14: Position of the 3 rightmost poles of original system($\omega_0 = 10, \delta_0 = 1.32, \psi = 14, \zeta = \kappa = 0.02$) and system with optimal feedback gain $\mathbf{K}$.

obtained are listed below:

$$\mathbf{K}_{\text{opt}} = \begin{bmatrix} 1.1655 & -0.3552 & -3.6722 & -1.9293 \end{bmatrix} \tag{5.24}$$

$$\mathbf{L}_{\text{opt}} = \begin{bmatrix} 0.2471 & 0.2455 & 0.2067 & 0.2013 \\ 0.2204 & -0.0013 & -0.2051 & -0.8115 \end{bmatrix}^T \tag{5.25}$$

The corresponding optimal objective functions satisfy $J(\mathbf{K}_{\text{opt}}) = -1.1963$, and $Q(\mathbf{L}_{\text{opt}}) = -0.7973$, implying that all the poles of the closed-loop system of drill-string dynamics combined with the observer based controller Eq.(5.13) are indeed in the left-half complex plane, thereby guaranteeing exponential stability of the system described by Eq.(5.11). The original poles positions and the controlled poles positions can be seen in Figure(5.14). As before, the author will investigate the

effectiveness of the controller on the motions of the dimensionless nonlinear system, wherein the state-dependent delay, friction, and loss of contact are taken into account as sources of nonlinearity. For parameter values of $\delta_0 = 1.33$ and $\omega_0 = 10$, the system response can be either be a stable limit cycle without stick-slip or a stick-slip limit cycle. To eliminate the undesired nonlinear vibrations in both cases, the observer-based control parameters $\mathbf{K}_{\text{opt}}$ and $\mathbf{L}_{\text{opt}}$ are set to be zero. With different initial conditions, the drill string system will merge to stable limit cycle and stick-slip limit cycle. With the control applied at $\hat{t} = 100$, the system of both cases are quickly stabilized to the equilibrium.

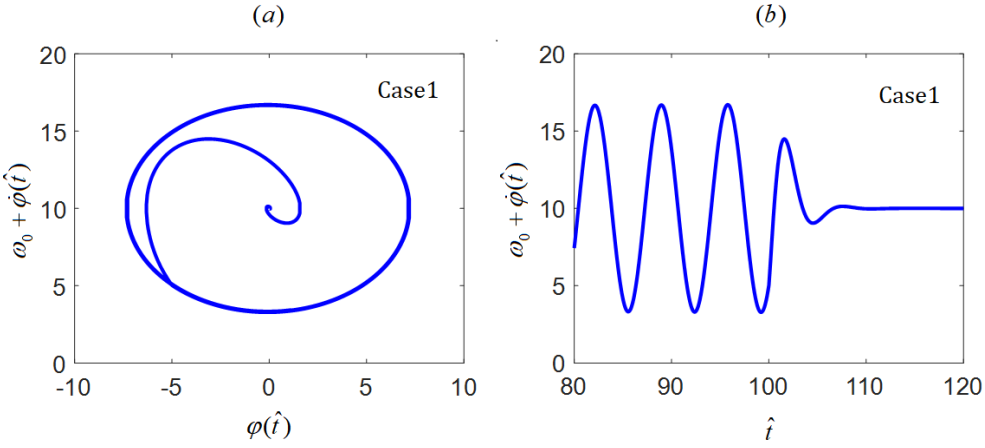

Figure 5.15: Simulation of nonlinear system($\omega_0 = 10, \delta_0 = 1.33, \psi = 14, \zeta = \kappa = 0.02$) with control at $\hat{t} = 100$. Case 1 - limit cycle without stick-slip (a) phase portrait projection and (b) torsional motion response.

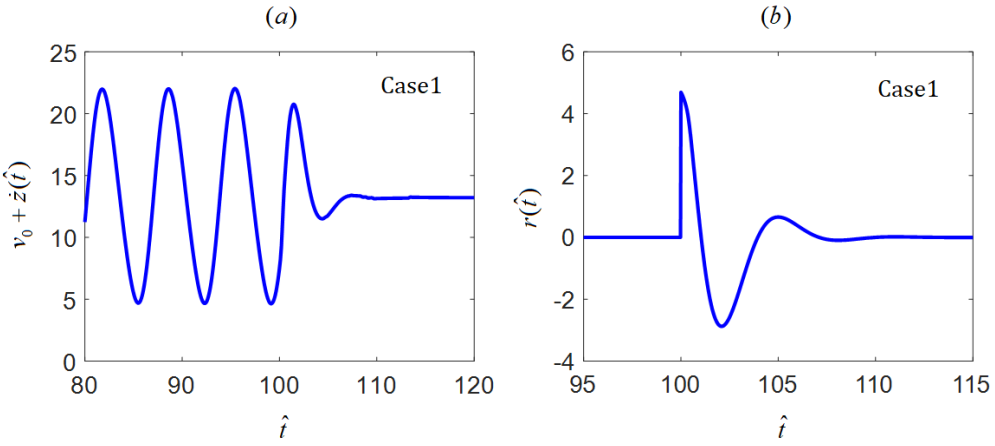

Figure 5.16: Simulation of nonlinear system($\omega_0 = 10, \delta_0 = 1.33, \psi = 14, \zeta = \kappa = 0.02$) with control at $\hat{t} = 100$. Case 1 - limit cycle without stick-slip (a) axial motion response, (b) control signal.

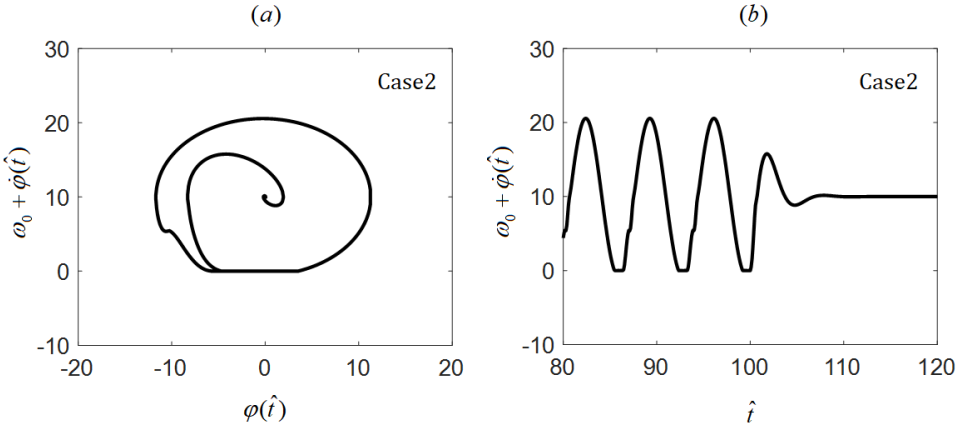

Figure 5.17: Simulation of nonlinear system($\omega_0 = 10, \delta_0 = 1.33, \psi = 14, \zeta = \kappa = 0.02$) with control at $\hat{t} = 100$. Case 2 - stick-slip limit cycle (a) phase portrait projection and (b) torsional motion response.

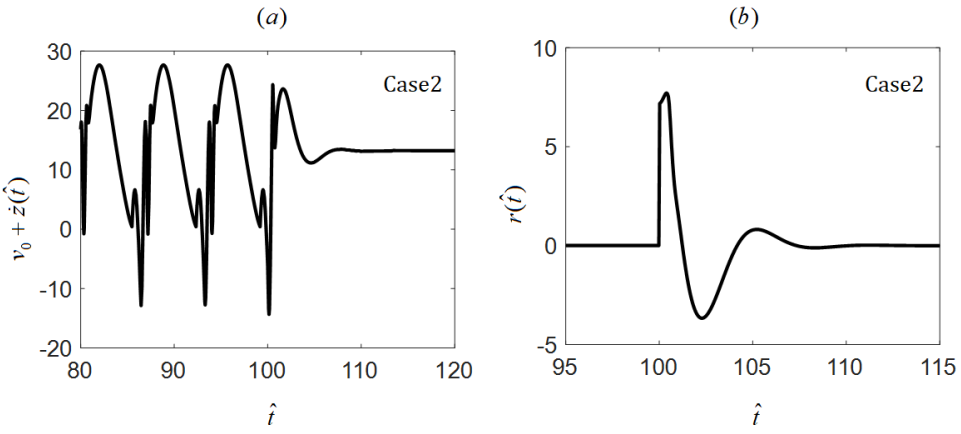

Figure 5.18: Simulation of nonlinear system($\omega_0 = 10, \delta_0 = 1.33, \psi = 14, \zeta = \kappa = 0.02$) with control at $\hat{t} = 100$. Case 2 - stick-slip limit cycle (a) axial motion response and (b) control signal.

Chapter 6: Summary of Contributions and Recommendations for Future Work

6.1 Summary of Contributions

In this section, the outcomes of the research studies presented in Chapter 2 to Chapter 5 are collected and discussed.

The nonlinear axial and torsion dynamics of oil drilling systems are considered with a reduced-order drill-string model. Nonlinear effects arise from cutting mechanics which include dry friction, loss of contact, and the state-dependent delay, are studied.

The main contributions are listed as follows:

1. The effects of state-dependent delay, dry friction, and loss of contact on drilling dynamics have been studied by considering a representative reduced-order model for coupled axial-torsional dynamics. The nondimesionalization has been conducted to reduce the number of parameters. The linearized constant time delay system holding the same local stability properties as the original state-dependent delay system has been found.(Xie Zheng and Balakumar Balachandran [66])

2. The local stability for the linearized system has been carried out analytically

using D-subdivision method. The stability crossing curves have been generated as well. The stable and unstable region have been classified by the number of poles on the right half plane.(Xie Zheng and Balakumar Balachandran [66])

3. The state-dependent delay are always nonlinear, since the state itself arises in its own argument through the delay. To study the effect of it, DDE-BIFTOOL, a continuation numerical continuation method software toolbox developed for systems with explicit time delays is used. From the bifurcation diagrams, two conclusions can be drawn as follows,

• When dimensionless drive space ω_0 is small, branches of periodic motions are unstable (subcritical bifurcation), as ω_0 increase, these periodic motion change from unstable to stable (supercritical bifurcation).

• With small value of dimensionaless axial and torsional damping ratio, periodic motions are subcritical, as damping ratio increases the Hopf bifurcation change from subcritical to supercritical.(Xie Zheng, Vipin Agarwal, and Balakumar Balachandran [67])

4. For a larger scale, the nonlinear effect of loss of contact and dry friction are considered by introducing a sigmoid function, a hyperbolic tangent function and an explicit form of state-dependent delay which is based on a Taylor expansion. The nonlinear instabilities are shown in bifucation diagrams, which reveal a route leading to stick-slip vibrations. From the results, the infer that the system is susceptible to the stick-slip phenomenon, even when the system is operating in a stable nominal state, in particular near the critical points. Moreover, apart from a stick0slip limit cycle, a stable limit cycle without stick-slip can occur due to the state-dependent

delay. This scenario with stable equilibrium branch, a stable limit cycle branch without stick slip, and a stable limit cycle branch with stick-slip has been reported for the first time. (Xie Zheng, Vipin Agarwal, Xianbo Liu, and Balakumar Balachandran [68])

5. To mitigate the stick-slip vibrations, controller design are presented. First, based on current and delayed torsional state, a Proportional and Differential controller are given. The feedback gain are determined by a numerical optimization method. The effectiveness is examined with nonlinear system for stable motions as well as the stick-slip motions. Furthermore, with an observer, the axial state are estimated and used for a new controller which are based on pole placement method for system with time delay. The position of poles are determined by the numerical optimization method as before. Similarly, the effectiveness of the linear system based controller are tested with the nonlinear system for suppressing limit cycle motions with and without stick-slip. It is noted that in both instances, the controller can be used to stabilize the system to an equilibrium state, thus showing that the controller is viable for the nonlinear system. (Xie Zheng, Vipin Agarwal, Xianbo Liu, and Balakumar Balachandran [68])

6.2 Recommendations for Future Work

In future work, a system with high number of degrees of freedom is to be considered. It is planned to include the effect of other nonlinear factors, for example, the friction between the drill0sting and well-bore associated with lateral motion.

In addition, the effectiveness of the control schemes in the presence of noise and parameter uncertainties is to be examined.

Appendix A: Derivation of Non-dimensional Governing Equations

As shown in the Introduction section, the original governing equation of the drill string system is

$$\begin{aligned} M\ddot{Z}(t) + C_a\dot{Z}(t) + K_a(Z(t) - V_0 t) &= W_s - W_b(t) \\ I\ddot{\Phi}(t) + C_t\dot{\Phi}(t) + K_t(\Phi(t) - \Omega_0 t) &= -T_b(t) \end{aligned} \tag{A.1}$$

To reduce the number of parameters, the equations of motion are cast into dimensionless form, with the procedures showing below:

Step 1: Write down the given constant.

One main objective of current research is the mitigation of stick-slip vibrations. Since it is torsion dominated, the torsional characteristic time and characteristic length will be employed here as the time and length constant.

$$t_* = \sqrt{\frac{I}{K_t}} \qquad L_* = \frac{2K_t}{\epsilon a^2} \tag{A.2}$$

Step 2: Write down variables and involved & units.

The physical quantities related to axial and torsional motions of drill string system are listed in the table below,

Table A.1: Variables involved for drilling operations

Name	Symbol	Unit
Axial displacement	$Z(t)$	m
Axial velocity	$\dot{Z}(t)$	$\mathrm{m\,s^{-1}}$
Axial acceleration	$\ddot{Z}(t)$	$\mathrm{m\,s^{-2}}$
Torsional displacement	$\Phi(t)$	rad
Torsional velocity	$\dot{\Phi}(t)$	rad $\mathrm{s^{-1}}$
Torsional acceleration	$\ddot{\Phi}(t)$	rad $\mathrm{s^{-2}}$

Step 3: Determine new non-dimensional variables.

The nominal solution for our drill string model, which represents the stable drilling without any vibration, can be described as:

$$\begin{aligned} \bar{Z} &= V_0 t + Z_0 \qquad & \dot{\bar{Z}} &= V_0 \\ \bar{\Phi} &= \Omega_0 t + \Phi_0 \qquad & \dot{\bar{\Phi}} &= \Omega_0 \end{aligned} \tag{A.3}$$

Here, Z_0 and Φ_0 are the respective constant deformations of the axial spring and the torsion spring.

$$\begin{aligned} Z_0 &= -\tfrac{1}{K_a}\left(2\pi\epsilon a\zeta\tfrac{V_0}{\Omega_0} + C_a V_0 + \sigma a l - W_s\right) \\ \Phi_0 &= -\tfrac{1}{K_t}\left(\pi\epsilon a^2\tfrac{V_0}{\Omega_0} + C_t\Omega_0 + \tfrac{1}{2}\mu\gamma a^2\sigma l\right) \end{aligned} \tag{A.4}$$

Then, the new non-dimensional variable are

Table A.2: Non-dimensional variables

Name	Symbol
Time	$\hat{t} = t/t_*$
State-dependent delay	$\hat{\tau} = \tau/t_*$
Axial displacement	$z(t) = \frac{Z-\bar{Z}}{L_*}$
Torsion displacement	$\varphi(t) = \Phi - \bar{\Phi}$

Step 4: Calculate all required derivatives in terms of non-dimensional variables.

For axial motions, one has $Z = z * L_* + \bar{Z}$, and the higher order derivatives are

$$\frac{dZ}{dt} = L_* \frac{dz}{dt} + \frac{\bar{Z}}{dt} = \frac{L_*}{t_*} \frac{dz}{d\hat{t}} + V_0 \tag{A.5}$$

$$\frac{d^2Z}{dt^2} = \frac{d}{dt}\left(\frac{L_*}{t_*} \frac{dz}{d\hat{t}} + V_0\right) = \frac{L_*}{t_*^2} \frac{dz^2}{d\hat{t}^2} \tag{A.6}$$

For torsional motions, since $\Phi = \varphi + \bar{\Phi}$, the higher order derivatives are

$$\frac{d\Phi}{dt} = \frac{d\varphi}{dt} + \frac{\bar{\Phi}}{dt} = \frac{1}{t_*} \frac{d\varphi}{d\hat{t}} + \Omega_0 \tag{A.7}$$

$$\frac{d^2\Phi}{dt^2} = \frac{d}{dt}\left(\frac{1}{t_*} \frac{d\varphi}{d\hat{t}} + V_0\right) = \frac{1}{t_*^2} \frac{d\varphi^2}{d\hat{t}^2} \tag{A.8}$$

Step 5: Rewrite governing equations with non-dimensional variables.

Substituting the non-dimensional variables and these derivatives into the original governing equations, one will have

$$\begin{aligned} \ddot{z}(\hat{t}) + 2\xi\eta\dot{z} + \eta^2 z(\hat{t}) &= -\psi\delta(\hat{t}, \hat{\tau}) + \hat{W}_{\text{bf}} \\ \ddot{\varphi}(\hat{t}) + 2\kappa\dot{\varphi}(\hat{t}) + \varphi(\hat{t}) &= -\delta(\hat{t}, \hat{\tau}) + \hat{T}_{\text{bf}} \end{aligned} \tag{A.9}$$

The dimensionless parameters are defined as

- Ratio of the axial natural frequency to the torsion natural frequency:

$$\eta^2 = \frac{K_a}{M} * t_*^2 = \frac{K_a}{M} \cdot \frac{I}{K_t}$$

- Non-dimensional axial damping ratio:

$$\xi = \frac{C_a}{2m} \cdot t_* / \eta = \frac{C_a}{2\sqrt{K_a M}}$$

- The quantity ψ is dependent upon the rock strength and drill-bit geometry.

$$\psi = \frac{\epsilon a \zeta L_*}{M L_* / t_*^2} = \frac{\epsilon a \zeta}{m} \cdot \frac{I}{K_t}$$

Furthermore, the dimensionless perturbation of cutting depth δ can be written as

$$\delta(\hat{t}, \hat{\tau}) = N \left[R \left(z(\hat{t}) - z(\hat{t} - \hat{\tau}) + v_0 \hat{\tau} \right) \cdot H(\dot{\varphi}(\hat{t}) + \omega_0) - v_0 \hat{\tau}_0 \right] \tag{A.10}$$

The dimensionless perturbation of friction components of the weight on bit $\hat{W}_{\text{bf}}$ can be expressed as

$$\hat{W}_{\text{bf}} = \frac{\sigma a l}{M L_*} t_*^2 \left[1 - H \left(z(\hat{t}) - z(\hat{t} - \hat{\tau}) + v_0 \hat{\tau} \right) \cdot H \left(\dot{z}(\hat{t}) + v_0 \right) \right] \tag{A.11}$$

and the dimensionless perturbation of friction components of the torque on bit $\hat{T}_{\text{bf}}$ takes the form

$$\hat{T}_{\text{bf}} = \frac{\mu \gamma \sigma a^2 l}{2I} t_*^2 \left[1 - \text{sgn}(\dot{\varphi}(\hat{t}) + \omega_0) \cdot H \left(z(\hat{t}) - z(\hat{t} - \hat{\tau}) + v_0 \hat{\tau} \right) \cdot H \left(\dot{z}(\hat{t}) + v_0 \right) \right] \tag{A.12}$$

where v_0 is the dimensionless penetration rate, ω_0 is the dimensionless angular speed,

and $\hat{\tau}_0$ is the constant time delay.

$$\omega_0 = \Omega_0 t_* \qquad v_0 = \frac{V_0 t_*}{L_*} \qquad \hat{\tau}_0 = \frac{2\pi}{N\omega_0} \tag{A.13}$$

Appendix B: Derivation of Stability Crossing Set

With the state variable $\mathbf{X} = (z(\hat{t}) \quad \dot{z}(\hat{t}) \quad \varphi(\hat{t}) \quad \dot{\varphi}(\hat{t}))^T$, the state space form of linearize system can be expressed in the form as

$$\dot{\mathbf{X}}(\hat{t}) = A_0\mathbf{X}(\hat{t}) + A_1\mathbf{X}(\hat{t} - \hat{\tau}_0) \tag{B.1}$$

Here, A_0, and A_1 are the coefficient matrix of current state and delayed state, which are given by

$$\mathbf{A_0} = \begin{bmatrix} 0 & 1 & 0 & 0 \\ -\eta^2 - N\psi & -2\xi\eta & N\psi\delta_0 & 0 \\ 0 & 0 & 0 & 1 \\ -N & 0 & N\delta_0 - 1 & -2\kappa \end{bmatrix} \tag{B.2}$$

$$\mathbf{A_1} = \begin{bmatrix} 0 & 0 & 0 & 0 \\ N\psi & 0 & -N\psi\delta_0 & 0 \\ 0 & 0 & 0 & 0 \\ N & 0 & -N\delta_0 & 0 \end{bmatrix} \tag{B.3}$$

Then one can define a matrix Δ as

$$\Delta(s) = sI - A_0 - A_1 e^{-\hat{\tau}_0 s} \tag{B.4}$$

the characteristic equation reads

$$det(\Delta(s)) = 0 \tag{B.5}$$

After a lengthy but straightforward calculation, one will arrive at the characteristic equation of following form:

$$P_0(s) + P_1(s)(1 - e^{-\hat{\tau}_0 s}) = 0 \tag{B.6}$$

Here, P_0, and P_1 are polynomials in the eigenvalue s and these polynomials can be expressed as

$$\begin{aligned} P_0(s) &= s^4 + (2\xi\eta + 2\kappa)s^3 + (\eta^2 + 4\kappa\xi\eta + 1)s^2 + (2\xi\eta + 2\kappa\eta^2)s + \eta^2 \\ P_1(s) &= (N\psi - Nv_0)s^2 + (2\kappa N\psi - 2\xi\eta N v_0)s + (N\psi - N\eta^2 v_0) \end{aligned} \tag{B.7}$$

By definition, the stability crossing set is a set where the poles of the characteristic equation cross the imaginary axis. In other words, the poles only contain the imaginary part $s = i\omega$. The ω denotes the crossing frequency. Substituting $s = i\omega$ and

$\hat{\tau}_0 = 2\pi N/\omega_0$ characteristic equation can be rewrite in to

$$\frac{P_1(i\omega)}{P_0(i\omega) + P_1(i\omega)} e^{-\frac{2\pi N}{\omega_0}\omega i} = 1 \tag{B.8}$$

Based on the magnitude condition, one has

$$||P_0(i\omega) + P_1(i\omega)|| = ||P_1(i\omega)|| \tag{B.9}$$

for phase condition, one has

$$\angle \frac{P_1}{P_0 + P_1} - \frac{2\pi N}{\omega_0}\omega = 2k\pi \qquad k = 1, 2, ..., \tag{B.10}$$

Since P_0 is not related to dimensionless drive speed ω_0 and drill bit design factor ψ, we can define the real part as α and the imaginary part as β, then $P_0(i\omega)$ can be written in the form

$$P_0(i\omega) = \alpha + \beta i \tag{B.11}$$

where,

$$\begin{aligned} \alpha(\omega) &= \omega^4 - (\eta^2 + 4\kappa\xi\eta + 1)\omega^2 + \eta^2 \\ \beta(\omega) &= -2\xi\eta + 2\kappa)\omega^3 + (2\xi\eta + 2\kappa\eta^2)\omega \end{aligned} \tag{B.12}$$

$P_1(i\omega)$ is in terms of drill-string design parameter ψ as,

$$P_1(i\omega) = \left(-\omega^2 + 2\kappa\omega i + 1\right) N\psi + \left(Nv_0\omega^2 - 2\xi\eta N v_0 \omega i - N\eta^2 v_0\right) \tag{B.13}$$

If one takes the square on both sides of the magnitude condition equation, after a rather lengthy calculation, we arrive at

$$\psi_{SDD} = \frac{1}{N[\alpha(\omega^2-1)-2\beta\kappa\omega]}[\frac{\alpha^2+\beta^2}{2} + (\alpha(\omega^2-\eta^2)+2\beta\xi\eta\omega)Nv_0] \tag{B.14}$$

Similarly from the phase condition, one can get

$$\omega_{0SDD} = \frac{2\pi\omega}{N(\Theta_1+(2k-1)\pi)}, \qquad k=1,2,..., \tag{B.15}$$

where,

$$\Theta_1 = \angle\frac{-P_1}{P_0+P_1} \tag{B.16}$$

When the terms with v_0 in P_1 are zero, the SD-DDE characteristic equation degenerate to CD-DDE characteristic equation:

$$P_0(s) + P_2(s)(1-e^{-\hat{\tau}_0 s}) = 0 \tag{B.17}$$

where P_2 can be expressed as

$$P_2(s) = N\psi(s^2+2\kappa s+1) \tag{B.18}$$

Following the same procedure as in the SD-DDE case, we get the stability crossing

set in the form of

$$\begin{aligned} \psi_{CD} &= \frac{1}{N[\alpha(\omega^2-1)-2\beta\kappa\omega]}\frac{\alpha^2+\beta^2}{2} \\ \omega_{0CD} &= \frac{2\pi\omega}{N(\Theta_2+(2k-1)\pi)}, \qquad k=1,2,..., \end{aligned} \tag{B.19}$$

and

$$\Theta_2 = \angle\frac{-P_2}{P_0+P_2} \tag{B.20}$$

Appendix C: MATLAB code of Observer-based Controller

```
clc; clear all; close all;


i) Drill String System Parameters

% Nondimension velocity:

v0 = 1.32;

% Nondimension angular velocity:

w0 = 10;

% Nondimension axial damping ratio:

xi =0.02;

% Nondimension torsional damping ratio:

kappa = 0.02;

[N, psi, eta, xi, kappa, Wf, Tf,A0,A1] = Parameters(v0,xi,kappa);


ii) Simulation Parameters

% Simulation time:

t_end = 200;

% Linearized time delay:
```

```
tau0 = 2*pi/(N*w0);

% Revolution of time delay:

ntn = 200;

% Time step size:

dt = tau0/ntn;

% Time vector

t = 0:dt:t_end-dt;

% Number of steps

nsteps = length(t);
```

ii) State Parameters

```
V0 = w0*v0;

X = zeros(4,nsteps);

dphi0 = 11;

z = V0*t;

phi = w0*t;

% Initial positions:

X(1,1:ntn*5+2) = z(1:ntn*5+2) ;

% Initial velocity

X(2,1:ntn*5+2) = V0;

% Initial angle

X(3,1:ntn*5+2) = phi(1:ntn*5+2);

% Initial angular velocity

X(4,1:ntn*5+2) = w0 + dphi0;
```

```
(1) Simulation without control

for i=ntn*2:nsteps-1

% find state-dependent time delay tau

if X(3,i) - X(3,i-ntn) > 2*pi/N

   while X(3,i) - X(3,i-ntn) > 2*pi/N

      ntn = ntn -1;

   end

else

   while X(3,i) - X(3,i-ntn) ¡ 2*pi/N

      ntn = ntn +1;

   end

ntn =ntn -1;

end

% depth of cut

delta = X(1,i)-X(1,i-ntn);

R_delta = (delta > 0)*delta;

H_delta = delta > 0;

H_dz = X(2,i) > 0;

H_dphi = X(4,i) > 0;

ddz = -2*xi*eta*(X(2,i)-V0) - eta**2*(X(1,i)-z(i))+ N*psi*V0*tau0 - N*psi*R_delta*H_dphi
+ Wf*(1-H_delta*H_dz);

X(2,i+1) = X(2,i) + ddz*dt;

X(1,i+1) = X(1,i) + X(2,i)*dt;
```

```
ddphi = -2*kappa*(X(4,i)-w0) - (X(3,i)-phi(i)) + N*V0*tau0 - N*R_delta*H_dphi
+ Tf*(1-sign(X(4,i))*H_delta*H_dz);
X(4,i+1) = X(4,i) + ddphi*dt;
X(3,i+1) = X(3,i) + X(4,i)*dt;
end
X_origin = X;

%(2) Simulation with control
% iv) Oberver Parameters B = [0;0;0;1];
C = [0, 0, 1, 0; 0, 0, 0, 1];
F = [ 1.1655, -0.3552, -3.6722, -1.9293];
L = [0.2471, 0.2204; 0.2455, -0.0013; 0.2067, -0.2051; 0.2013, 0.8115];
LC =L*C;
BF = B*F;
Ob = zeros(4,nsteps);
dOb = zeros(4,nsteps);
U = zeros(4,nsteps); u =0;
uc =zeros(1,nsteps);
% v) Simulation
for i=ntn*2:nsteps-1    if X(3,i) - X(3,i-ntn) ¿ 2*pi/N
    while X(3,i) - X(3,i-ntn) ¿ 2*pi/N
      ntn = ntn -1;
    end
```

```
    else
      while X(3,i) - X(3,i-ntn) ¡ 2*pi/N
        ntn = ntn +1;
      end
    ntn =ntn -1;
  end
  % Dynamics of Observer
  dOb(:,i) = A0*Ob(:,i) + A1*Ob(:,i-ntn)+ BF*Ob(:,i) + LC*(U(:,i) - Ob(:,i));
  Ob(:,i+1) = Ob(:,i) + dOb(:,i)*dt;
  % Nonlinear Parameters
  delta = X(1,i)-X(1,i-ntn);
  R_delta = (delta¿0)*delta;
  H_delta = delta¿0;
  H_dz = X(2,i)¿0;
  H_dphi = X(4,i)¿0;
  ddz = -2*xi*eta*(X(2,i)-V0) - eta**2*(X(1,i)-z(i)) + N*psi*V0*tau0 - N*psi*R_delta*H_dphi
+ Wf*(1-H_delta*H_dz);
  X(2,i+1) = X(2,i) + ddz*dt;
  X(1,i+1) = X(1,i) + X(2,i)*dt;
  % Control input if t(i) ¿ 100      u = F(1)*Ob(1,i) + F(2)*Ob(2,i) + F(3)*Ob(3,i)+F(4)*Ob(4
end uc(i) = u;
  ddphi = -2*kappa*(X(4,i)-w0) - (X(3,i)-phi(i)) + N*V0*tau0 - N*R_delta*H_dphi
+ Tf*(1-sign(X(4,i))*H_delta*H_dz)+ u;
```

```
X(4,i+1) = X(4,i) + ddphi*dt;

X(3,i+1) = X(3,i) + X(4,i)*dt;

U(:,i+1) =[X(1,i+1)-z(i+1); X(2,i+1)-V0; X(3,i+1)-phi(i+1); X(4,i+1)-w0];

end

Phi = X(3,:) - phi;

dPhi = X(4,:) - w0;

figure(1)

plot(t,X_origin(4,:),'b','linewidth',4);

figure(2)

plot(t,X(4,:),'k','linewidth',3);

xlim([80,120])

set(gca,'FontSize',20)

figure(3)

stat = 1e5;

plot(Phi(stat:end),dPhi(stat:end)+10,'k','linewidth',3);

set(gca,'FontSize',20)

figure(4)

plot(t,uc,'k','linewidth',3)

xlim([95,115])

set(gca,'FontSize',20)
```

Bibliography

[1] What is onshore drilling versus offshore drilling? https://www.entranceconsulting.com/onshore-versus-offshore-drilling/, 2019. Accessed: 02-26-2020.

[2] Xianbo Liu. *Dynamics and Control of a Slender, Flexible Rotor with Time-Delay Effects*. PhD thesis, Shanghai jiaotong university, Shanghai, China, 7 2017.

[3] Guangjian Dong and Ping Chen. A review of the evaluation, control, and application technologies for drill string vibrations and shocks in oil and gas well. *Shock and Vibration*, 2016, 2016.

[4] Liu Hong, Irving P Girsang, and Jaspreet S Dhupia. Identification and control of stick–slip vibrations using kalman estimator in oil-well drill strings. *Journal of Petroleum Science and Engineering*, 140:119–127, 2016.

[5] Xianbo Liu, Nicholas Vlajic, Xinhua Long, Guang Meng, and Balakumar Balachandran. Coupled axial-torsional dynamics in rotary drilling with state-dependent delay: stability and control. *Nonlinear Dynamics*, 78(3):1891–1906, 2014.

[6] History of oil. https://www.ektinteractive.com/history-of-oil/, 2020. Accessed: 01-27-2020.

[7] History of the petroleum industry. https://en.wikipedia.org/wiki/History_of_the_petroleum_industry, 2019. Accessed: 01-27-2020.

[8] Paul Michael Bommer. *A Primer of Oilwell Drilling*. University of Texas at Austin Austin, 2008.

[9] Martha Belem Saldivar Márquez, Islam Boussaada, Hugues Mounier, and Silviu-Iulian Niculescu. Analysis and control of oilwell drilling vibrations. In *A Time-Delay Systems Approach, ser. Advances in Industrial Control*. Springer, 2015.

[10] MP Dufeyte, H Henneuse, et al. Detection and monitoring of the slip-stick motion: field experiments. In *SPE/IADC drilling conference*. Society of Petroleum Engineers, 1991.

[11] DR Pavone, JP Desplans, et al. Application of high sampling rate downhole measurements for analysis and cure of stick-slip in drilling. In *SPE Annual Technical Conference and Exhibition*. Society of Petroleum Engineers, 1994.

[12] N Mihajlovic, AA Van Veggel, N Van de Wouw, and H Nijmeijer. Analysis of friction-induced limit cycling in an experimental drill-string system. *J. Dyn. Sys., Meas., Control*, 126(4):709–720, 2004.

[13] Chien-Min Liao, Balakumar Balachandran, Mansour Karkoub, and Youssef L Abdel-Magid. Drill-string dynamics: reduced-order models and experimental studies. *Journal of Vibration and Acoustics*, 133(4), 2011.

[14] Christophe Germay, Vincent Denoël, and Emmanuel Detournay. Multiple mode analysis of the self-excited vibrations of rotary drilling systems. *Journal of Sound and Vibration*, 325(1-2):362–381, 2009.

[15] E. Detournay and P. Defourny. A phenomenological model for the drilling action of drag bits. *Int. J. Rock Mech. Min. Sci. Geomech. Abstr.*, 29(1):13–23, 1991.

[16] X. Liu, N. Vlajic, X. Long, G. Meng, and B. Balachandran. State-dependent delay influenced drill-string oscillations and stability analysis. *ASME. J. Vib. Acoust.*, 136(5):051008, 2014.

[17] T. Richard, C. Germay, and E. Detournay. Self-excited stick-slip oscillations of drill bits. *C.R.Mec.*, 332(8):619–626, 2004.

[18] X. Long, B. Balachandran, and B. Mann. Dynamics of milling processes with variable time delays. *Nonlinear Dynamics*, 47(1):49–63, 2007.

[19] T. Insperger, G. Stepan, and J. Turi. State-dependent delay in regenerative turning processes. *Nonlinear Dynamics*, 47(1-3):275–283, 2007.

[20] K Nandakumar and Marian Wiercigroch. Stability analysis of a state dependent delayed, coupled two dof model of drill-stringvibration. *Journal of sound and vibration*, 332(10):2575–2592, 2013.

[21] T. Insperger, D.A.W. Barton, and G. Stepan. Criticality of hopf bifurcation in state-dependent delay model of turning processes. *Int. J. Non-linear Mechanics*, 43:140–149, 2007.

[22] Pilkee Kim, Sanghyun Bae, and Jongwon Seok. Bifurcation analysis on a turning system with large and state-dependent time delay. *Journal of Sound and Vibration*, 331(25):5562–5580, 2012.

[23] Sunit K Gupta and Pankaj Wahi. Bifurcations in the axial–torsional state-dependent delay model of rotary drilling. *International Journal of Non-Linear Mechanics*, 99:13–30, 2018.

[24] C. Germay, V. Denoel, and E. Detournay. Multiple mode analysis of the self-excited vibrations of rotary drilling systems. *J. Sound and Vib.*, 325(12):362–381, 2009.

[25] Jack K Hale, Sjoerd M Verduyn Lunel, Lunel S Verduyn, and Sjoerd M Verduyn Lunel. *Introduction to functional differential equations*, volume 99. Springer Science & Business Media, 1993.

[26] Vladimir Borisovich Kolmanovskii and Valerij Romanovič Nosov. *Stability of functional differential equations*, volume 180. Elsevier, 1986.

[27] Wim Michiels and Silviu-Iulian Niculescu. *Stability and stabilization of time-delay systems: an eigenvalue-based approach*. SIAM, 2007.

[28] Damoon Soudbakhsh, Yang Zhang, and Jingang Yi. Stability analysis of human rider's balance control of stationary bicycles. In *2012 American Control Conference (ACC)*, pages 2755–2760. IEEE, 2012.

[29] Jingang Yi, Damoon Soudbakhsh, Yizhai Zhang, and Yang Zhang. Why some parkinson's disease patients cannot stand or walk but can ride a bicycle: A control system-based analysis. In *ASME 2012 5th Annual Dynamic Systems and Control Conference Joint with the JSME 2012 11th Motion and Vibration Conference*, pages 225–232. American Society of Mechanical Engineers Digital Collection, 2012.

[30] Reza Olfati-Saber, J Alex Fax, and Richard M Murray. Consensus and cooperation in networked multi-agent systems. *Proceedings of the IEEE*, 95(1):215–233, 2007.

[31] Bernd Krauskopf. Bifurcation analysis of lasers with delay. *Unlocking dynamical diversity: Optical feedback effects on semiconductor lasers*, pages 147–183, 2005.

[32] D John Runia, Sicco Dwars, Ivo Petrus Jozef Maria Stulemeijer, et al. A brief history of the shell" soft torque rotary system" and some recent case studies. In *SPE/IADC Drilling Conference*. Society of Petroleum Engineers, 2013.

[33] Aage Kyllingstad et al. A comparison of stick-slip mitigation tools. In *SPE/IADC Drilling Conference and Exhibition*. Society of Petroleum Engineers, 2017.

[34] Md Mejbahul Sarker, D Geoff Rideout, and Stephen D Butt. Advantages of an lqr controller for stick-slip and bit-bounce mitigation in an oilwell drillstring. In *ASME 2012 International Mechanical Engineering Congress and Exposition*, pages 1305–1313. American Society of Mechanical Engineers, 2012.

[35] Thijs Vromen. *Control of stick-slip vibrations in drilling systems*. PhD thesis, Eindhoven University of Technology, Eindhoven, Netherlands, 11 2015.

[36] B. Besselink, T. Vromen, N. Kremers, and N. Wouw. Analysis and control of stick-slip oscillations in drilling systems. *IEEE transactions on control systems technology*, 24:1582–1593, 2016.

[37] X. Zheng and B. Balachandran. State-dependent delay and drill string dynamics. *Procedia IUTAM*, 22:31–38, 2017.

[38] T. Richard, C. Germay, and E. Detournay. A simplified model to explore the root cause of stick-slip vibrations in drilling systems with drag bits. *J. Sound Vib.*, 305(3):432–456, 2007.

[39] B. Besselinkm, N. Wouw, and H. Nijmeijer. A semi-analytical study of stick-slip oscillations in drilling systems. *ASME J. Comput. Nonlinear Dyn.*, 6(2):p.021006, 20011.

[40] C. Germay, N. van de Wouw, H. Nijmeijer, and R. Sepulchre. Nonlinear drill string dynamics anlysis. *SIAM J. Appl. Dyn. Syst.*, 8(2):527–553, 2009.

[41] Tamás Insperger, Gábor Stépán, and Janos Turi. State-dependent delay model for regenerative cutting processes. In *Fitfth EUROMECH Nonlinear Dynamics Conference, 2005, Eindhoven, Netherlands*. Citeseer, 2005.

[42] Ferenc Hartung and Janos Turi. Linearized stability in functional differential equations with state-dependent delays. In *Conference Publications*, volume 2001, page 416. American Institute of Mathematical Sciences, 2001.

[43] Ferenc Hartung. Linearized stability in periodic functional differential equations with state-dependent delays. *Journal of Computational and Applied Mathematics*, 174(2):201–211, 2005.

[44] Ferenc Hartung and Janos Turi. On differentiability of solutions with respect to parameters in state-dependent delay equations. *journal of differential equations*, 135(2):192–237, 1997.

[45] Lev Semionovitch Pontryagin. On the zeros of some elementary transcendental functions. *Amer. Math. Soc. Transl*, 2(1):95–110, 1955.

[46] Elena N Gryazina, Boris Teodorovich Polyak, and Andrey Aleksandrovich Tremba. D-decomposition technique state-of-the-art. *Automation and Remote Control*, 69(12):1991–2026, 2008.

[47] Sim Borisovich Norkin et al. *Introduction to the theory and application of differential equations with deviating arguments*. Academic Press, 1973.

[48] Gábor Stépán. *Retarded dynamical systems: stability and characteristic functions*. Longman Scientific & Technical, 1989.

[49] Keqin Gu and Xie Zheng. An overview of stability crossing set for systems with scalar delay channels. In *Proceedings of the 33rd Chinese Control Conference*, pages 2676–2681. IEEE, 2014.

[50] Norbert Hohenbichler. All stabilizing pid controllers for time delay systems. *Automatica*, 45(11):2678–2684, 2009.

[51] K. Engelborghs, T. Luzyanina, and D. Roose. Numerical bifurcation analysis of delay differential equations using dde-biftool. *ACM Trans. Math. Software.*, 28(1):1–21, 2002.

[52] K. Engelborghs, T. Luzyanina, and G. Samaey. *DDE-BIFTOOL v.2.00: a Matlab package for bifurcation analysis of delay differential equations*. Department of Computer Science, K.U.Leuven, Leuven, Belgium, 2001.

[53] Jan Sieber, Koen Engelborghs, Tatyana Luzyanina, Giovanni Samaey, and Dirk Roose. Dde-biftool manual-bifurcation analysis of delay differential equations. *arXiv preprint arXiv:1406.7144*, 2014.

[54] Peng Lin, Yingmin Jia, and Lin Li. Distributed robust consensus control in directed networks of agents with time-delay. *Systems & control letters*, 57(8):643–653, 2008.

[55] Rifat Sipahi, Tomáš Vyhlídal, Silviu-Iulian Niculescu, and Pierdomenico Pepe. *Time delay systems: Methods, applications and new trends*. Springer, 2012.

[56] M Shahabuddin, AM Liaquat, HH Masjuki, MA Kalam, and M Mofijur. Ignition delay, combustion and emission characteristics of diesel engine fueled with biodiesel. *Renewable and Sustainable Energy Reviews*, 21:623–632, 2013.

[57] Balakumar Balachandran, Tamás Kalmár-Nagy, and David E Gilsinn. *Delay differential equations*. Springer, 2009.

[58] Keqin Gu and Silviu-Iulian Niculescu. Survey on recent results in the stability and control of time-delay systems. *J. Dyn. Sys., Meas., Control*, 125(2):158–165, 2003.

[59] Guillermo J Silva, Aniruddha Datta, and Shankar P Bhattacharyya. *PID controllers for time-delay systems*. Springer Science & Business Media, 2007.

[60] Ing-Rong Horng and Jyh-Horng Chou. Analysis, parameter estimation and optimal control of time-delay systems via chebyshev series. *International Journal of Control*, 41(5):1221–1234, 1985.

[61] Jing Zhou. Decentralized adaptive control for large-scale time-delay systems with dead-zone input. *Automatica*, 44(7):1790–1799, 2008.

[62] Yang Song, Jian Fan, Minrui Fei, and Taicheng Yang. Robust control of discrete switched system with time delay. *Applied Mathematics and Computation*, 205(1):159–169, 2008.

[63] Ozer Elbeyli and JQ Sun. On the semi-discretization method for feedback control design of linear systems with time delay. *Journal of Sound Vibration*, 273:429–440, 2004.

[64] David A Close, Steven C Owens, and Trevor KC Pugh. Downhole vibration monitoring of a drillstring, February 20 1990. US Patent 4,903,245.

[65] J. V. Burke, A. S. Lewis, and M. L. Overton. A robust gradient sampling algorithm for nonsmooth, nonconvex optimization. *SIAM J. Optim.*, 15(3):751–779, 2005.

[66] Xie Zheng and Balakumar Balachandran. State-dependent delay and drill-string dynamics. *Procedia IUTAM*, 22:31–38, 2017.

[67] Xie Zheng, Vipin Agarwal, and Balakumar Balachandran. State-dependent delay effect in drilling. *Nonlinear Dynamics and Control of Deep Drilling Systems*, page 1, 2018.

[68] Xie Zheng, Vipin Agarwal, Xianbo Liu, and Balakumar Balachandran. Nonlinear instabilities and control of drill-string stick-slip vibrations with consideration of state-dependent delay. *Journal of Sound and Vibration*, page 115235, 2020.